Ultrasonic Nondestructive Evaluation of Type 316 Austenitic Stainless Steel by Time-Frequency Analysis Methods

By

GOVIND KUMAR SHARMA

(Enrolment No: ENGG02200704001)

Indira Gandhi Centre for Atomic Research, Kalpakkam

A thesis submitted to the

Board of Studies in Engineering Sciences

In partial fulfillment of requirements

for the Degree of

DOCTOR OF PHILOSOPHY

of

HOMI BHABHA NATIONAL INSTITUTE

January, 2014

Homi Bhabha National Institute

Recommendations of the Viva Voce Committee

As members of the Viva Voce Board, we certify that we have read the dissertation prepared by **Govind Kumar Sharma** entitled **"Ultrasonic Nondestructive Evaluation of Type 316 Austenitic Stainless Steel by Time-Frequency Analysis Methods"** and recommend that it may be accepted as fulfilling the thesis requirement for the award of Degree of Doctor of Philosophy.

M. Sai Baba 22. 11. 2014

Chairman – Dr. M. Sai Baba **Date:**

22 NOV 2014

Guide/Convener – Dr. T. Jayakumar **Date:** 22/11/2014

Member 1 – Dr. A. K. Bhaduri **Date:**

22/11/2014

Member 2 – Dr. B. K. Panigrahi **Date:**

N N Kishore

External Examiner **Date:** 22/11/14

Prof. N N Kishore
IIT Kanpur

Final approval and acceptance of this dissertation is contingent upon the candidate's submission of the final copies of the dissertation to HBNI.

I hereby certify that I have read this dissertation prepared under my direction and recommend that it may be accepted as fulfilling the dissertation requirement.

Date: 22 NOV 2014

Place: Kalpakkam **Guide** 22/11/2014

STATEMENT BY AUTHOR

This dissertation has been submitted in partial fulfilment of requirements for an advanced degree at Homi Bhabha National Institute (HBNI) and is deposited in the Library to be made available to borrowers under rules of the HBNI.

Brief quotations from this dissertation are allowable without special permission, provided that accurate acknowledgement of source is made. Requests for permission for extended quotation from or reproduction of this manuscript in whole or in part may be granted by the Competent Authority of HBNI when in his or her judgment the proposed use of the material is in the interests of scholarship. In all other instances, however, permission must be obtained from the author.

Date: 21. 11. 2014

Place: Kalpakkam

Govind Sharma

(Govind Kumar Sharma)

DECLARATION

I, hereby declare that the investigation presented in the thesis entitled **"Ultrasonic Nondestructive Evaluation of Type 316 Austenitic Stainless Steel by Time-Frequency Analysis Methods"** submitted to **Homi Bhabha National Institute (HBNI)**, Mumbai, India, for the award of **Doctor of Philosophy** in **Engineering Sciences** is the record of work carried out by me under the guidance of **Dr. T. Jayakumar**, Director, Metallurgy and Materials Group, Indira Gandhi Centre for Atomic Research, Kalpakkam. The work is original and has not been submitted earlier as a whole or in part for a degree/diploma at this or any other Institution / University.

Date: 21. 11. 2014

Govind Sharma.

Place: Kalpakkam

(Govind Kumar Sharma)

List of publications arising from the thesis

Journals (3)

1. **Govind K. Sharma**, Anish Kumar, C. Babu Rao, T. Jayakumar and Baldev Raj, "Short time Fourier transform analysis for understanding frequency dependent attenuation in austenitic stainless steel, ***NDT&E International***, Vol. 53, pp. 1-7, 2013.
2. **Govind K. Sharma,** Anish Kumar, B. Purnachandra Rao and T. Jayakumar, "Continuous wavelet transform analysis for enhancement of signal to noise ratio in coarse grained austenitic stainless steel", ***Materials Evaluation***, Vol. 72, No. 12, pp. 1519-1529, 2014.
3. **Govind K. Sharma**, Anish Kumar, T. Jayakumar, B. Purnachandra Rao and N. Mariyappa, "Ensemble Empirical Mode Decomposition analysis of ultrasonic signals for adaptive defect detection in coarse grain austenitic stainless steels", ***Ultrasonics,*** In press, 2014.

Conferences (2)

1. **Govind K. Sharma**, Anish Kumar, C. Babu Rao, T. Jayakumar, and Baldev Raj, "Wavelet and short time Fourier transform analysis for understanding frequency dependent scattering", presented in ***Review of Progress in Quantitative Non Destructive Evaluation***, Kingston Rhode Island, USA, July 26-31, 2009.
2. **Govind K. Sharma,** Anish Kumar, T. Jayakumar and B. Purnachandra Rao, "Ultrasonic C-scan imaging of defects in coarse grain austenitic stainless steels- wavelet based approach", presented in ***Asia Pacific Conference on Non-Destructive Testing***, Mumbai, India, November 18-22, 2013.

Solely dedicated to my parents

ACKNOWLEDGEMENTS

I owe my deep sense of gratitude to my research supervisor and mentor **Dr. T. Jayakumar**, Director, Metallurgy and Materials Group (MMG), Indira Gandhi Centre for Atomic Research (IGCAR) for his whole hearted support, encouragement, guidance and patience during the research work. Without his untiring mentorship, constant inspiration, valuable discussions and suggestions, this thesis wouldn't have been possible. I appreciate him for critically going through the draft of my thesis and research papers.

I express my sincere gratitude to **Dr. Anish Kumar**, Head, Ultrasonic Microstructural Section (UMS), MMG, IGCAR for his valuable advice in my work, spending his precious time to read and correct my thesis and research papers. He patiently provided the vision, encouragement and advice necessary for me to proceed through the entire research program.

I express my sincere gratitude to **Dr. B. P. C. Rao**, Head, Non Destructive Evaluation Division (NDED), MMG, IGCAR for his inspiration, encouragement and support during the course of this thesis work.

I am indebted to **Dr. A. Joseph,** Head In-Service Inspection and Residual Stress Measurements Section (ISI&RSM), MMG, IGCAR for his constant encouragement and support in all respects.

I am thankful to **Dr. C. Babu Rao,** Raja Ramanna Fellow (RRF), IGCAR for many useful discussions and his support during the course of thesis work. I would like to extend my heartfelt thanks to **Dr. C. V. Krishnamurthy,** Associate Professor, Dept. of Physics and **Dr. Krishnan Balasubramanian,** Professor, Dept. of Mechanical Engineering, IIT Madras, Chennai for their unconditional support and giving me permission to utilise some of the software facilities.

My sincere thanks to my Doctoral Committee Chairman **Dr. M Sai Baba,** and members **Dr. A. K. Bhaduri** and **Dr. B. K. Panigrahi** for regularly evaluating the progress of the research work and giving many useful suggestions.

I am grateful to former and present Directors, IGCAR, **Dr. Baldev Raj, Shri S. C. Chetal** and **Dr. P. R. Vasudeva Rao** for providing me permission and encouragement to purse this work.

I take this opportunity to specially thank **Shri S. Mahadevan** for giving many useful suggestions throughout my research work. His support and friendship have been invaluable both on the academic front and at a personal level. I would like to thank **Shri S. T. Arasu, Shri M. M. Narayanan, Shri N. Mariyappa, Dr. K. V. Rajkumar, Shri S. Shuaib Ahmed** and **Shri A. Viswanath** for various useful discussions. I am thankful to **Smt. T. Nivedha** for helping me to cross check the order of references. I am grateful to **Dr. B. K. Choudhary** for going through the draft of the thesis and his valuable suggestions. I thank **Smt. Deepshikha Sharma** for helping me in editing work of my thesis. I sincerely acknowledge the support received from my friend **Bhuwan Chandra Sati** during tough times. I would also like to thank all the colleagues of NDE Division for their help and support.

I express my profound gratitude to my grandparents, my father **Shri Umashanker Sharma** and my mother **Smt. Sarla Sharma**, my uncles, parents-in-laws, my brother, my sister and other family members for their personal support and encouragement.

Finally, I express my sincere thankfulness to my wife **Deepshikha** and son **Deepankar** for their love, patience and sacrifices to make this achievement a reality.

Above all, I owe it all to almighty **God** for granting me wisdom, health and strength to undertake this research work and enabling me to take it to completion.

Contents

Abstract xi
List of Figures xiv
List of Tables xxii
Symbols and Abbreviations xxiv

Chapter 1. Introduction 1
1.1 Introduction 1
1.2 Microstructural characterisation 2
1.3 Defect characterisation 3
1.4 The scope of investigation 7
1.5 Outline of thesis 8
Chapter 2. Review of Literature and Motivation 11
2.1 Introduction 11
2.2 Ultrasonic attenuation in polycrystalline materials 11
2.2.1 Scattering of ultrasonic waves 12
2.2.2 Absorption of ultrasonic waves 14
2.3 Grain size characterisation 15
2.3.1 Spectral analysis 18
2.3.2 Homomorphic processing 20
2.4 Defect characterisation 22
2.4.1 Frequency domain analysis techniques 23
2.4.1.1 Split spectrum processing 24
2.4.1.2 Other techniques 27
2.4.2 Time-frequency domain analysis techniques 28
2.4.2.1 Wigner – Ville distribution 28
2.4.2.2 Short time Fourier transform 29
2.4.2.3 Wavelet transform 32
2.4.2.4 Hilbert–Huang processing 42
2.5 Imaging of defects in highly attenuating media 47
2.6 Appraisal of the problem 49

Chapter 3. Ultrasonic Measurements 51
3.1 Introduction 51
3.2 Experimental setup 51
3.3 Software for selection of window length for STFT 53
3.3.1 Peak frequency estimation using STFT 54
3.4 Software for estimating pseudo peak frequencies of CWT 54
3.5 Model based peak frequency estimation 57
3.6 Algorithm for C-scan imaging using CWT approach 57
Chapter 4. Time-Frequency based Analysis for Understanding Frequency Dependent Attenuation and Quantitative Evaluation of Grain Size 60
4.1 Introduction 60
4.2 Experimental 61
4.2.1 Specimen preparation 61
4.2.2 Microstructural characterization 61
4.3 Results and discussion 63
4.3.1 Short time Fourier transform 63
4.3.1.1 Optimisation of window length for STFT analysis 63
4.3.1.2 Frequency dependent attenuation analysis using STFT 67
4.3.1.3 Quantitative evaluation of grain size using longitudinal waves 74
4.3.1.4 Quantitative evaluation of grain size using shear waves 77
4.3.1.5 Conclusions from STFT analysis 80
4.3.2 Continuous wavelet transform 82
4.3.2.1 Optimization of mother wavelet 82
4.3.2.2 The Pseudo frequency approach 83
4.3.2.3 Comparison of STFT spectrogram and CWT coefficient plot 86
4.3.2.4 Correlation between SNR and pseudo frequency 87
4.3.2.5 Quantitative grain size evaluation 90
4.3.2.6 Comparative analysis between STFT and CWT based approaches 92
4.3.2.7 Conclusions from CWT studies 94
Chapter 5. Continuous Wavelet Transform based C-Scan Imaging of Defects 95
5.1 Introduction 95
5.2 Experimental 96
5.2.1 Specimen preparation 96

5.3 Results and discussion 100
5.3.1 Conventional C-scan imaging 100
5.3.2 Optimisation of ultrasonic frequency 101
5.3.3 Evaluation of frequency shifts using STFT 103
5.3.3.1 Specimen 1 (360 µm grain size) 104
5.3.3.2 Specimens 2 and 3 (200 µm grain size) 105
5.3.4 Model based evaluation of frequency shifts 108
5.3.5 Comparison of experimental and model based peak frequencies 111
5.3.6 Wavelet based C-scan imaging 112
5.3.6.1 Specimen 2 (Flat bottom holes) 114
5.3.6.2 Specimen 3 (Side drilled holes) 118
5.3.6.3 Qualitative evaluation of defect detection sensitivity 124
5.4 Conclusions 126
Chapter 6. Ensemble Empirical Mode Decomposition based Adaptive Processing of Ultrasonic Signals 127
6.1 Introduction 127
6.2 Experimental 129
6.2.1 Specimen preparation 129
6.3 Results and discussion 129
6.3.1 Comparison between EMD and EEMD analysis 129
6.3.1.1 Effect of mode mixing 130
6.3.2 Suitability of EEMD processing for signal reconstruction 133
6.3.3 Adaptive reconstruction of signals using EEMD 134
6.3.4 EEMD processing for detection of defects 138
6.4 Adaptive defect detection in a B-scan 142
6.5 Conclusions 145
Chapter 7. Summary and Future Works 146
7.1 Summary 146
7.2 Future works 149
References 150

Abstract

The primary aim of the ultrasonic non-destructive investigations carried out in this thesis is to develop various time-frequency based signal processing methodologies to analyse ultrasonic signals for enhanced microstructural characterisation and imaging of defects in type 316 austenitic stainless steel. The time-frequency (TF) based signal processing techniques including short time Fourier transform (STFT), continuous wavelet transform (CWT) and Ensemble Empirical Mode Decomposition (EEMD) have been used. Specific software have been developed in LabVIEW and Matlab programming systems for accurate estimation of ultrasonic spectral parameters.

Specimens with a range of grain sizes (30-210 μm) were made by suitable heat treatments to the AISI type 316 austenitic stainless steel. The ultrasonic signals acquired from these specimens were analysed by time-frequency methods for microstructural characterisation. The understanding of frequency dependent attenuation is improved by using STFT and CWT analysis of these signals. The spectral information of the back-wall and backscatter could be obtained simultaneously by these approaches. Reliable peak frequency information could be obtained for back-wall echoes, even in the case of poor signal to noise ratio (SNR). The spectral information from back-wall echoes has been utilised for grain size characterisation. The STFT and CWT based time-frequency analysis techniques are established as useful tools for enhanced materials characterisation applications.

The application of time-frequency analysis techniques was extended to defect detection and imaging in coarse grain austenitic stainless steel. Specially designed coarse grained specimens with flat bottom holes (FBH) and side drilled holes (SDH) were made from suitably heat treated AISI type 316 stainless steel samples. The shift in the peak frequency of ultrasonic waves with propagation distance is measured by STFT approach. The ultrasonic signals obtained from artificial defects made at different depths were used for this purpose. The simultaneous availability of time and frequency information in STFT is utilised effectively. The systematic variation in the peak frequency with the propagation distance has been validated by theoretical approach. The spectral information obtained at defect locations by STFT showed a definite range of frequencies for the defects at different depths. This information has been utilised to propose CWT based scheme for imaging of defects.

The wavelet based techniques require optimisation of mother wavelets and optimum selection of scales to reconstruct the signal. However, the recently proposed EEMD processing has the distinct advantage that it does not rely on a set of predefined basis functions and derives the basis functions from the signal itself, known as Intrinsic Mode Functions (IMFs). A novel adaptive signal processing methodology is proposed in this study for enhancing the signal to noise ratio of ultrasonic signals obtained from austenitic stainless steels of different grain sizes. The proposed method comprises of employing the signal minimisation algorithm to the IMFs obtained by Ensemble Empirical Mode decomposition (EEMD) of ultrasonic signals. It is possible to adaptively reconstruct the signal with enhanced signal to noise ratio based on a selected range of IMFs for a particular probe frequency. This proposed method works well for the range of grain sizes (30-210 μm) used in this study.

The time-frequency based approaches used in the study provided better understanding of frequency dependent scattering in austenitic stainless steel. The

limits imposed by conventional ultrasonic methods for grain size evaluation could also be extended by the proposed approaches. The shift in the peak frequency with propagation distances observed by the experimental results and mathematical model, paved the path for development of a single wavelet scale based CWT approach. This approach was used successfully for imaging of defects at various depths in thick coarse grain austenitic stainless specimens. The novel adaptive methodology proposed by employing signal minimisation algorithm on selected IMFs showed better than 15 dB enhancement in the SNR of the ultrasonic signals, can be used as a signal analysis approach for automatic defection of defects with improved sensitivity.

List of Figures

Fig. 2.1. Influence of grain size on (a) ultrasonic first back-wall echo and (b) its autopower spectrum in AISI type 316 stainless steel [47]. 19

Fig. 2.2. Variation in peak frequency (PF) and full width at half maximum (FWHM) of the autopower spectrum of the first back-wall echo with grain sizes (d) and ($d^{-1/2}$) [47]. 20

Fig. 2.3. Homomorphic wavelet recovery system (a) system sketch, (b) backscattered grain signal, (c) magnitude spectrum of grain signal, (d) log magnitude of the signal, (e) magnitude cepstrum of signal and (f) recovered log magnitude spectrum of ultrasonic wavelet [49].....................21

Fig. 2.4. Schematic of processing steps being carried out for enhancement of SNR using split spectrum processing (SSP) technique [9]...........................26

Fig. 2.5. The comparison of improvement in SNR of an ultrasonic signal from a flat bottom hole by applying different recombination algorithms to the SSP processed signal (a) squared wideband echo signal (unprocessed), (b) average of decomposed squared signals, (c) square of the decomposed averaged signals and (d) minimisation of decomposed squared signals [6]. 26

Fig. 2.6. A synthetic trace and its time-frequency spectra generated with Wigner-Ville distribution. The cross term interference can be observed in the WVD spectra between the echo locations at time scales of 200 and 400 ms [65]. 29

Fig. 2.7. Schematic of STFT processing indicating the importance of the window length determination. The time and frequency resolutions are fixed for entire analysis depending on the window length chosen. 31

Fig. 2.8. Schematic of CWT processing indicating the inherent flexible window analysis for processing of signal. The time and frequency resolution changes depending on the scale of analysis..34

Fig. 2.9. The processing of ultrasonic signal for different wavelet scales and application of minimisation algorithm to the CWT processed signal at selected scales [75]. 35

Fig. 2.10. Schematic of dyadic filtering scheme being used in the DWT based processing of signals. 37
Fig. 2.11. The improvement of SNR with wavelet processing of signals (a) original ultrasonic signal, (b) whiter noise added and (c) output of wavelet transform [7] 39
Fig. 2.12. Typical plots of original signals and processed signals used to identify flaws in pipelines: (a) original ultrasonic signal with crack near the inner wall, (b) processed result of (a), (c) original signal with a crack near the outer wall and (d) processed results of (c) [81]. 39
Fig. 2.13. The performance of wavelet filtering when spectral content of noise and signal are similar (a) typical frequency band of grain noise and frequency response of ultrasonic transducer, (b) time domain signal of ultrasonic signal merged in noise and (c) ultrasonic echo recovered with improved SNR by wavelet filtering (db6 with hard thresholding) [82] 41
Fig. 2.14. Sliced time–frequency spectrum at a particular frequency based on (a) EMD and (b) EEMD processing of a seismic record [18]. 47
Fig. 3.1. Schematic of ultrasonic measurement set-up used for data acquisition. 52
Fig. 3.2. Photograph of the experimental set-up. 53
Fig. 3.3. Front panel of LabVIEW program developed for optimization of window length. 55
Fig. 3.4. Front panel of the LabVIEW software developed for calculating SNR of ultrasonic signal by considering the first three back-wall echoes. 56
Fig. 3.5. Algorithm used to perform wavelet based C-scan imaging of defects in thick coarse grain austenitic stainless steel specimens. 58
Fig. 4.1. Photomicrographs of the austenitic stainless steel specimens with different grain sizes (a) 30 μm, (b) 78 μm and (c) 210 μm. 62
Fig. 4.2. Ultrasonic signal acquired from top surface (water - specimen interface) of 30 μm grain size specimen in immersion mode 64
Fig. 4.3. The amplitude spectrum of the reference signal evaluated by FFT (peak frequency ~15.9 MHz and -3 dB bandwidth ~4.13 MHz). 65

Fig. 4.4. Typical variation in the peak frequency with increase in window length from 64 to 1280 data points (0.12 μs to 2.5 μs) calculated using STFT of the reference signal. The frequency resolution increases with increase in the window length which can be clearly observed by better localisation of peak frequency and decrease in the bandwidth of the processed signal. 66

Fig. 4.5. Effect of time window size for generating spectrogram on the measured peak frequency and -3 dB bandwidth. Dotted lines show peak frequency and -3 dB bandwidth obtained by FFT. (The results are shown for the top surface echo of specimen with 30 μm grain size, for which the centre frequency and -3 dB bandwidth were measured to be 15.9 MHz and 4.13 MHz, respectively). 66

Fig. 4.6. (a) Time domain ultrasonic signal from the specimen of 121 μm grain size (obtained by 25 MHz unfocussed transducer), (b) its spectrogram and (c) frequency content of first back-wall echo peak location by STFT (typical at cursor location, shown in red colour). 69

Fig. 4.7. The spectral content of the first three back wall echoes obtained by STFT processing of ultrasonic A-scan signal obtained from 121 μm grain size specimen. 69

Fig. 4.8. (a) Ultrasonic time domain signal obtained from a 210 μm grain size specimen, (b) its spectrogram and (c) frequency content of first back-wall at cursor location. 71

Fig. 4.9. Variation in the peak frequencies of front surface (FS) reflection, first back-wall (FBW), second back-wall (SBW) and third back-wall (TBW) echoes and spectral distribution of the backscatter estimated using STFT for different grain size specimens is illustrated. 72

Fig. 4.10. Peak frequencies of first, second and third back-wall echo locations obtained by STFT processing of ultrasonic signals showed a linear correlation with the grain size parameter ($d^{-1/2}$) 76

Fig 4.11. Experimental set up used to acquire corner reflection using shear wave 78

Fig. 4.12. Typical angle beam B-scan image showing corner reflections at multiple skip distances and (b) radio frequency signal at the half skip corner reflection from a specimen of 106 μm grain size. 79

Fig. 4.13. Correlation between peak frequency of shear wave signal from corner reflection and grain size parameter. 80
Fig. 4.14. The SNR of ultrasonic signal obtained from 210 µm grain size specimen initially increases with increasing wavelet scales and decreases after reaching maximum. The improvement of SNR was monitored by using different mother wavelets. 83
Fig. 4.15. (a) A-scan signal from the top surface of specimen with 138 µm grain size, (b) CWT coefficient plot of the A-scan signal using 'Morlet' wavelet, (c) change in the peak amplitude of coefficients with scale and (d) comparison of amplitude spectra of A-scan signal and its wavelet coefficient at scale 21. 85
Fig. 4.16. The change in the pseudo frequencies with scales of 'Morlet' wavelet is presented, where the central frequency of 'Morlet' wavelet is 0.8125 Hz [96], and sampling rate of signal is 500 MS/s. 86
Fig. 4.17. (a) A-scan signal from the 210 µm grain size specimen of 10 mm thickness, (b) STFT spectrogram of the signal and (c) wavelet coefficient plot of the signal. The locations of first three back-wall echoes are highlighted with dotted boxes. 87
Fig. 4.18. The improvement in SNR with wavelet scales by considering first back-wall echo (FBWE), second back-wall echo (SBWE), third back-wall echo (TBWE) and entire signal for 210 µm grain size specimen. The ultrasonic signal was processed by 'Morlet' wavelet. 89
Fig. 4.19. The RF signal obtained from a 210 µm grain size specimen and its wavelet coefficients at different scales (25, 50, 86, 125 and 143 and 175). Scales 86, 125 and 143 correspond to the maximum SNR for the FBWE, SBWE and TBWE respectively. 89
Fig. 4.20. Variations in CWT pseudo frequencies with grain size parameter. 91
Fig. 4.21. The correlation between STFT peak frequencies and CWT pseudo frequencies with grain size parameter ($d^{-1/2}$). 92
Fig. 5.1. Photomicrographs obtained by metallography for (a) Specimen 1-360 µm, (b) Specimen 2- 200 µm and (c) Specimen 3 -200 µm. 97

Fig. 5.2. Schematic of Specimen 1 (360 μm grain size) and Specimen 2 (200 μm grain size) used in this study for evaluation of peak frequency shift of ultrasonic waves with propagation distance. The defect identification numbers are also given below the defect dimensions. 98

Fig. 5.3. Schematic of Specimen 3 with side drilled holes (SDH) made at different depths (fine dotted lines, blue colour) as well as in same plane (coarse dotted lines, red colour) in inclined manner so the distance between two holes decreases towards centre of the specimen. 99

Fig. 5.4. (a) The ultrasonic signal obtained from water-specimen surface using 5 MHz transducer and (b) its amplitude spectrum. 102

Fig. 5.5. Ultrasonic C-scans obtained by conventional time domain method for Specimen 2 (a) amplitude based and (b) time of flight (TOF) based, using 5 MHz immersion transducer......102

Fig. 5.6. Ultrasonic reflection from a 3 mm dia. FBH at 25 mm depth in Specimen 2 using 5 MHz transducer (shown by dotted rectangle, red colour) and (b) its STFT spectrogram. The back-wall echo is observed at the end of the signal (shown by solid rectangle, red colour). 103

Fig. 5.7. (a) Time domain signal from 6 mm diameter FBH at 25 mm depth in Specimen 1, (b) its spectrogram, where the defect signal location is indicated by dotted circle and back-wall echo location is indicated by solid circle and (c) frequency content at the defect location. 106

Fig. 5.8. (a) Time domain signal from 3 mm diameter FBH at 30 mm depth in Specimen 2, (b) its spectrogram, where defect signal location is indicated by dotted circle and back-wall echo location is indicated by solid circle and (c) frequency content at the defect location. 106

Fig. 5.9. (a) Time domain signal from 3 mm diameter SDH at 30 mm depth in Specimen 3, (b) its spectrogram, where defect signal location is indicated by dotted circle and back-wall echo location is indicated by solid circle and (c) frequency content at the defect location. 107

Fig. 5.10. Variation in peak frequency values of ultrasonic waves with propagation distance. The peak frequency values at different depths were evaluated by analysing ultrasonic echoes from artificial defects at different depths using STFT. 112

Fig. 5.11. C-scan images generated by unprocessed data from Specimen 2 (a) amplitude and (b) time of flight based C-scans. 116

Fig. 5.12. C-scan images generated by CWT processed data at optimum scale from Specimen 2 (a) amplitude and (b) time of flight based C-scan, arrow indicates deepest defect at 45 mm from scanning surface in the Specimen 2. 116

Fig. 5.13. 3D representation of the time of flight data shown in Fig. 5.12 (b), the location of the defects from the top surface in terms of depth is shown in this graph. The reflection from edge of the specimen is indicated by an arrow in the figure. 117

Fig. 5.14. C-scan images generated by unprocessed data from Specimen 2 (a) amplitude and (b) time of flight based C-scans. Only back-wall echo region was used for gating. 117

Fig. 5.15. C-scan images generated by CWT processed data at optimum scale from Specimen 2 (a) amplitude and (b) time of flight based C-scans. Only back-wall echo region was used for gating. 118

Fig. 5.16. C-scan images generated by unprocessed data from Specimen 3 (side 1) (a) amplitude and (b) time of flight based C-scans. 121

Fig. 5.17. C-scan images generated by CWT processed data at optimum scale from Specimen 3 (side 1) (a) amplitude and (b) time of flight based C - scans. 121

Fig. 5.18. C-scan images generated by unprocessed data from Specimen 3 (side 2) (a) amplitude and (b) time of flight based C-scans. 122

Fig. 5.19. C-scan images generated by CWT processed data at optimum scale from Specimen 3 (side 2) (a) amplitude and (b) time of flight based C-scans. 122

Fig. 5.20. 3D representation of the time of flight data shown in Fig. 5.17 (b), the locations of the side drilled holes from top surface (side 1) of specimen are given in terms of depth. 123

Fig. 5.21. A 3D representation of the time of flight data shown in Fig. 5.19 (b), the location of the side drilled holes from top surface (side 2) of specimen are given in terms of depth. 123

Fig. 6.1. The comparison of IMFs (im1-im7) obtained by (a) EMD processing, the effect of mode mixing in different IMFs is marked by solid circles and (b) EEMD processing, in comparison to EMD processing the minimal mode mixing is present and marked by dotted circles. The multiple ultrasonic back-wall echoes obtained from 78 µm grain size specimen are selected for the comparison. 132

Fig. 6.2. The Hilbert spectra, for a representative IMF (IMF-5) obtained from (a) EMD and (b) EEMD processing of ultrasonic signals obtained from 78 µm grain size specimen. It can be observed that the mode mixing is significantly reduced by EEMD processing. 132

Fig. 6.3. (a) Typical ultrasonic A-scan signal obtained from 30 µm grain size specimen and its IMFs (im1-im7) obtained by EEMD processing and (b) amplitude spectrum of the signal S(f) and corresponding IMFs (IM(f)-IM(f)7). The ultrasonic signal was acquired with 10 MHz transducer and 100 MS/s sampling rate...134

Fig. 6.4. The IMFs (im1-im7) obtained by EEMD processing of ultrasonic signals obtained from (a) 30 µm and (b) 210 µm grain size specimen. Typical three multiple back-wall echoes are selected for processing. It can be inferred that typical IMFs (3-5) can be used to reconstruct the signal irrespective of the vast difference in the grain size..........................136

Fig. 6.5. Comparison of IMFs (im1-im7) obtained by EEMD processing for the ultrasonic signals obtained with (a) 10 MHz probe frequency and 100 MS/s sampling rate, (b) 10 MHz probe frequency and 500 MS/s sampling rate and (c) 25 MHz probe frequency and 500 MS/s sampling rate for 210 µm grain size specimen. The rectangular boxes represent the range of IMFs containing meaningful information of the signal...137

Fig. 6.6. (a-b) shows the ultrasonic signals obtained from 30 and 210 μm grain size specimens, the data range is selected including first three back-wall echoes, (c-d) The reconstruction of the ultrasonic signals by selected IMFs (3-5) obtained by EEMD processing and (e-f) The reconstruction of ultrasonic signals obtained by application of minimisation on selected IMFs (3-5) obtained by EEMD processing. The zoomed part of third back-wall echo is shown in the inset. 138

Fig. 6.7. The IMFs (im1-im7) obtained by EEMD processing of ultrasonic signals obtained from flat bottom holes (FBH) at (a) 25 mm, (b) 30 mm and (c) 35 mm distance from scanning surface in Specimen 2. The data range is selected to include back-wall echo for the processing also. 140

Fig. 6.8. (a-c) shows the ultrasonic signals obtained from flat bottom holes (FBH) at (a) 25 mm (b) 30 mm and (c) 35 mm distance from scanning surface in Specimen 2, (d-f) The reconstruction of the ultrasonic signals by selected IMFs (3-5) sum obtained by EEMD processing and (g-i) The reconstruction of ultrasonic signals obtained by application of minimisation on selected IMFs (3-5) obtained by EEMD processing. The defect and the back-wall echoes are indicated with arrows. 141

Fig. 6.9. The ultrasonic B-scan was acquired by automatic scanning covering the three flat bottom holes including 9 (3 mm dia., 15mm deep), 13 (6 mm dia., 25 mm deep) and 3 (6 mm dia., 35 mm deep). 143

Fig. 6.10. The original B-scan acquired. The ultrasonic frequency used for scanning was 10 MHz and data were acquired at 100 MS/s sampling rate. 144

Fig. 6.11. The B-scan reconstructed by sum of IMFs (3-5) obtained by EEMD processing. 144

Fig. 6.12. The B-scan reconstructed by applying minimisation algorithm to the IMFs (3-5) obtained by EEMD processing. 145

List of Tables

Table 4.1. Chemical composition (wt%) of AISI type 316 austenitic stainless steel 61

Table 4.2. Details of the heat treatments given to AISI type 316 austenitic stainless steel specimens and the corresponding grain sizes obtained by metallographic examinations are presented. 62

Table 4.3. Details of ultrasonic peak frequencies obtained by STFT at the front surface (FS), first back-wall (FBW), second back-wall (SBW) and third back-wall (TBW) echo signals in different grain size specimens. 71

Table 4.4. Details of pseudo frequencies calculated for the scale values corresponding to optimum SNR by considering three back-wall echoes. 91

Table 4.5. Comparative analysis of STFT and CWT based methods in terms of microstructural characterization of austenitic stainless steels. 93

Table 5.1. Details of the heat treatments given to AISI Type 316 stainless steel specimens and grain size obtained, these specimens were used to fabricate artificial defects. 97

Table 5.2. Dimensional details of flat bottom holes (FBH) fabricated in the Specimen 1 (360 μm grain size) and Specimen 2 (200 μm grain size), the FBH were made by electric discharge machining (EDM) process. 98

Table 5.3. The location of the centre of side drill holes (SDHs) fabricated in Specimen 3 is presented. All the holes were made of 3 mm diameter. Since both the sides are available for scanning, the depth of centre of SDHs from both surfaces are given. 100

Table 5.4. The peak frequency values obtained by STFT for flat bottom holes (FBHs) at different depths in Specimen 2. 107

Table 5.5. The peak frequency values obtained by STFT for side drilled holes (SDHs) at different depths in Specimen 3. 108

Table 5.6. Qualitative analysis for defect detection capability of conventional and continuous wavelet transform based approaches in Specimen 2. 125

Table 5.7. Qualitative analysis for defect detection capability of conventional and continuous wavelet transform based approaches in Specimen 3. 125

Table 6.1. Comparison of EEMD with STFT and CWT approaches 128
Table 6.2. Signal to noise ratio improvement in ultrasonic signals obtained from artificially made flat bottom holes in 200 µm grain size, 50 mm thickness austenitic stainless steel specimen (Specimen 2)........................141

Symbols and abbreviations

Symbols		Abbreviations	
α	Attenuation coefficient	**BWE**	Back wall echo
f_0	Peak frequency	**CGASS**	Coarse grain austenitic stainless steel
f_c	Downshifted peak frequency	**CWT**	Continuous wavelet transform
dB	Decibel	**DWT**	Discrete wavelet transform
ρ	Density	**EEMD**	Ensemble empirical mode decomposition
f	Frequency of the ultrasonic wave	**EMD**	Empirical mode decomposition
d	Grain size	**FBH**	Flat bottom hole
ω	Instantaneous frequency	**FBWE**	First back-wall echo
K	Kelvin	**FFT**	Fast Fourier transform
MHz	Megahertz	**FSE**	Front surface echo
µm	Micrometer	**FWHM**	Full width half maximum
θ	Phase	**HHT**	Hilbert-Huang transform
F_s	Pseudo frequency	**IMF**	Intrinsic mode function
S	Scattering coefficient	**JTFA**	Joint time-frequency analysis
C_{ij}	Single crystal elastic coefficients	**NDE**	Nondestructive evaluation
V_L	Ultrasonic longitudinal wave velocity	**RF**	Radio frequency
V_T	Ultrasonic shear wave velocity	**SBWE**	Second back-wall echo
λ	Wavelength of the ultrasonic wave	**SD**	Standard deviation
s	Wavelet scale	**SDH**	Side drilled hole
		SNR	Signal to noise ratio
		SSP	Split spectrum processing
		STFT	Short time Fourier transform
		SWT	Stationary wavelet transform
		TBWE	Third back-wall echo
		TF	Time-frequency
		TOF	Time of flight
		UA	Ultrasonic attenuation
		WQ	Water quench
		WT	Wavelet transform
		WVD	Wigner-Ville distribution
		YS	Yield strength

Chapter 1. Introduction

1.1 Introduction

Nondestructive evaluation (NDE) techniques are commonly employed for the detection and characterization of flaws in components. Apart from flaw characteristics, another parameter which is equally important to assess the structural integrity of engineering components is the material property. NDE techniques offer several advantages over the conventional coupon-based techniques for evaluation of material properties. There are different NDE methods available for structural integrity evaluation of components and structures. Each NDE method is based on a particular physical principle and has its own field of application, advantages and disadvantages. Among various NDE techniques, ultrasonic testing is the most versatile NDE method which is applicable to both metallic and non-metallic materials [1]. By this method, surface and internal discontinuities as well as the microstructure can be evaluated. The volumetric inspection capability with one side access requirement makes the ultrasonic technique unique among other NDE techniques [1].

Ultrasonic waves propagate through materials and are reflected/scattered by inhomogeneities or discontinuities present in the material and grain structure. The measurement of transmitted and reflected ultrasonic waves in a material can be correlated with structural integrity, which is a function of material inhomogeneities and defect parameters. Besides, ultrasonic measurements provide quantitative information about grain size, thickness of the component, size and orientation of the detected discontinuity. Ultrasonic evaluation of these parameters aids in evaluating structural integrity. The two different areas where the scope of ultrasonic testing is widely explored are (i) microstructural characterisation and (ii) defect detection and imaging. The ultrasonic examination of coarse grained material has always been a challenge due to presence of grain noise. The spectral content of the ultrasonic waves changes with propagation distance in high scattering materials due to their non-stationary nature in such media. The non-stationary nature of the ultrasonic signals obtained from coarse grain materials limits the use of conventional Fourier transform (FT) based methods for reliable measurements. Hence, the primary aim of this study is to develop suitable time-frequency (TF) signal processing algorithms for application on ultrasonic signals obtained from coarse grain austenitic stainless steel (CGASS), for enhanced microstructural and defect characterisation. In this study, comparative advantages and limitations of different time-frequency approaches used for grain size evaluation, defect detection and imaging are discussed in detail.

1.2 Microstructural characterisation

The propagation of ultrasonic waves is influenced by the microstructure of a material through which it propagates. The propagating ultrasonic waves will be attenuated depending on the properties of the medium. Ultrasonic attenuation is governed by absorption and scattering. The frequency dependent scattering of ultrasonic waves by coarse grain materials is a key ultrasonic parameter in estimating the grain size [2]. The high frequency content of the beam is scattered more compared to the low frequency. Studies have been reported to correlate the peak frequency shifts of backscatter and back-wall echoes with grain sizes, by Fourier transform based approaches. However, the FT based ultrasonic measurements are limited to relatively low attenuating materials with reasonably good signal to noise ratio (SNR). For this purpose, there is a strong need for time-varying (non-stationary) ultrasonic signals obtained from coarse grain materials to be analysed by approaches other than FT based methods. This necessitates the use of TF analysis methods for microstructural characterisation (grain size) which has not been attempted so far.

Short time Fourier transform (STFT) is a widely used joint time-frequency analysis (JTFA) tool. The STFT is able to retrieve both frequency and time information simultaneously from a signal [3]. The STFT calculates the Fourier transform of a windowed part of the original signal, where the window shifts along the time axis. The time and frequency resolution is governed by the Heisenberg inequality [3]. Hence, there is a need for suitable selection of window length to obtain optimum time and frequency resolution. Even with the optimum window, the time and frequency resolution is fixed for entire analysis.

In order to overcome the fixed resolution problem, a more flexible TF approach known as continuous wavelet transform (CWT) has been used, which can perform multiresolution analysis. CWT is defined in terms of basis functions obtained by compression/dilation and shifting of mother wavelet. The property of self-adjusting the analysis windows, according to the signal frequency makes CWT suitable for the analysis of transient non-stationary signals [4]. Comparative analysis has been carried out between the microstructural characterisation capabilities of STFT and CWT.

1.3 Defect characterisation

The detection of defects in CGASS is a challenging task. The amplitudes of defect echoes may be comparable to that of the microstructural scattering noise in CGASS. Ultrasonic characterization of defects in this medium requires enhancement of signal to noise ratio (SNR) for identification of defects. The analysis of ultrasonic signals by spectral analysis methods showed a downward shift in maximum energy frequency of ultrasonic echoes at defect locations in CGASS [5]. However, no systematic experimental and theoretical studies are reported to evaluate the frequency shifts in coarse grain medium. In view of this, there is a need to carry out a systematic investigation to understand the frequency shifts being observed in high scattering materials. Different signal processing approaches like split spectrum processing (SSP) [6] and wavelet transform (WT) [7] have been proposed for enhancement of SNR in highly scattering coarse grain media.

The improvement in SNR by split spectrum processing is achieved by partitioning a wide band received spectrum to obtain frequency shifted bands. These bands are further processed using different recombination algorithms such as signal minimisation and polarity thresholding to improve the signal [8]. Signal minimisation algorithm showed superior flaw detection capabilities compared to other recombination algorithms. However, the capabilities of split spectrum processing for enhancement of SNR are critically dependent on the selection of the processing parameters such as location of the signal in the spectrum, number of filters, type of filters and transducer bandwidth and its useful range [9].

Wavelet transform based approaches are unique due to their time-frequency localisation capabilities. Different wavelet approaches such as continuous wavelet transform [10], discrete wavelet transform (DWT) [7] and time-invariant wavelet approaches such as undecimated wavelet transform (UWT) [11] are being used for SNR enhancement and detection of defects in noisy environment. Wavelets are an attempt to overcome the shortcoming of Fourier analysis, which cannot provide time information. Wavelets provide a meaningful way to do time-frequency analysis.

Wavelet transform decomposes a signal into a set of frequency bands (popularly known as scales) by projecting the signal onto an element of a set of predefined basis functions. The projection of signal onto different scales is equivalent to band pass filtering with a bank of filters.

Different signal processing approaches have been reported in literature to process ultrasonic A-scan signals obtained from high scattering and attenuating media to improve the SNR. However, very few studies are reported to image the defects by utilising signal processing methods in highly attenuating materials [12, 13, 14]. These studies have utilised the back-wall echo location for gating and imaging purposes. This may provide information related to the presence of defects in material but are limited with respect to their position. Hence, there is a need for an improved approach which can provide reliable information about the defects with their positional information.

The amplitude and the time of flight are the ultrasonic parameters being used in conventional time domain based C-scan imaging methods. However, these parameters are not suitable for imaging purposes when the echoes are merged in backscatter noise. In frequency domain, the peak frequency information cannot be correlated with target due to multiple peaks in the frequency spectra of the gated regions and absence of time information. This necessitates the use of suitable TF parameter, which can be used for imaging of defects in CGASS. The CWT is a simple time-frequency analysis technique which provides the flexibility of signal analysis based on the wavelet scales. The wavelet based approaches are found to be very useful in improving SNR and time-frequency localisation, but they are limited with respect to the selection of mother wavelets, selection of optimum scales and decomposition levels. Therefore, it is necessary to utilise new approaches which are adaptive in nature.

Recently, a new signal processing technique known as Empirical Mode Decomposition (EMD) is proposed for processing non-linear and non-stationary signals [15]. Unlike wavelet based techniques, EMD has the distinct advantage that it does not rely on a set of predefined basis functions. EMD derives the basis functions known as Intrinsic Mode Functions (IMFs) adaptively from the data set itself through a shifting process. A few studies have reported the use of EMD processing of ultrasonic signals obtained from coarse grain materials, where sums of selected IMFs have been used for reconstruction of signals with enhanced SNR [16]. This method is, however, prone to mode mixing, especially when the noise is present intermittently. The mode mixing refers to the existence of same time scale in different IMFs. The mode mixing effect in EMD is significantly reduced by a modified noise assisted data analysis method known as Ensemble Empirical Mode Decomposition (EEMD) method [17]. EEMD has been widely used for geophysical purposes [18]. However, the usefulness of this method has not been explored for processing of ultrasonic signals. The frequency content of the IMFs obtained by EEMD processing decreases with increasing order of IMFs and is achieved adaptively. However, the frequency content of the neighboring IMFs can be overlapped, and shows minimal mode mixing. An IMF represents a simple oscillatory mode of variable amplitude and frequency related to the processed signal, and usually has individual physical meaning.

1.4 The scope of investigation

The scope of this study involves the application of time-frequency analysis techniques on ultrasonic signals for evaluation of grain sizes to improve the limits imposed by the conventional methods. Further, these methods are also employed to develop better understanding of frequency dependent attenuation in high scattering media. Secondly, it is also essential to develop time-frequency methodologies for improved defect detection and imaging by understanding the frequency shifts of ultrasonic waves. Further, new methodologies are explored for adaptive detection of defects by ultrasonic waves in high scattering coarse grain austenitic stainless steels media.

The work detailed in this thesis has the following aims:

(i) Ultrasonic characterisation of grain size in type 316 austenitic stainless steel and extending the limit of grain size evaluation using time-frequency signal processing techniques as compared to existing ultrasonic NDE approaches.

(ii) Experimental evaluation of changes in the spectral content of ultrasonic signals obtained from artificial reflectors at different depths in coarse grain austenitic stainless steel and its theoretical validation.

(iii) Development of continuous wavelet transform based method for ultrasonic imaging of defects in coarse grain austenitic stainless steel.

(iv) Development of an adaptive approach which can be applied for detection of defect with enhanced signal to noise ratio in specimens with a wide range of grain sizes.

The above goals were achieved through the following approaches:

(i) Understanding the limitations of the existing ultrasonic NDE methodologies for grain size evaluation and defect characterisation by examining various approaches reported in the literature.

(ii) Developing computer algorithm for time-frequency analysis of ultrasonic signals using the STFT and CWT approaches for quantitative evaluation of grain size.

(iii) Developing the experimental and theoretical approaches for evaluating the changes in the spectral content of ultrasonic waves with propagation distance in coarse grain austenitic stainless steel medium.

(iv) Developing the computer algorithms for continuous wavelet transform based C-scan imaging of defects in coarse grain stainless steels based on experimental and theoretical understanding of frequency shifts.

(v) Development of a novel adaptive signal analysis methodology utilising EEMD in conjunction with signal minimisation algorithm for detection of defects in coarse grain austenitic stainless steel specimens.

1.5 Outline of thesis

Chapter 1 covers the need of time-frequency analysis based approach for analysis of ultrasonic signals obtained from coarse grain austenitic stainless steel. The brief details of TF analysis approaches developed for enhanced grain size evaluation, defect detection and imaging are given.

Chapter 2 gives a brief introduction of ultrasonic scattering that occurs in polycrystalline materials and their dependence on material properties. A brief survey of the literature on various frequency and time-frequency based signal processing techniques for enhancement of SNR in ultrasonic signals is covered. The motivation and objectives of the work carried out in the thesis are also given.

Chapter 3 provides details of the experimental set up used for ultrasonic measurements. In addition, the chapter also gives the details of various time-frequency algorithms used in the study for processing of ultrasonic signals obtained from coarse grain stainless steel.

Chapter 4 describes the use of STFT spectrogram for understanding frequency dependent attenuation and evaluation of grain size in austenitic stainless steel. A novel scheme developed for selection of suitable window length to obtain optimum time-frequency resolution from a spectrogram is covered. The spectral content obtained from back-wall and backscatter echo signals of different grain size specimens of austenitic stainless steel using STFT is discussed. In addition, this chapter also presents the details of CWT processing carried out for grain size evaluation. The details of the pseudo frequency parameter established for quantitative evaluation of grain size is given. Finally, a comparative analysis of grain size evaluation using STFT and CWT based approaches is presented.

Chapter 5 deals with understanding the changes in the spectral content of ultrasonic wave with propagation distance in a coarse grain material. The details of determination of peak frequencies from artificial reflectors at different depths in coarse grain specimens using STFT are given. The application of a mathematical model, based on ultrasonic scattering theory, for understanding the ultrasonic frequency shift with wave travel path has been discussed in detail. The experimentally observed frequency shifts are validated with this mathematical model. The selection of optimum wavelet scale for imaging of defects is decided based on experimental and theoretical evaluation of frequency shifts. The procedure for C-scan imaging of defects based on CWT processing is discussed.

Chapter 6 gives the details of adaptive time-frequency analysis methods, based on EMD and EEMD methods. These methods do not require any prior information for processing the signals. The advantages of EEMD over EMD is discussed. The details of the proposed novel EEMD based signal reconstruction methodology with signal minimisation algorithm is discussed. The application of this methodology for adaptive detection of artificial defects at different depths in a coarse grain austenitic stainless steel specimen is presented.

Chapter 7 presents the summary of the research findings and the scope for possible improvement in this direction for further investigations.

Chapter 2. Review of Literature and Motivation

2.1 Introduction

This chapter provides a comprehensive review of the ultrasonic studies carried out by various authors for microstructural characterisation, defect detection and imaging in high scattering coarse grain austenitic stainless steels. The attenuation of ultrasonic wave, which is a key ultrasonic parameter for the analysis of high scattering material is explained briefly. A summary of various signal processing approaches reported in literature for analysis of ultrasonic signals in frequency and time-frequency domains, towards evaluation of grain sizes and detection of defects in highly attenuating medium is presented.

2.2 Ultrasonic attenuation in polycrystalline materials

Acoustic wave loses its energy during the propagation through a material by a variety of processes [19, 20, 21], and this energy loss is known as attenuation. In simple terms, the difference in the amplitudes of the first and the second back-wall echoes gives the total attenuation. For plane waves of small amplitudes, the energy intensity (I) at a distance x from the source of ultrasound is given by

$$I = I_0 \, exp(-\alpha x) \qquad (2.1)$$

where α is total attenuation coefficient and I_0 is the intensity of the incident ultrasonic beam. The total attenuation is understood to be caused by basic processes such as beam spreading (diffraction), scattering and absorption. Beam spreading is primarily a geometrical function, where intensity decreases with the square of distance travelled by a wave [1]. The total attenuation coefficient α may be expressed as $\alpha = \alpha_a + \alpha_s$.

The α_a stands for the losses due to internal friction, i.e. ultrasonic absorption and α_s takes into account losses due to scattering of ultrasonic waves.

The scattering of ultrasonic waves caused by grain structure of the material is a limiting factor for detection of flaws in high scattering medium. The grain noise appears between back-wall echoes due to the continuous scattering of ultrasonic waves. In order to understand the reason for the presence of noise in coarse grain stainless steels, it is essential to understand the basics of ultrasonic attenuation. Ultrasonic attenuation is an important parameter which has been extensively used for microstructural characterisation [22]. Due to high attenuation rates of ultrasonic signals in coarse grained materials, it is difficult to obtain flaw information by conventional methods. A brief description of the ultrasonic attenuation in materials due to scattering and absorption are given in the sections 2.2.1 and 2.2.2.

2.2.1 Scattering of ultrasonic waves

Ultrasonic scattering is caused by the elastic interaction such as reflection at grain boundaries, small cracks and other anomalies [20]. Roderick et al. [23] described the contribution of grain boundary scattering to the ultrasonic attenuation in polycrystalline materials. In the successive investigations, attempts have been made to examine the theoretical aspects of the contribution of grain scattering on ultrasonic attenuation in polycrystalline materials [24] along with experimental verification [25, 26, 27]. However, the well-developed theories exist only for grain boundary scattering from equiaxed grains in isotropic single phase polycrystalline solids.

Scattering is governed by the grain size (*d*), frequency of the wave (*f*) and the elastic anisotropy of the material [21]. Depending on the ratio of the wavelength of the ultrasonic wave (λ) to grain size (*d*), the ultrasonic scattering phenomenon can be classified into three regimes namely,

$$\begin{aligned} \alpha_s &\propto d^3.f^4 \text{ (Rayleigh scattering; when } \lambda > 2\pi d) \\ &\propto d.f^2 \text{ (Stochastic scattering; when } \lambda \leq 2\pi d) \\ &\propto 1/d \text{ (Diffusion scattering; when } \lambda \ll 2\pi d) \end{aligned} \quad (2.2)$$

The practical range of the frequencies of the ultrasonic waves used for microstructural and defect characterisation lies between 0.5 to 50 MHz. In this frequency range, λ lies in the range of 12 mm to 120 μm for ultrasonic longitudinal wave velocity of 6000 m/s. Assuming, the average grain size of the structural materials as 50 μm, the range of λ shows that most of the microstructural characterisation studies fall in the Rayleigh scattering regime. In view of this the attenuation due to grain scattering in the Rayleigh regime is discussed in detail. The attenuation of ultrasonic longitudinal waves due to grain scattering in the Rayleigh regime can be given as

$$\alpha_s = S1.T.f^4 \quad (2.3)$$

where *T* is the grain volume and *S1* is the proportionality constant which is primarily dependent upon the acoustic anisotropy of the grains, density and ultrasonic velocities in the material. For grains with spherical geometry, *T* can be written as

$$T = \frac{1}{6}\pi d^3 \quad (2.4)$$

Substituting the value of *T* in the Eq. 2.3 gives

$$\alpha_s = S.d^3.f^4 \quad (2.5)$$

where *S* (dB/cm (MHz)^4 cm^3) for cubic materials is defined as [2]

$$S = \frac{8\,\pi^4\,C^2}{1125\,\rho^2\,V_L^3}\left(\frac{1}{V_L^5} + \frac{1}{V_T^5}\right) \quad (2.6)$$

where C represent elastic anisotropy, ρ is density, V_L is longitudinal wave velocity and V_T is shear wave velocity. The elastic anisotropy, C is defined as [2]

$$C = C_{11} - C_{12} - 2C_{44} \tag{2.7}$$

where C_{11}, C_{12} and C_{44} are the single crystal elastic coefficients. It can be concluded from Eq. 2.5 that ultrasonic attenuation not only varies with grain size and frequency but also depends on the scattering factor of the materials. Papadakis [2] has reported the grain scattering factor for various metallic materials. It has been shown that the grain scattering factor depends on the microstructural features of the alloy [2]. Gao et al. [28] have studied the frequency dependence of ultrasonic attenuation in cast iron using broad band frequency in the three characteristic regions of scattering. It has been demonstrated that the scatter size of samples can be evaluated from ultrasonic measurements. Average scatter size obtained from the ultrasonic and metallographic examinations showed good correlation [28].

2.2.2 Absorption of ultrasonic waves

During the propagation of ultrasonic wave, absorption is caused by the inelastic interaction of wave with structure of medium. The absorption in a material is quantified by a quantity called absorption coefficient (α_a) expressed by the following equation

$$\alpha_a = a_1 f^{0.5} + a_2 f + a_3 f^2 \tag{2.8}$$

where a_1, a_2 and a_3 are constants and f is the frequency of the ultrasonic wave. The first, second and third terms on the right side of Eq. 2.8 corresponds to thermo - elastic losses, magnetic losses and losses due to dislocation damping, respectively.

At room temperature and in the frequency range of 0.1 - 20 MHz, the dominant absorption losses are usually associated with the interaction of ultrasonic wave fields with dislocations. In addition to this, interactions also occur with magnetic domains [29]. Ultrasonic absorption has been used to characterise the cold work and for the assessment of fatigue [30] and creep damage [31] in materials, since a dislocation structure is strongly affected by plastic deformation. In many attenuation studies, mainly the scattering from prior austenite grain size has been taken into consideration for analysing the results. It has been shown that in austenitic stainless steel, only 5% of the total attenuation results from the absorption, while the remaining 95% is attributed to the grain scattering [32]. In ferritic steels, the contribution from absorption to the total attenuation is expected to be higher. The reverberation technique have been used to measure the absorption in material, where either a contact or non-contact type ultrasonic methodology can be adopted [33]. The application of ultrasonic absorption measurements for materials characterization is limited by the fact that sufficiently precise measurements of absorption are not possible with conventional techniques employing couplant.

2.3 Grain size characterisation

Different conventional ultrasonic methods have utilised velocity and attenuation as basic tools for grain size measurements. The grain size of a material is an important engineering parameter which influences the mechanical properties such as yield strength, creep, fatigue and impact transition temperature, and is widely used for monitoring the quality of the product during manufacturing processes [19, 34]. The dependence of yield strength (YS) and impact transition temperature (TT) with grain size is expressed by well-known Hall-Petch relations given below [35] as

$$YS = Y_0 + k_y d^{-1/2} \tag{2.9}$$

$$TT = T_0 + k_0 d^{-1/2} \tag{2.10}$$

where Y_0 and T_0 depend on composition and temperature, k_y and k_0 are constants and d is the average grain diameter. Generally grain size is measured from optical methods by analysing the micrographs, which are produced by metallography technique [36]. Such measurements using conventional metallographic technique is time consuming and sometimes requires cutting of specimens from the component. In addition to this, the metallographic technique provides the grain size only at the selected locations. The spatial variation in grain size present in the material cannot be obtained using this technique. It is advantageous to use a non-destructive method for the measurement of the grain size of a material.

Palanichamy et al. [37] observed a decrease in ultrasonic velocity with increase in grain size (in the range of 60-110 µm) in AISI type 316 austenitic stainless steel. A linear relationship was reported between the velocity and the grain size obtained by metallography [37]. The variation in longitudinal wave velocity with grain size has been explained based on the theory proposed by Hirsekorn [38, 39]. According to this theory, the product of the wave number (*k*) and the average grain diameter (*d*), i.e. *kd*, is the deciding factor for the change in velocity with grain size. It has been shown that the velocity passes through a minima when the conditions i.e., grain size–wavelength combination are favourable for resonance interaction between ultrasonic waves and the grains. The pioneering work in the area of grain size evaluation by utilising ultrasonic attenuation (UA) is reported by Papadakis [2]. In UA measurements, the amplitudes of the successive back-wall echoes are used. However, for highly attenuating austenitic stainless steel with thick specimens or specimens with large grain size, the amplitudes of the second and subsequent back-wall echoes are usually very small. The smaller amplitudes of the back-wall echoes limit the use of conventional ultrasonic velocity and attenuation measurements for grain size evaluation. In such cases, ultrasonic relative attenuation (URA) method can be employed [40]. The URA uses the amplitude of the first back-wall echo as the parameter correlating with the grain size. But this approach is also limited for use due to higher dependencies on the coupling condition and the variation in the thickness.

The scattering induced ultrasonic attenuation also offers a simple way for material inhomogeneity characterisation including grain size measurement in polycrystalline materials [2], porosity assessment in cast metal [41, 42] and in composites [43]. Ultrasonic backscattering techniques have been used for grain size characterisation [44, 45], by evaluating the attenuation coefficients from the exponential decay of the backscattered signals. Nagy et al. [46] have shown that the ultrasonic attenuation measured using backscatter technique is limited to samples of evenly distributed inhomogeneties. The backscatter technique works well with polycrystalline materials where grain structure and size distribution are uniform. However, the accuracy of attenuation measurements from backscattering technique is lower compared to coherent transmission technique. The scattering caused by inhomogeneties takes place in forward as well as in backward directions, but the scattering induced attenuation of the backscattered signal tends to be approximately half of the plane wave attenuation [46]. Apart from conventional amplitude based measurements, Fourier transform based spectral analysis techniques have been reported for grain size characterisation in austenitic stainless steels [47]. The frequency shifts estimated by homomorphic processing technique from backscatter echoes is also correlated with grain size [48, 49].

2.3.1 Spectral analysis

Ultrasonic spectroscopy is a further development of the pulse-echo technique, which uses broadband ultrasound and analyses the spectra of echo pulses. Analogous to light, the specimen is insonified with white sound. The variation in microstructure or the presence of defects alter the 'color' of the wave travelled through the material and the change in the 'color' of the sound wave provides information about the material. Ultrasonic spectroscopy has been successfully used for the characterization of defects and microstructural features [50]. The wide application of this technique includes, the measurement of depth of surface opening cracks [51] and quality testing of interfacial bonding [52]. Gericke et al. [53] have demonstrated the use of ultrasonic spectroscopy for grain size determination, by interrogating metal plates with broadband ultrasound. The 'loop frequency' responses of steels of varying grain size showed that, as the mean grain size increased from 50 µm to 100 µm, the ratio of the heights of the two frequency humps changed and the higher frequencies preferentially get attenuated by coarser grained material. The shift in the spectral peak frequency has been used for the evaluation of structural variations induced during tensile deformation in SUS304 stainless steels [54]. In this case, the spectral peak frequency was found to increase with increase in the tensile elongation. This is attributed to the deformation induced martensitic transformation during tensile deformation resulting in smaller crystalline grains, thereby reducing the attenuation due to ultrasonic scattering [54].

Kumar et al. [47] have studied the influence of grain size on ultrasonic spectral parameters in AISI type 316 austenitic stainless steel. The peak frequency and the full width at the half maximum (FWHM) of the autopower spectrum of the first back-wall echo have been correlated with the grain size. Fig. 2.1 (a) and (b) show the effect of grain size on ultrasonic first back-wall echo and its autopower spectrum, respectively. Amplitudes of both the first back wall echo and its autopower spectrum decreased with increase in the grain size due to the increased attenuation. Furthermore, with increase in the grain size, the higher scattering for high frequency results a decrease in the peak frequency and the FWHM. These ultrasonic spectral parameters were found to vary linearly with the inverse of the square root of the grain size (Fig. 2.2) exhibiting Hall - Petch type of relationship and hence can be linearly correlated with the yield stress, if the other microstructural features remain same [47]. The proposed methodology has useful practical significance that the devised parameters are independent for different coupling conditions and the error involved due to couplant variations can be minimised.

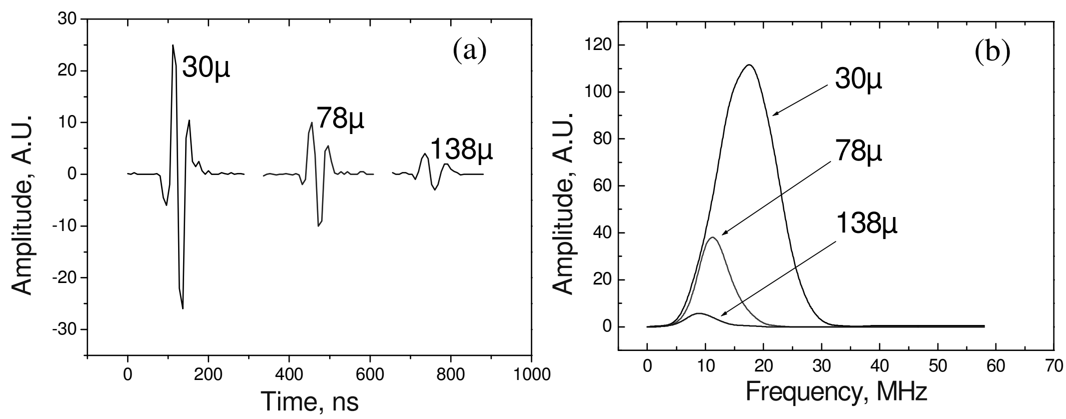

Fig. 2.1. Influence of grain size on (a) ultrasonic first back-wall echo and (b) its autopower spectrum in AISI type 316 stainless steel [47].

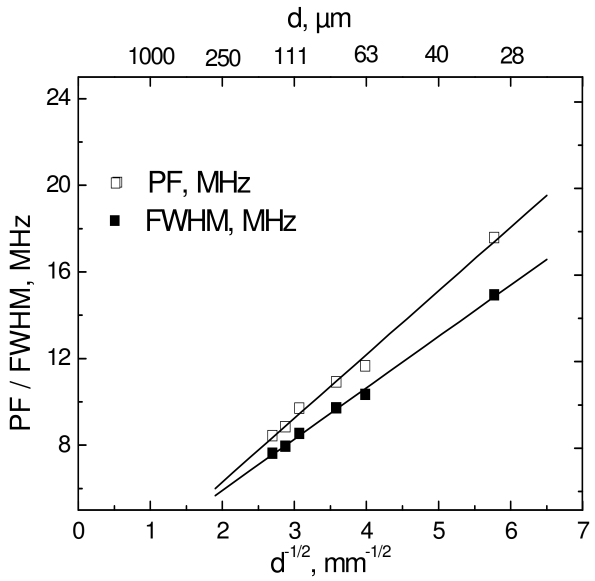

Fig. 2.2. Variation in peak frequency (PF) and full width at half maximum (FWHM) of the autopower spectrum of the first back-wall echo with grain sizes (d) and ($d^{-1/2}$) [47].

2.3.2 Homomorphic processing

A homomorphic system is one in which the output is a superposition of the input signals, i.e., the input signals are combined by an operation comprising of algebraic characteristics of addition [55]. Homomorphic processing is a complex nonlinear signal processing technique proposed by Saniie et al. [48, 49], which utilizes Fourier transform and logarithmic operations to convert convolutional signals to additive form, which can then be decomposed conveniently. The homomorphic wavelet recovery system is shown in Fig. 2.3 (a-f) [49], in which the grain signal is Fourier transformed to determine the magnitude spectrum. Following this, a logarithmic operator is applied to convert the multiplicative relationship between the mean echo wavelet and the grain impulse response to an additive relationship. The inverse Fourier transform of this provides grain signal power cepstrum. The cepstrum is the outcome of taking the Fourier transform of the log spectrum as a signal. The name cepstrum is derived by reversing the first four letters of 'spectrum'. One of the important properties of cepstrum is that it is a homomorphic transformation. The spectrum of the mean echo wavelet is approximately Gaussian shaped in the frequency domain and its power cepstrum has a time width which is shorter than the power cepstrum of the grain impulse response. Therefore, when a short pass filter of duration equivalent to echo duration is applied to the grain signal power cepstrum, the power spectrum of the echo wavelet can be recovered.

The homomorphic technique was used to analyse ultrasonic backscattered signals from specimens of different grain sizes [48]. This technique was able to remove randomness in the backscattered signals and it was possible to extract frequency dependent attenuation coefficient. Further, the feasibility of grain size characterisation using the developed approach has been demonstrated [48].

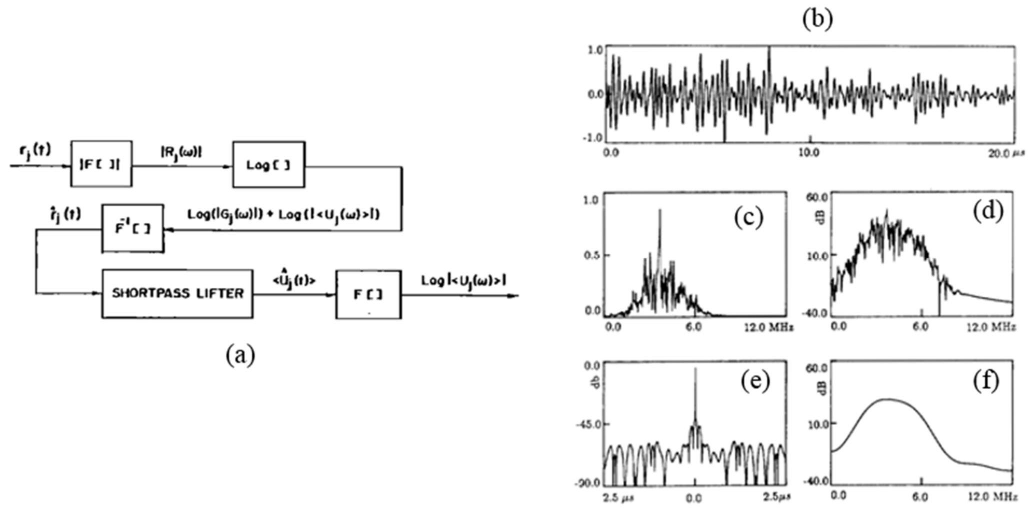

Fig. 2.3. Homomorphic wavelet recovery system (a) system sketch, (b) backscattered grain signal, (c) magnitude spectrum of grain signal, (d) log magnitude of the signal, (e) magnitude cepstrum of signal and (f) recovered log magnitude spectrum of ultrasonic wavelet [49].

Various approaches reported in literature for grain size characterisation are based on spectral analysis of ultrasonic echoes by Fourier transform (FT). Individually back-wall echoes or backscatter of the ultrasonic signals have been utilised for this purpose. A signal processed with the FT can only give the frequency distribution over the entire signal window. It can be compared to sinusoidal functions spread over the entire signal, but they are not connected to any ultrasonic pulse timings. As a result, the classical Fourier transform does not provide the evolution of frequency contents with time in non-stationary signals, as seen in materials with high ultrasonic scattering. This demands the use of methods which can deal with non-stationary signals and provide time-frequency localisation for enhanced analysis of noisy signals.

To the best of author's knowledge, time-frequency based studies have not been carried out for grain size characterisation of austenitic stainless steels. In the thesis, the details of systematic studies carried out using two time-frequency approaches, viz., short time Fourier transform (STFT) and continuous wavelet transform (CWT) for characterisation of grain size in austenitic stainless steel are presented. The proposed time-frequency approaches have been qualified using a set of specimens with a range of grain sizes (30-210 μm) generated by suitable heat treatment. An attempt has been made to provide better insight into new aspects of data analysis for microstructural characterisation in type 316 austenitic stainless steel using time-frequency methodologies developed in this study.

2.4 Defect characterisation

The scattering of an ultrasonic wave converts energy of the coherent, collimated ultrasonic beam into incoherent, divergent waves. For example, the ultrasonic signals obtained from coarse grain materials contain many overlapping echoes, which result from grain boundary scattering. The grain boundary scattering limits the detection of small cracks, flaws or other defects, as it reduces the SNR. Often, the flaw echo is completely merged into the grain or backscatter noise. In view of this, the use of time domain analysis of such signals becomes difficult. Several approaches based on frequency and time-frequency domains have been reported to improve the SNR in materials with high ultrasonic scattering. A brief review of different signal processing methods employed for detection of defects in highly scattering materials using ultrasonic waves is presented and this is followed by an overview of defect imaging methodologies.

2.4.1 Frequency domain analysis techniques

Ultrasonic pulse echo signals contain grain noise echoes, which result from random reflectors such as grains. The detection of flaws in the presence of grain noise echoes becomes difficult even when the size of flaws are substantially larger than grains. In frequency based filtering approaches, different types of filters such as band pass and low pass are utilised based on requirements of the bandwidth of the signal of interest. One could use conventional frequency domain filtering technique if the signal and noise have separate bandwidths. However, the overlapping of signal and noise in the frequency domain may lead to the distortion in the signal when a filter attenuates the noise components. Besides, the technique based on Fourier decomposition cannot be applied to nonlinear and non-stationary signals.

Krauss et al. [56] and Kennedy et al. [57] proposed the grain echo decorrelation resulting from the shift in the transducer position. They have reported the use of broadband transducer to transmit a set of narrow band signals and rectification and averaging operations on received echoes for flaw to grain echo enhancement [56].

Similar processing techniques have been reported for processing of radar signals. However, a more robust approach based on frequency diversity popularly known as split spectrum processing (SSP) was proposed by Newhouse et al. [6]. This technique showed promising results for flaw to grain echo enhancement, and the brief details related to this technique are given below.

2.4.1.1 Split spectrum processing

Split Spectrum Processing uses the frequency diversity to determine if a signal originates from a real flaw or a grain boundary. The implementation of SSP, therefore, makes use of multiple frequencies to inspect a component. This is best achieved by the use of a broadband signal, which can then be decomposed into a number of frequency bands [6]. The reported studies have utilised SSP for enhancement of SNR in coarse grain stainless steel specimens of 75-160 μm grain sizes. This method produces frequency diverse quasi-decorrelated signals from the received wide band signal by digital filtering. The wideband ultrasonic transducer is used to send and receive the pulses into the medium. The receiver output is then Fourier transformed to obtain frequency and bandwidth information of the received echo. The amplitude spectrum of the received signal is divided into a number of bands by digital filtering. Afterwards, inverse Fourier transform is performed at each band to obtain the individual frequency shifted signals. The centre frequencies of these signals shall be positioned within the half power bandwidth of the transducer. The splitting of the signals is achieved using Gaussian shaped filters in frequency domain. Karpur et al. [8] have made studies to compare the effect of Gaussian and raised Cosine filters on improvement of signal to noise ratio. Once the signal has been decomposed into a number of frequency bands, these frequency bands (filtered signals) are recombined. This recombination technique must be able to identify flaw signal, based on frequency diversity. A number of algorithms are reported to perform the recombination [9]. The minimisation and polarity thresholding algorithms are the most widely used recombination algorithms among others to process the frequency diverse signals obtained by splitting process [6].

Studies have also been made to improve the existing method by using the bandwidth of each filter proportional to central frequency, whereas in conventional methods fixed bandwidth filters are used [9]. A typical diagram representing the steps involved in the SSP processing of an ultrasonic signal is shown in Fig. 2.4 [9]. The performance of the split spectrum processing is found to be very useful in grain noise suppression, but it is very sensitive to the spectral range selected for processing. Secondly, the optimisation of various parameters need to be carried out to perform the processing. The signal to noise ratio enhancement capabilities of the SSP is critically dependent on the selection of the processing parameters such as location of the signal in the spectrum, number of filters and bandwidth [58].

An example of SSP processing towards SNR improvement of an ultrasonic signal is shown in Fig. 2.5. The improvement in the SNR of an ultrasonic signal obtained from a flat bottom hole in titanium specimen along with comparative analysis of different algorithms developed to process the ultrasonic signal shown in Fig. 2.5 indicated that, the minimisation of squared signals (Fig. 2.5 (d)) brings out the best improvement in SNR among other algorithms [6].

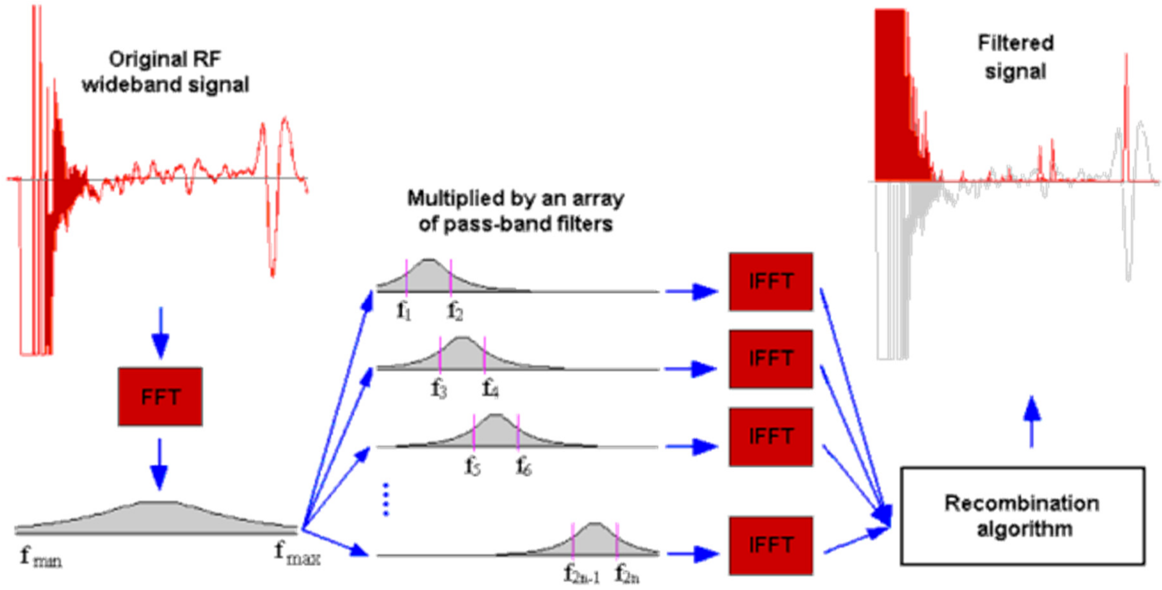

Fig. 2.4. Schematic of processing steps being carried out for enhancement of SNR using split spectrum processing (SSP) technique [9].

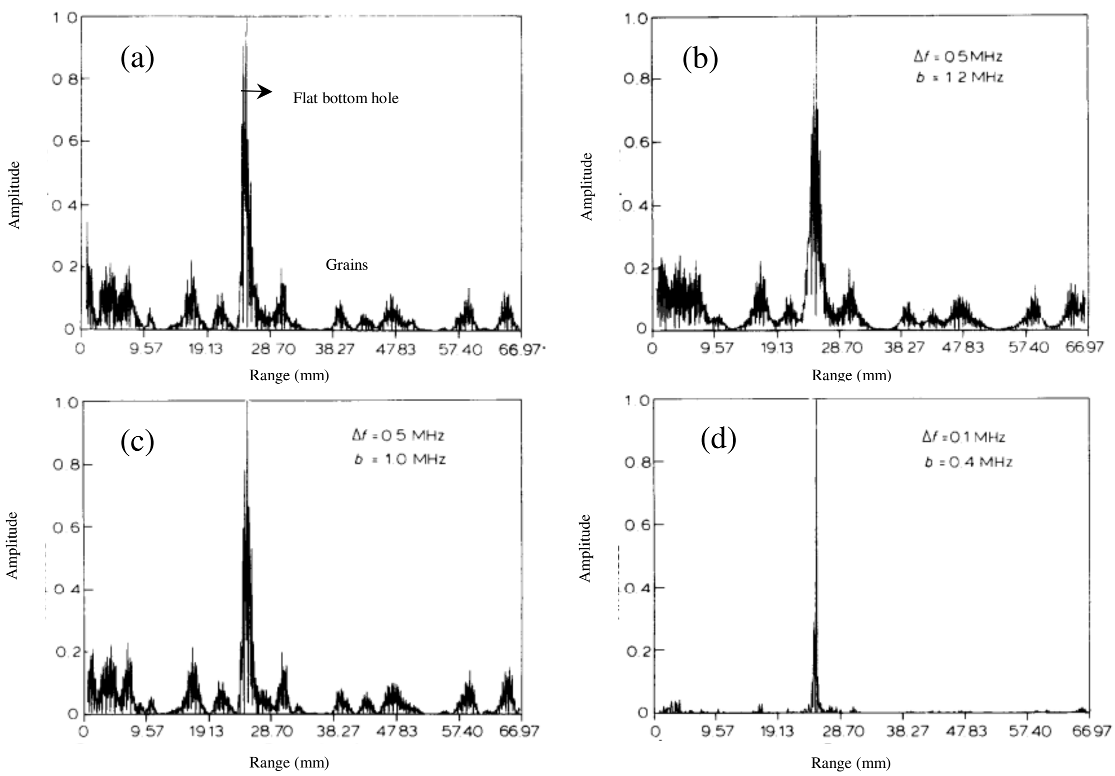

Fig. 2.5. The comparison of improvement in SNR of an ultrasonic signal from a flat bottom hole by applying different recombination algorithms to the SSP processed signal (a) squared wideband echo signal (unprocessed), (b) average of decomposed squared signals, (c) square of the decomposed averaged signals and (d) minimisation of decomposed squared signals [6].

2.4.1.2 Other techniques

Besides SSP, other approaches for structural noise removal such as Wiener filtering techniques based on group delay statistics have been used [59, 60]. The group delay of noise will be random, however it will be constant at the flaw location. This information is utilised for the detection of a flaw. These algorithms are based on designing a filter that has a high gain at frequencies where the SNR is large, and a low gain where the SNR is small. The main characteristics of this processing are to balance the conflicting goals of reducing the noise at filter output without distorting the signal [61]. The maximum likelihood estimation [62] and adaptive filtering [63] have been used for noise suppression and SNR improvement in ultrasonic testing. The artificial neural network based on the framework of adaptive FIR filtering has been used to enhance the SNR of ultrasonic signals in highly scattering materials such as large grained stainless steels and composites [64]. It has been shown that the artificial neural network based adaptive filter provides better signal enhancement compared to conventional adaptive filter [64].

The spectral analysis of backscatter has also been used to predict the presence or absence of a flaw based on the frequency shifts at the defect locations in coarse grain materials. The performance of autoregressive (AR), Pony's algorithm and multiple signal classification (MUSIC) methods have been compared for the detection of defect in coarse grained stainless steels [5]. The second order AR model produces better instantaneous frequency estimation in terms of resolution and accuracy [5]. The instantaneous frequency determined by the above mentioned methods showed promising results for flaw detection capabilities in the steel material.

In addition to the above, method based on the time varying spectral content of the ultrasonic echoes has been used to predict the presence or the absence of flaw echo in the received echo from highly scattering materials. The errors predicted by linear and time-varying parametric model for structural noise are less. However, in the presence of flaw, errors are large and change locally at the flaw location [61]. Due to the frequency dependent attenuation of ultrasonic signals in coarse grain steel, the use of time-frequency (TF) analysis becomes essential for improved understanding and extraction of hidden information.

2.4.2 Time-frequency domain analysis techniques

2.4.2.1 Wigner – Ville distribution

The evaluation of TF distribution plays an important role in flaw detection and characterisation in ultrasonic non-destructive evaluation. Wigner – Ville distribution (WVD) provides an actual TF representation of an ultrasonic echo on a joint time-frequency plane. WVD being superior in energy distribution concentration, is confronted with cross-terms interference (CTI) when signals are multi-component [65]. Fig. 2.6 shows a synthetic seismic trace comprised of three components constructed by adding with Ricker wavelets of different centre frequencies [65]. The seismic trance was modelled for a time duration is 0.6 s. The first seismic event (at 100 ms) is an isolated wavelet with a centre frequency of 50 Hz. The second seismic event (at 300 ms) consists of a 50 Hz wavelet and a 20 Hz wavelet arriving at the same time. The last one occurring at 500 ms is the superposition of two 40 Hz wavelets with a delay arrival time of 25 ms. The artefacts due to CTI can be clearly observed between the echo locations in WVD spectra at time scales of 200 and

400 ms as shown in Fig. 2.6. Wu et al. [65] have proposed advanced processing methods to alleviate the problems of cross terms interference in WVD.

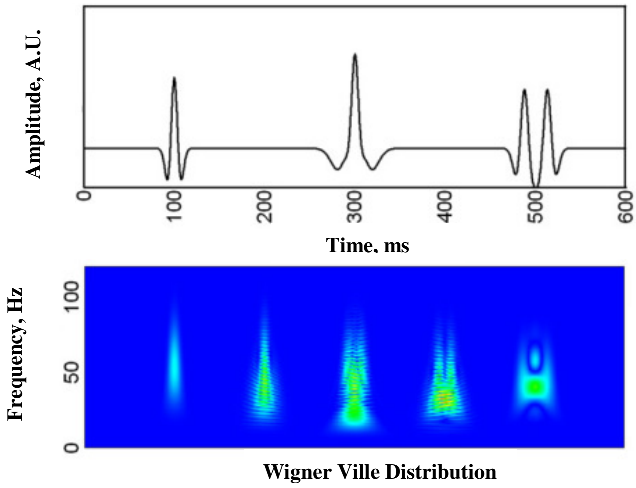

Fig. 2.6. A synthetic trace and its time-frequency spectra generated with Wigner-Ville distribution. The cross term interference can be observed in the WVD spectra between the echo locations at time scales of 200 and 400 ms [65].

2.4.2.2 Short time Fourier transform

The STFT is one of the most widely used algorithms in joint time-frequency analysis (JTFA) based on detailed FT centred at each time point. From the perspective of signal processing, there is minor difference between STFT and FT based processing. In STFT processing, the signal is divided into small segments, where the signal can be assumed to be stationary. To achieve this, a window function is chosen. Since the bases are no longer of infinite extent in time, it is possible to monitor the variations in signal frequency spectrum as a function of time. This is accomplished by the translation of the window as a function of time t, resulting in a 2D joint time-frequency representation STFT (t, ω) of the original time signal. The window function is first located at the very beginning of the signal and will be shifted in specified intervals till the end of the signal. At each window location, the FT is obtained. The spectra at any particular time are then stacked to reflect the lateral variation of signal behavior in both time and frequency in JFTA. The magnitude display $|\mathrm{STFT}\ (t,\omega)|$ is called the spectrogram of the signal. The STFT algorithm and the window function can be mathematically represented as

$$STFT[s(t)] = S(\tau,\omega) = \int_{-\infty}^{+\infty} s(t)\chi(t-\tau).e^{-j\omega t}dt \tag{2.11}$$

where, $\chi(t)$ is the window function which has a user defined time duration and $s(t)$ is the waveform signal in time domain. This operation (Eq. 2.11) differs from the Fourier transform only by the presence of window function $\chi(t)$. As the name implies, the STFT is generated by taking the Fourier transform of smaller durations of the original waveform. Alternatively, we can interpret the STFT as the projection of the function $s(t)$ onto a set of bases $\chi(t-\tau).e^{-j\omega t}$ with parameters τ and ω.

The result of this analysis depends on the choice of the window function leading to a tradeoff between time localization and frequency resolution. If the window length is too small, spectral leakage of low frequency component appears and when it is too long, the target of interest would be blurred [3]. The analytical and numerical evaluation of resolutions achieved by STFT for ultrasonic applications has been reported [66]. The study concluded that, with the a prior knowledge of the measurements system characteristics and using developed TF characteristic curves, the optimal window parameter for STFT can be obtained [66]. The window parameter determines the time and frequency resolution, which is constant for a particular window size. In the context of time–frequency analysis, uncertainty principles are referred to as the Gabor limit, or the Heisenberg–Gabor limit as described below in Eq. 2.21 [66, 67] as

$$\Delta t \Delta f \geq \frac{1}{4\pi} \tag{2.12}$$

Δt is decided by the window length which is selected only once for the entire analysis and accordingly Δf is also fixed. The width of the window function relates to how the signal is represented, whether there is good frequency resolution (frequency components close together can be separated) or good time resolution (the time at which frequencies change). A wide window gives better frequency resolution but poor time resolution, while narrower window gives good time resolution but poor frequency resolution. A schematic of the STFT time-frequency plane is shown in Fig. 2.7. Time and frequency resolutions are constant and being determined by window size, and this is represented by squares in the time-frequency plane [68].

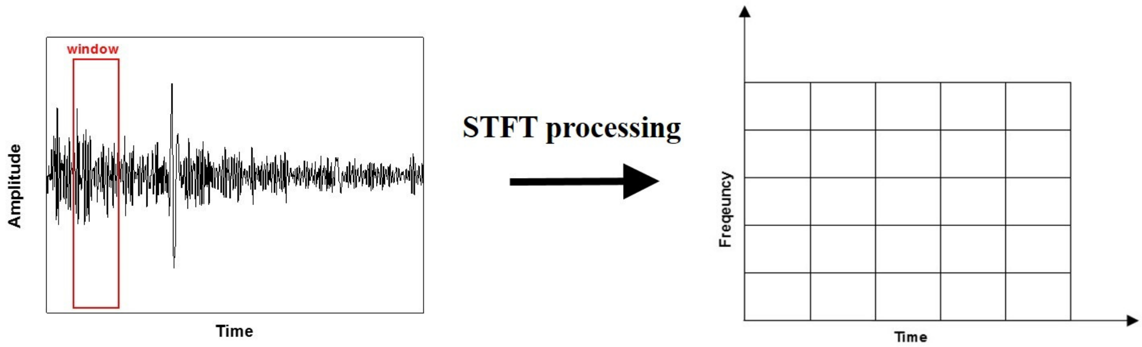

Fig. 2.7. Schematic of STFT processing indicating the importance of the window length determination. The time and frequency resolutions are fixed for entire analysis depending on the window length chosen.

The STFT and WVD processing have been successfully employed in resolving complicated issues by utilising their time-frequency analysis capabilities. For example, acoustic spectrum of a transmitting aircraft, when received by stationary receiver, changes with time due to acoustical Doppler effect. The STFT and WVD have been used in estimating the propeller blade rate at short time intervals for an aircraft flying at a constant altitude and speed over an acoustic sensor located above the ground level. The temporal variation in the observed blade rate is then used to estimate the speed and altitude of the aircraft [69].

Determination of acoustic attenuation and dispersion has important applications in ultrasound tissue characterisation and non-destructive testing of materials. Generally, Fourier transform based signal processing methods are used to get the amplitude and phase spectra of ultrasonic signal to estimate the attenuation and dispersion of the given medium. However, these methods require phase unwrapping to be carried out for unambiguous measurements. Zhao et al. [70] used STFT to estimate ultrasonic attenuation and dispersion. The attenuation measurements are carried out based on the amplitude decay of ultrasonic pulse, and the phase velocities are evaluated based on the mono frequency components extracted by STFT. This method was very useful in eliminating ambiguity issues in phase angle calculations [70].

2.4.2.3 Wavelet transform

The wavelet transform (WT) is an alternate approach to the STFT to overcome the constant resolution problem. Wavelet transform mainly consists of two different processing techniques called as continuous and discrete wavelet transforms.

Continuous wavelet transform (CWT)

The wavelet transform is defined in terms of basis functions obtained by compression/dilation and shifting of mother wavelet [4]. It acts as a mathematical microscope which allows one to zoom in on the fine structure of a signal or alternatively to reveal large scale structures by zooming out. The property of self-adjusting the analysis window according to signal frequency makes it more suitable for the analysis of transient non-stationary ultrasonic signals. In the wavelet analysis, the signal is multiplied with a function called mother wavelet, similar to the window function in the STFT, and the transform is computed separately for different segments of the time-domain signal. The width of the window is changed as the transform is computed for every single spectral component, which is the most significant characteristic of the wavelet transform [71]. The continuous wavelet transform is defined [68] as

$$\mathrm{CWT}_x^{\psi}(\tau, s) = \psi_x^{\psi}(\tau, s) = \frac{1}{\sqrt{s}} \int x(t)\psi^*\left(\frac{t-\tau}{s}\right) dt \qquad (2.13)$$

It can be observed from Eq. 2.13, that the transformed signal is a function of two variables, τ (translation) and s (scale) parameters. The $\psi(t)$ is the transforming function, and it is called the mother wavelet. According to the Eq. 2.13, for every τ and s, we have a wavelet coefficient, representing how much the scaled wavelet is similar to the function at location $t = (\tau/s)$. The term “wavelet” means a small wave. The “smallness” refers to the condition that this (window) function is of finite length, i.e., compactly supported. The “wave” refers to the condition that this function is oscillatory. The term “mother” implies that the functions with different regions of support that are used in the transformation process are derived from one main function, or the mother wavelet. Hence, the “mother wavelet” is a prototype for generating the other window functions.

The term “translation” is used in the same sense as it is used in the STFT. It is related to the location of the window, as the window is shifted through the signal. This term, corresponds to time information in the transform domain. However, in the wavelet analysis, frequency parameter is not used, as it is assigned for STFT analysis. Instead, a scale parameter is used. The inverse of the scale can be correlated with pseudo frequency [68]. A schematic of the CWT time-frequency plane is shown in Fig. 2.8, every box in this figure corresponds to a value of the WT in the time-frequency plane. Though the widths and heights of the boxes change, the area is constant. At higher scales (low frequencies), the heights of boxes are shorter (better frequency resolution, since there is less ambiguity regarding the value of exact frequency), but their widths are longer (which correspond to poor time resolution, since there is more ambiguity regarding the value of exact time). At lower scales (higher frequencies), the widths of boxes decrease indicating better time resolution, however, the heights of boxes increase indicating poor frequency resolution.

The CWT has been used for extracting the local effects of frequency components in ultrasonic impact echo signals [72] which have been correlated with the embedded structures such as steel reinfrocement and PVC tubes in concrete slab. The features of structures embedded in the concrete could be resolved by the difference in the wavlet scales and magnitude plot of wavelet coefficients [72].

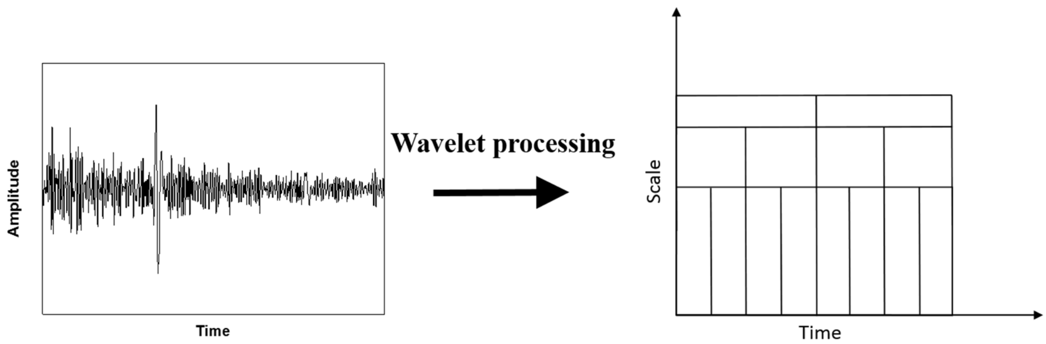

Fig. 2.8. Schematic of CWT processing indicating the inherent flexible window analysis for processing of signal. The time and frequency resolution changes depending on the scale of analysis.

The CWT has also been used for calculating the frequency dependent ultrasonic velocity of the longitudinal and shear waves using wavelet scales in the cement based materials [73]. A recently reported study utilizes the combination of CWT and the fast

Fourier transform (FFT) to study the changes in the fundamental frequency of impact echo signals [74]. In the reported study [74], first, the CWT is applied to the signal and then appropriate time window is selected based on the wavelet analysis. Further, the FFT is applied to the time window optimized by the wavelet to obtain better frequency resolution. The 'scal2frq' function in Matlab program have been used by Trivedi et al. [74] to obtain pseudo frequency values for the corresponding wavelet scales. The continuous wavelet transform has been utilised for SNR enhancement of ultrasonic signals merged in coherent noise, which were obtained from highly absorbing material [75]. The reconstruction of signal with minimisation algorithm to selected wavelet scales showed good improvement in SNR. The typical example of processing the ultrasonic signals from a highly absorbing material is shown in Fig. 2.9 [75].

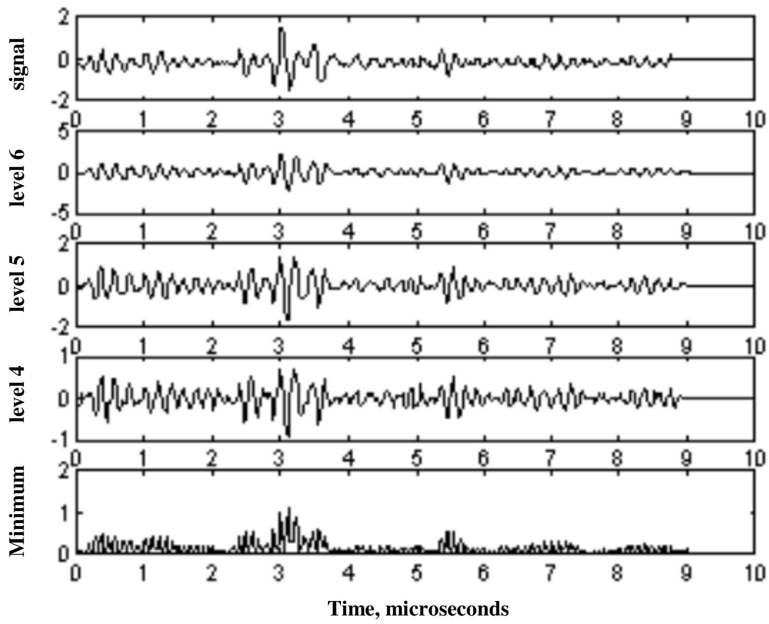

Fig. 2.9. The processing of ultrasonic signal for different wavelet scales and application of minimisation algorithm to the CWT processed signal at selected scales [75].

Discrete wavelet transform (DWT)

Discrete wavelet transform (DWT) was developed to save computation time by eliminating redundancy in CWT analysis. In CWT analyses of ultrasonic echoes, the time-frequency plane is sampled uniformly, but for the higher scales (lower frequencies), the sampling rate can be decreased according to Nyquist's rule. The scale parameter is discretized first on a logarithmic grid. The time parameter is then discretized with respect to the scale parameter. This means different sampling rates are used for each scale or the sampling is done on the dyadic sampling grid. The DWT can be interpreted as decomposing a signal into a set of frequency channels having the same bandwidth on the logarithmic scale [71]. This processing, not only gives information in the time and frequency domains simultaneously, but also act as a sub-band filter which performs mathematical operations to separate certain frequencies of a signal. With the DWT, an original signal can be decomposed into a series of approximations ('A' components, or low frequency components') and details ('D' components, or high frequency components) that reveal useful information on the signal characteristics which may not appear in the original signal. Fig. 2.10 represents the concept of dyadic filtering of an ultrasonic signal by DWT processing. The original signal can first be decomposed in to A1 and D1 components and this step is repeated. The repetition number is called the level and at the n^{th} level, the original signal can be represented as, $s(t) = A_n + \sum_{i=1}^{n} D_i$, where i is an integer. The time-domain signals are passed through various high-pass and low-pass filters to filter out either high frequency or low frequency portions of the signal [71]. Chen et al. [10] reported the use of DWT for enhancement of SNR in coarse grain 304 SS. The study showed that DWT has good potential to improve SNR during ultrasonic inspection of coarse grained materials [10].

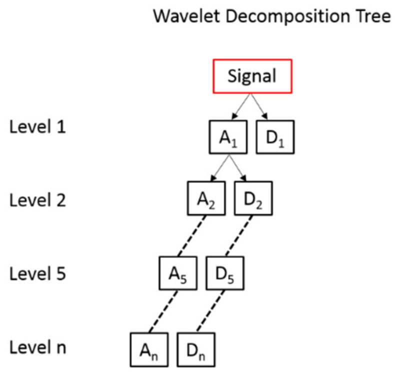

Fig. 2.10. Schematic of dyadic filtering scheme being used in the DWT based processing of signals.

Erdal et al. [76] have used DWT for decorrelating flaw echoes from clutter echoes and the benefits of DWT in utilizing both temporal and spectral properties have also been discussed. The improvement of the flaw to clutter enhancement of ultrasonic signals is dependent on the frequency scales used and type of wavelet kernel used for processing the data [76]. The use of DWT has been reported to estimate the porosity content of composite material from ultrasonic backscattered signals. The ultrasonic echoes from a composite material comprise of multiple reflections from plies, porosities as well as background noise. Due to the presence of signals from different sources, the backscattered signals have various frequency bands. The ultrasonic backscattered signals were recorded from specimens of different porosity levels and decomposed into approximation and details coefficients by DWT processing. The peak frequency of the decomposed signal with different porosity content was recorded. Good correlation was found between the porosity content and the maximum amplitude of peak frequency of the decomposed signal [77].

The wavelets have been found to be very useful in detecting single targets, however, they are less effective in resolving closely spaced targets in comparison with SSP [78]. The comparative studies for noise suppression using DWT and Weiner filter based methods have been reported, where the DWT based denoising method is found to be more effective in removing the high frequency noise from the signal [79]. The pioneering work in the area of wavelets was done by Abbate et al. [7], where wavelets have been used as a band pass filter by using filter banks to cover the tested ultrasonic frequency band. They have utilised wavelet transform for improved ultrasonic flaw detection. Simulated white and coloured noise was added to the experimental signals to determine the SNR improvement due to wavelet filtering. 'Morlet' mother wavelet with a set of filters have been utilised to understand the improvement in SNR. The typical example of ultrasonic signal corrupted with white noise and the improvement with WT is shown in Fig. 2.11. It has been reported that the use of WT filtering for ultrasonic signals buried in noise without any loss of accuracy in time measurement helps in the accurate evaluation of flaw depth [7]. The 1-dimensional time signal transformed to 2-dimensional representation using wavelet approach results in redundancy, however, this can be advantageously utilised to improve the interpretation of experimental data [7]. Zhang et al. [80] proposed a theoretical model to estimate the optimal frequency to bandwidth ratio of the Gaussian wavelet. The proposed model was verified with experimental investigations [80]. Peng et al. [81] have treated WT as band pass filter whose central frequency and frequency bandwidth are determined by spectral distribution of a real ultrasonic signal obtained from a specimen. They have carried out the simulation studies to validate their approach and experimentally verified on real pipeline specimens for evaluation of defects. Typical example for improvement of SNR of ultrasonic signals from cracks near to inner and outer walls of pipeline is shown in Fig. 2.12. The processing of signals improved the appearance of flaw indications, which were otherwise merged in high frequency noise.

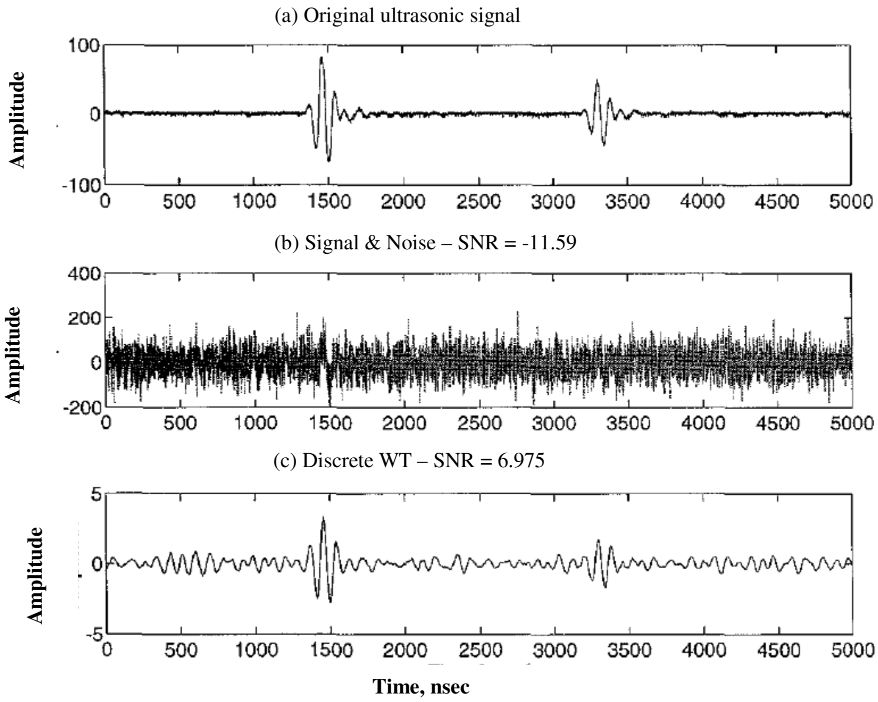

Fig. 2.11. The improvement of SNR with wavelet processing of signals (a) original ultrasonic signal, (b) whiter noise added and (c) output of wavelet transform [7].

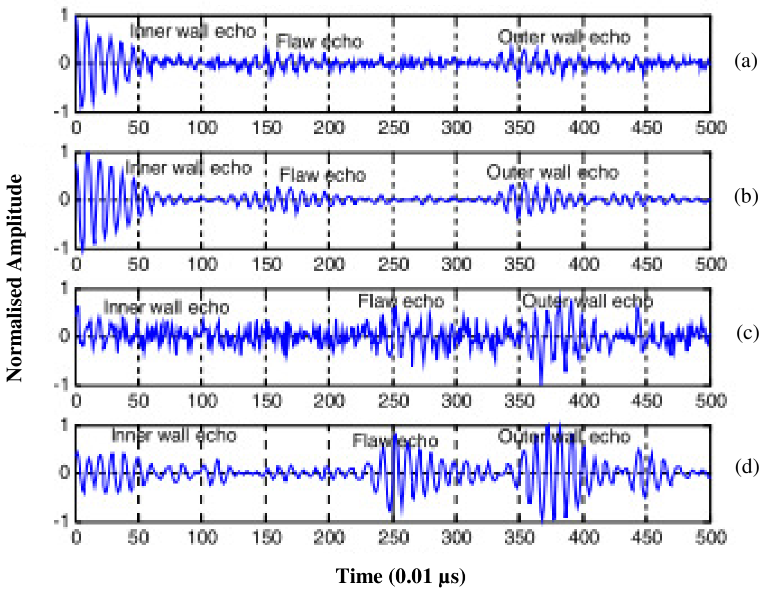

Fig. 2.12. Typical plots of original signals and processed signals used to identify flaws in pipelines: (a) original ultrasonic signal with crack near the inner wall, (b) processed result of (a), (c) original signal with a crack near the outer wall and (d) processed results of (c) [81].

The denoising performance of the wavelet processing of an ultrasonic signal depends on various parameters including type of wavelet, thresholding method and threshold selection rules. The use of level dependent thresholding has been reported for improvement of SNR in ultrasonic non-destructive evaluation of sound scattering materials such as carbon fibre reinforced plastic composites [82]. The universal thresholding rule is found to be more appropriate for enhancement of SNR compared to other selection rules. A typical example of SNR improvement with hard thresholding procedure is shown in Fig. 2.13. The application of thresholding rules on DWT processed signals shows good improvement of SNR, even when the frequency band of the grain noise and flaw signal are similar [82]. The higher order wavelets have been used for analysing denoising performance of time of flight diffraction (TOFD) signals obtained for austenitic stainless steel welds [83]. The studies showed that higher order wavelets give better SNR improvement compared to lower order wavelets [83].

Undecimated wavelet transform

The most significant problem with DWT is that it is not shift invariant transform. The shift variance results from the use of decimation in the DWT. Decimation implies the removal of odd indices in each decomposition level of DWT. This down sampling results in wavelet coefficients with position dependence. This can add large change in reconstructed waveforms. The study has also reported achieving shift invariance by using undecimated wavelet transform instead of discrete wavelet transform, where zero padding is used to up-sample the filter bank coefficients. The proposed method showed good SNR improvement compared to conventional wavelet method [84].

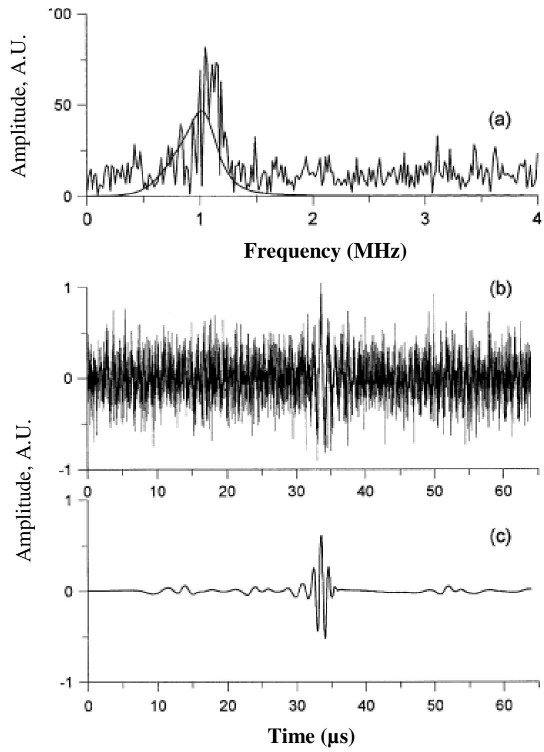

Fig. 2.13. The performance of wavelet filtering when spectral content of noise and signal are similar (a) typical frequency band of grain noise and frequency response of ultrasonic transducer, (b) time domain signal of ultrasonic signal merged in noise and (c) ultrasonic echo recovered with improved SNR by wavelet filtering (db6 with hard thresholding) [82].

Other methods

Time-frequency analysis methods are mainly used to improve the defect detection resolution. The S-transform, a hybrid of STFT and CWT, has been used for detection of echoes in the presence of poor SNR. The S-transform retains absolute phase information, while preserving good time-frequency resolution for all frequencies. However, STFT has low resolution and WT does not provide any phase information. The proposed method based on modified S-transform is able to show correct time-frequency information of multiple Gaussian echoes with low SNR. The usefulness of the proposed approach was demonstrated by resolving closely spaced ultrasonic echoes obtained from side drilled holes in a steel block [85].

2.4.2.4 Hilbert–Huang processing

The combination of empirical mode decomposition (EMD) technique with Hilbert transform is known as Hilbert–Huang processing technique [15]. EMD is designed to decompose, non-stationary, non-linear data into a series of Intrinsic Mode Functions (IMFs) adaptively. This procedure is automatic, data-driven and time-variant. The IMFs are generated by data shifting operations and then Hilbert transform is applied to these IMFs. The following conditions need to be satisfied for a signal to be an IMF:

1. $\left|Num_{extremet} - Num_{zero-crossing}\right| \leq 1$ (2.14)

   where, $Num_{extreme}$: The number of local extreme points (includes local maxima and local minima); $Num_{zero-crossing}$: The number of zero-crossing points.

2. $|m(t)| = \left|\frac{h_{max}(t)+h_{max}(t)}{2}\right| = 0$ (2.15)

   where, $h_{max}(t)$: The envelope interpolated by all the local maxima; $h_{min}(t)$: The envelope interpolated by all the local minima; m(t): The mean sequence of local maxima and minima envelopes.

The algorithm to decompose a signal into a series of IMFs is established with the definitions of local maxima and minima of the signal s(t). The local maxima $s_{max}(t)$ and minima $s_{min}(t)$ are connected by a cubic spline line to produce respective upper $u_s(t)$ and lower $l_s(t)$ envelopes. The respective mean is denoted as $m_l(t)$ and is given by

$$m_l(t) = \frac{u_s(t)+l_s(t)}{2} \quad (2.16)$$

The difference between the original signal s(t) and the so-called running mean is the first component as $h_l(t)$, $h_l(t)$=s(t)-$m_l(t)$. The shifting processing has to be repeated upto k times, as it is required to reduce the extracted signal to an IMF as $h_{1k}(t) = h_{1(k-1)}(t) - m_{1k}(t)$, where subsequent component $h_{1(k-1)}$ is treated as original signal. The resulting time series is the first IMF as $c_1(t)=h_{1k}(t)$. To check, if $h_{1k}(t)$ is an IMF, the following conditions must be satisfied:

1) the component $h_{1k}(t)$ should not display undershots or overshots riding on the original signal and produce local extremes without zero crossing.
2) should display symmetry of the upper and lower envelopes with respect to zero.
3) the number of zero crossings and extremes should be same for both functions.

The criterion for the shifting process to terminate comes from the size of the standard deviation (SD), computed from the two consecutive shifting results and is given by

$$SD = \frac{1}{m}\sum_{t=0}^{T}\left[\frac{\left|(h_{1(k-1)}(t)-h_{1(k-1)}(t))\right|^{2}}{h_{1(k-1)}^{2}}\right] \tag{2.17}$$

where m is the maximum number of the original signal digitising rate cells, T is the total length of the signal. A typical value for SD can be smaller than 0.3. The first IMF c(t) is subtracted from the original signal as $r_1(t) = s(t)-c_1(t)$ and this difference is called as the residue $r_1(t)$. It is treated as the new signal and subjected to the same shifting process. The process of finding intrinsic modes c_j continues until the final residue $r_n(t)$ will be a constant or a monotonic function. Then original signal is decomposed into n-empirical modes and a residue as

$$s(t) = \sum_{j=1}^{n} c_{j+} r_n \tag{2.18}$$

The second step is to apply the Hilbert transform to the decomposed IMFs. Each IMF component has its Hilbert transform

$$y_j(t) = \frac{1}{\pi}\, P \int_{-\infty}^{+\infty} \frac{c_j(t')}{t-t'}dt' \tag{2.19}$$

where P indicates the Cauchy principal value. With this definition, the analytic signal is defined as

$$z_t = c_j + iy_j(t) = a(t)e^{i\theta(t)} \tag{2.20}$$

in which,

$$a_j(t) = \sqrt{c_j^2 + y_j^2} - is\ the\ magnitude$$

$$\theta_j = arctan\left(\frac{y_j(t)}{c_j(t)}\right) - \text{is the phase}$$

To analyse the analytic signal z(t), the Hilbert amplitude spectrum H(ω,t) is used. Therefore, one can define an instantaneous frequency ω_j given by

$$\omega_j = \frac{d\theta_j(t)}{dt} \tag{2.21}$$

Thus, the original signal can be expressed as

$$s(t) = Re\left[\sum_{j=1}^{n} a_j(t).\, e^{\left(i\int \omega_j(t)dt\right)}\right] \tag{2.22}$$

Equation 2.16 enables to represent the amplitude (or the energy) and the instantaneous frequency. The HH based processing has been applied for the detection of defects in multi-layered fiber-reinforced plastic pipes [86]. The artificially made defects were detected and imaged using this method. However, to improve the capability of defect detection, the method of subtraction has been proposed [86]. The HH based methodology has also been used for the analysis of ultrasonic backscattered signals from coarse grain material [87]. Here, the summation of the IMFs is used for signal reconstruction, however, only the first IMF has been used for examining the time-frequency representation of the signal. The results have been compared with the other time-frequency analysis method called as chirplet signal decomposition [87], and are found to be accurate with respect to time and frequency representation. A chirplet is a piece of chirp similar to as wavelet is a piece of a wave. More precisely, a chirplet is a windowed portion of a chirp function, where the window provides time localization property. A comparative study between wavelet and HH based analysis is reported for coarse grained materials. The usefulness of HH based denoising method in comparison to wavelets is discussed [87]. The experimental and theoretical studies have also been reported to understand the SNR improvement of ultrasonic signals obtained from coarse grain stainless steel by EMD based processing [16]. The details of the Ensemble Empirical Mode Decomposition (EEMD) processing, which is found to be very useful in alleviating the mode mixing problem of EMD, is given below [17].

Introduction of EEMD

In the EEMD, white noise having the amplitude of a fraction (typically 0.1-0.4) of the standard deviation of the signal is added before performing EMD to decompose the signal into IMFs. In each trial, the ensemble average of each IMF is taken over all the trials to represent the true IMFs. The noise added in each trial to prevent the mode mixing effect, tends to diminish by $\varepsilon_0/\sqrt{M}$, where ε_0 is the noise amplitude and M is the number of ensemble members. The procedure for the EEMD analysis can be described as follows [17]:

1. Add a finite amplitude of white noise to the targeted data and then decompose it into IMFs using EMD as

$$\widetilde{x_n}(t) = x(t) + \varepsilon_0 \omega_n(t) \tag{2.23}$$

where $\widetilde{x_n}(t)$ is the signal after adding the white noise during the nth trial, $x(t)$ is the targeted data, ε_0 is a scaling factor to be multiplied by the white noise at each trial and $\omega_n(t)$ is the white noise added during the nth trial.

2. Repeat the above steps with different sets of white noise added over a large number of trials.

3. Find the mean of each IMF obtained in different trials to arrive at the final IMFs.

Determination of noise amplitude

One of the crucial issues in the EEMD method to prevent mode mixing is the determination of amplitude of noise (ε_0). It has been reported that the optimum amplitude of the noise to be added is in the range of 0.1-0.4 times the standard deviation of the signal [17]. If the amplitude of the added noise is too small, it would not be sufficient for preventing mode mixing. Different time scales present in the signal may not get separated when the signal is decomposed into IMFs. If the amplitude of noise added is too high, the number of ensemble averages required may be too large for a reasonable suppression of noise in the ensemble averaged IMFs. Thus, there is a trade-off between the computational efficiency (based on number of ensemble averages taken) and the signal to noise ratio finally achieved (based on residual noise in the IMFs). Mariyappa [88], has proposed a method for determination of noise amplitude by using the second order derivative of the signal. Wang et al. [18] have reported the superiority of EEMD processing for detection of underground sink holes in a seismic survey. They have shown that in the time–frequency analysis of seismic profiles, the time–frequency spectrum obtained by EEMD reflects the geological subsurface geology more accurately compared to EMD as shown in Fig. 2.14.

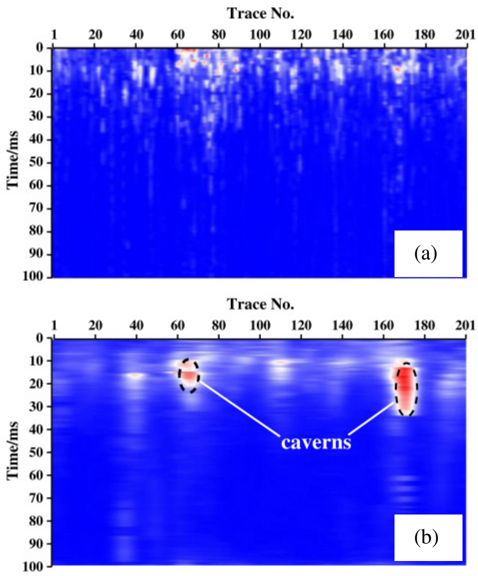

Fig. 2.14. Sliced time–frequency spectrum at a particular frequency based on (a) EMD and (b) EEMD processing of a seismic record [18].

2.5 Imaging of defects in highly attenuating media

A review of a few studies reported in the literature for imaging of defects in high scattering media is presented in this section. Partial spectra approach has been used to visualise the defect echo merged with noise in coarse grain steels. The partial spectra approach, i.e., the temporal or spatial frequency components of B-scan image are used individually to obtain information regarding the flaw location. This approach has been found to be very useful compared to conventional two dimensional spectrum [89].

The block filtering approach has been used to increase the lateral resolution thereby improving the flaw sizing accuracy in mild steel specimens. In the block-filtering process, the returned ultrasonic echoes are Fourier transformed and a band of frequency information is used to construct the C-scan image. However, in case of deconvolution, the block-filtered C-scan image is deconvolved with respect to the point spread function of a transducer used for acquiring the data. The deconvolution process is achieved by a frequency domain Weiner deconvolution algorithm. The block filter removes the dominant low frequency components in the returned echoes and C-scan image is generated with enhanced lateral resolution. This technique has shown improvements in sizing of flaw when the central frequency of the block filtering is not too far from the central frequency of the returned echoes [12].

A wavelet based method for C-scan imaging of defects in composite materials has been reported [14]. This method overcomes limitations of FT method in having a meaningful frequency analysis of peak frequency shifting. The mother wavelet was chosen by considering the similarity of wavelet shape with ultrasonic signal to be detected. The proposed methodology was used to examine the presence or absence of the back-wall echo reflection. The absence of back-wall reflection can be considered as an indication of a potential defect. The quantification of the amplitude received at the back-wall echo location was performed by a wavelet based characterising parameter. However, this technique is not suitable for thick structures as the back-wall reflection may be undetectable [14].

The Hilbert transform based C-scan images of the blind holes in specimens has been compared with conventional amplitude based images. Simultaneous real-time display of the complex and C-scan images is also possible. It has been reported that attributes of instantaneous amplitude can enhance the weak events, but the resolution of the image is not improved. However, the instantaneous phase and frequency attributes are very sensitive to the boundaries of the holes, and they show clear demarcation of the boundaries compared to amplitude based C-scan image [13].

2.6 Appraisal of the problem

The review of literature on materials characterisation reveals that the microstructural features which affect the scattering and absorption of the wave such as grain size can be effectively characterised by ultrasonic attenuation. The ultrasonic spectral analysis can be used for characterising the microstructure due to frequency dependent attenuation. In the reported studies, correlation of the frequency shifts of the backscatter and back-wall echoes with grain size has been studied. Fourier transform based approaches are used to obtain the frequency information, but they are limited to the analysis of signals from relatively lower grain sizes. Besides, the Fourier transform based measurements are also not suitable for analysing the ultrasonic signals in coarse grain austenitic stainless steel, which are non-stationary in nature. Hence, there is a need to use more appropriate signal processing techniques, which are suitable to analyse non-stationary signals to understand frequency dependent attenuation and to characterise grain size in high scattering austenitic stainless steel. To the best of the author's knowledge, this has not been studied earlier and hence, this problem has been taken up as a part of the current study. Austenitic stainless steel materials are of prime importance for applications in nuclear and chemical industries due to their higher mechanical and corrosion resistant properties compared to other counterparts.

Further, for ultrasonic characterisation of defects in highly scattering and attenuating materials such as authentic stainless steel and composites, various frequency and time-frequency analysis based methodologies have been developed. However, most of these analyses methods are limited to simulated signals, and only a few studies are reported for imaging of defects in these materials. In view of this, there appears to a need for systematic experimental and theoretical studies to understand the frequency shifts with beam path in coarse grain materials and devise a suitable imaging technique based on time-frequency parameter. It is important to mention that, no systematic study has been reported earlier in this domain. Therefore, efforts have been made to develop suitable experimental and theoretical understanding of frequency shifts generally observed in coarse grain materials. Further, attempts have also been made to develop an imaging methodology based on a time-frequency parameter in the present study.

Furthermore, the SNR improvement of ultrasonic signals by wavelet based approaches in highly scattering materials has been reported. However, these approaches have limitations with respect to the selection of a mother wavelet, optimum scales and decomposition levels. A few studies have also been reported on the use of a new adaptive signal processing technique known as EMD for enhancement of SNR of ultrasonic signals in coarse grained materials. Form the literature it is well known that the EMD suffers from mode mixing and hence it is essential to use alternative methods which can alleviate this problem and can be used adaptively. The mode mixing can be minimised by EEMD processing, and this method has been widely used for geophysical applications. In the thesis, a novel approach of EEMD processing of ultrasonic signals in conjunction with signal minimisation algorithm is proposed. This approach was successfully employed on ultrasonic signals obtained from austenitic stainless steel specimens with a range of grain sizes (30 - 210 μm). It has been demonstrated that adaptive reconstruction of ultrasonic signals can be achieved with enhanced signal to noise ratio for the grain size range undertaken in present work.

Chapter 3. Ultrasonic Measurements

3.1 Introduction

This chapter provides the details of experimental set-up used in this study. The details of the specific software developed for time-frequency analysis of ultrasonic signals obtained from coarse grain austenitic stainless steel are also given. Further, the application of a theoretical model for evaluation of peak frequency shift in high scattering medium is elucidated.

3.2 Experimental setup

The schematic of experimental setup used to carry out ultrasonic immersion measurements in this study is shown in Fig. 3.1. The photograph of the experimental setup is also shown in Fig. 3.2. Water was used as a coupling medium. Ultrasonic immersion transducers having the nominal frequencies of 25 MHz and 10 MHz were used to acquire the signals. The transducers were of 6 mm diameter with unfocussed nature. The transducers consist of piezoelectric crystals, which vibrate upon the application of electrical pulse across the thickness and generate the ultrasonic waves. A 35 MHz broadband ultrasonic pulser receiver was used to generate and receive the ultrasonic signals from the transducers. The experimentally measured peak frequencies of the transducers were found to be 16 MHz (25 MHz nominal frequency) and 9 MHz (10 MHz nominal frequency).

The ultrasonic reflections observed from the specimens were received by the same transducer (pulse echo mode) and were converted to electrical signals. These electrical signals were acquired by the receiver at an optimum gain and damping settings, and the received radio frequency (RF) ultrasonic signals were fed to the PC based digitizer. The ultrasonic signals were digitized at 500 MS/s as well as 100 MS/s sampling intervals, using a 500 MS/s, 8 bit digitizer card. The influence of different data lengths achieved by changing the digitization rates were used to understand the adaptive reconstruction of ultrasonic signals by Ensemble Empirical Mode Decomposition (EEMD) processing.

The ultrasonic signals were recorded at specified locations as well as in raster scan mode using an automated scanner. The scanner was controlled by an interface program developed in LabVIEW. The ultrasonic signals including the water - specimen reflection and user specified multiple back-wall echoes were stored in a computer using a LabVIEW program. All the waveforms were averaged for 100 times to eliminate random noise. The specimens were kept in the far field of the ultrasonic transducers.

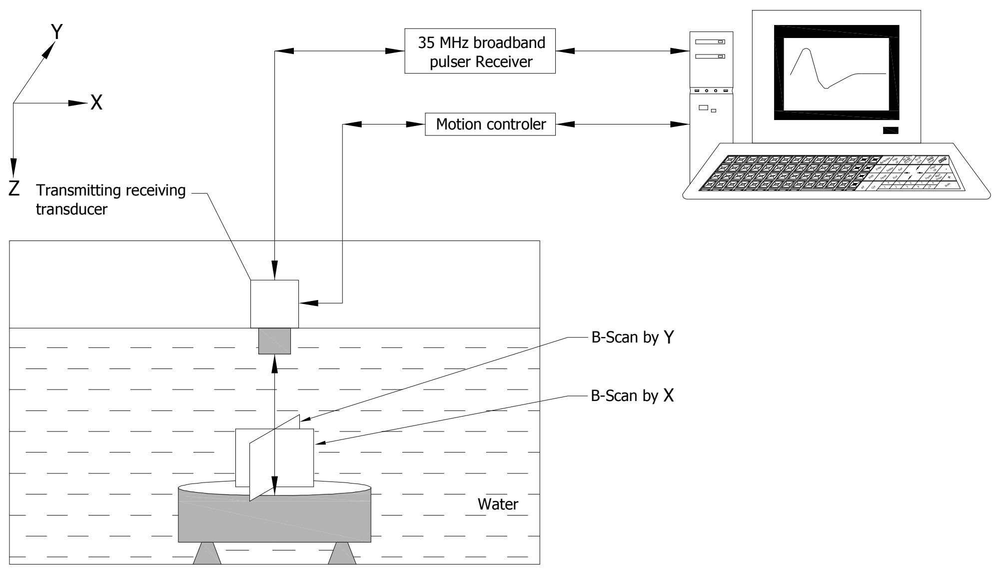

Fig. 3.1. Schematic of ultrasonic measurement set-up used for data acquisition.

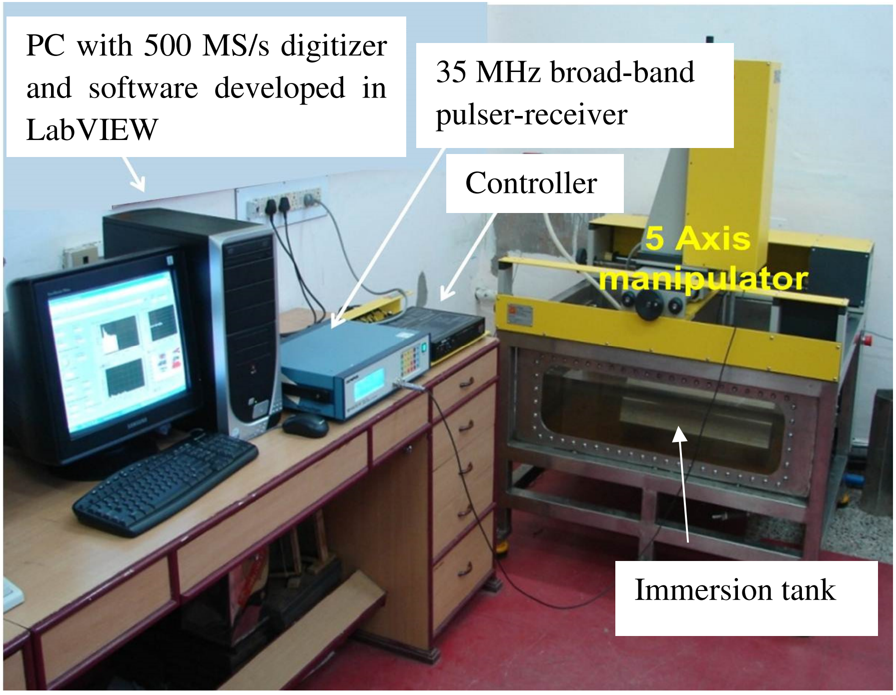

Fig. 3.2. Photograph of the experimental set-up.

3.3 Software for selection of window length for STFT

The determination of peak frequency at the back-wall or defect echo location by short time Fourier transform (STFT) is highly dependent on the window length. Therefore, it is essential to determine the optimum window length to process the ultrasonic signals with STFT. Software is developed in LabVIEW to monitor the peak frequency and -3 dB bandwidth of a signal from STFT with change in window size. Typical incremental variation of 64 data points (window length) was chosen to monitor the change in the peak frequency of the ultrasonic signal. The peak frequency and -3 dB bandwidth were also calculated using standard FFT algorithm. The results obtained from STFT and FFT were compared to make the optimisation process robust. The front panel of the developed program is given in Fig. 3.3. Detailed investigations were carried out to obtained spectral information of the ultrasonic echoes merged in backscatter, and the developed software has been used successfully.

3.3.1 Peak frequency estimation using STFT

An algorithm is developed to determine peak frequency information corresponding to peak echo location in the time domain signal by using STFT spectrogram. The software developed for peak frequency evaluation at the back-wall locations provides the vital input to understand the change in the spectral content of the ultrasonic signal.

3.4 Software for estimating pseudo peak frequencies of CWT

Since, the time-frequency resolution achieved by STFT is limited due to fixed window length, studies have been carried out to utilise parameters based on the continuous wavelet transform (CWT) based processing of ultrasonic signals. The ultrasonic signal has been normalised with respect to peak amplitude of the first back-wall echo signal for CWT analysis. The wavelet coefficients were obtained by CWT processing of ultrasonic waveforms obtained from specimens of different grain sizes. The wavelet coefficient up to 200 wavelet scales were obtained by using ‘Morlet’ wavelet. Further, the signal to noise ratio (SNR) was calculated for different wavelet scales. A specific software is developed to estimate SNR up to three back-wall echoes. The software was developed in LabVIEW using Matlab script mode for this purpose. The program requires start of the data, end of the data and individual back-wall echoes start and end positions. These values are fed manually. The range of data points between the back-wall echoes locations are assumed as backscatter locations. The high amplitude front surface reflection was not included for analysis. The data length up to three back-wall echoes was used for the calculation of SNR. The front panel of the developed LabVIEW program is given in Fig. 3.4.

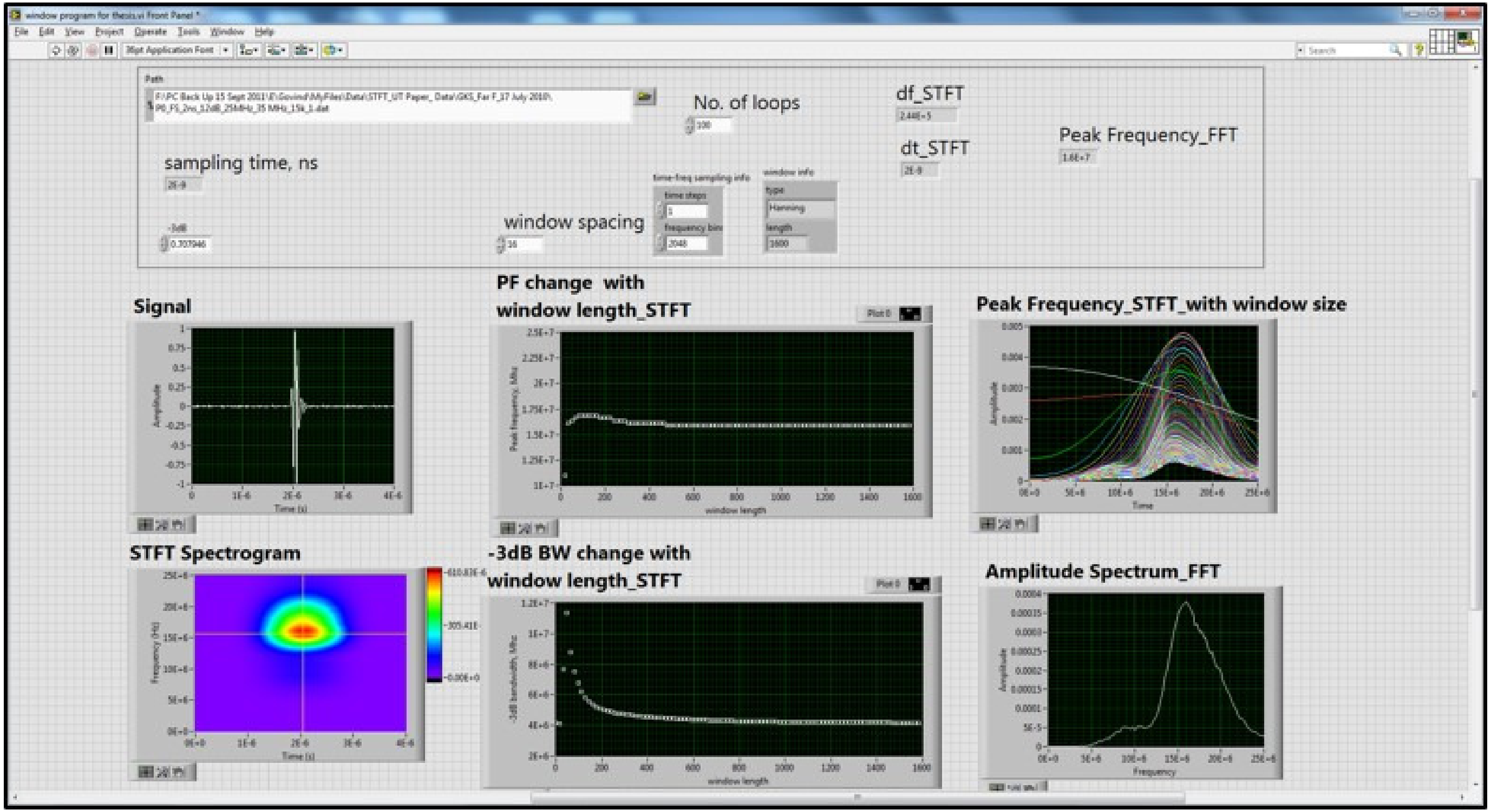

Fig. 3.3. Front panel of LabVIEW program developed for optimization of window length.

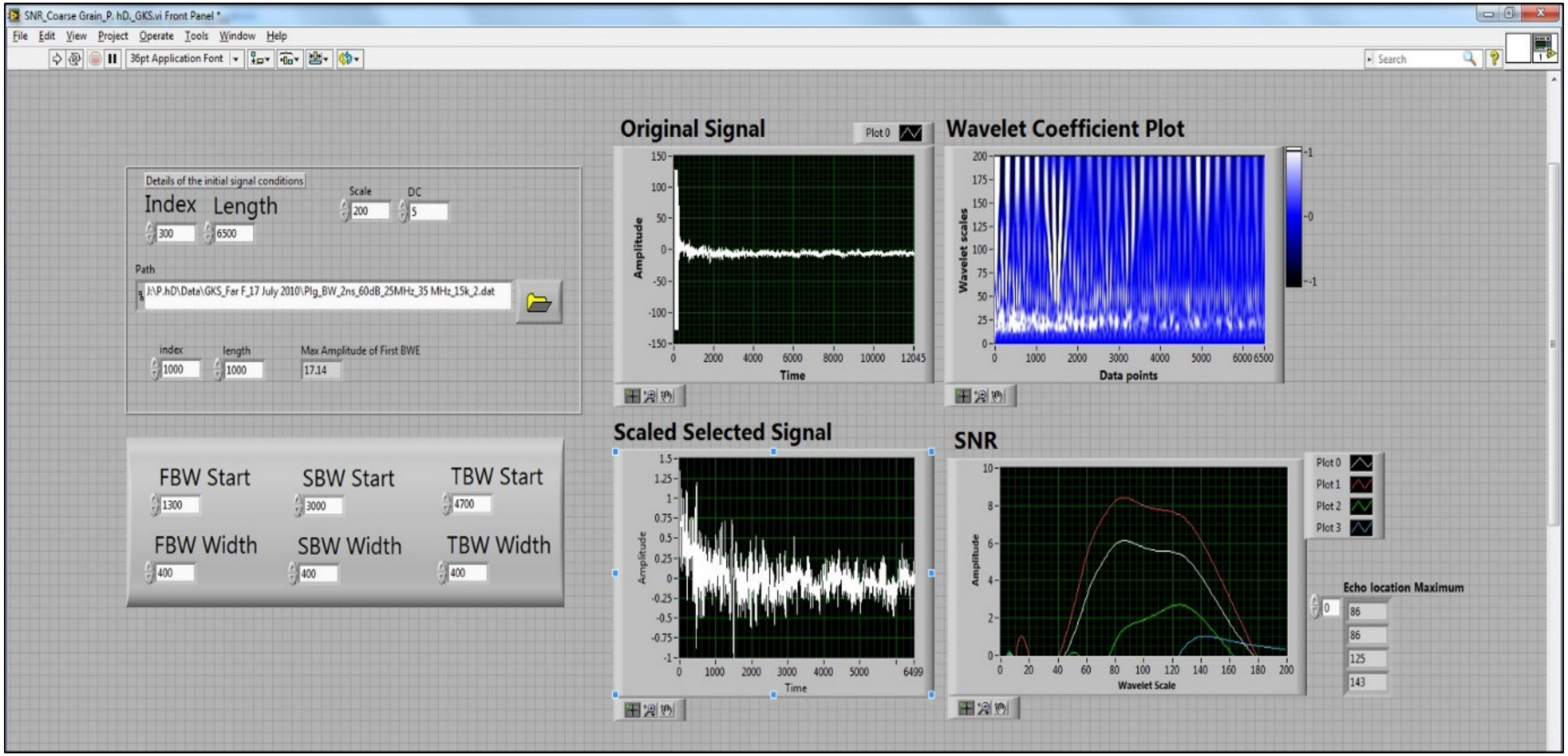

Fig. 3.4. Front panel of the LabVIEW software developed for calculating SNR of ultrasonic signal by considering the first three back-wall echoes.

3.5 Model based peak frequency estimation

The shift in ultrasonic peak frequency due to beam travel in coarse grain stainless steel is evaluated by STFT based approach reported in section 5.3.2 of the Chapter 5. The peak frequency shift obtained based on this approach is compared with that obtained from the mathematical model reported in the literature [90]. This model has been suitably modified to be used for our application by incorporating scattering induced attenuation.

Ophir et al. [90] have investigated the relationship between centre frequency downshift and transmitted bandwidth in tissue equivalent material by theoretical approach. The theoretical model proposed by them was used for a general case of frequency shift of a Gaussian pulse in an attenuating medium exhibiting nonlinear power law dependency on frequency. It was observed that a wideband ultrasonic pulse propagating through such a medium will suffer distortion due to the high rate of attenuation of its high frequency components. They have used this model for simple cases where close form solutions are available for lower orders ($n = 1$ and 2) [90]. However, for our requirement ($n = 4$), closed form solution is not available, hence, the solution was obtained by an iterative procedure. The details of the program developed for iterative solution of this problem is given in Appendix 3.1.

3.6 Algorithm for C-scan imaging using CWT approach

Software was developed in LabVIEW to generate C-scan images from the wavelet processed ultrasonic A-scans. Typical algorithm which has been used to process the ultrasonic signals obtained from coarse grained stainless steel specimens is shown in Fig. 3.5. This algorithm is similar to that being used for conventional C-scan imaging, where individual ultrasonic A-scans are processed to obtain amplitude and time of flight information of the gated regions. However, in the present study wavelet coefficients obtained by CWT processing of ultrasonic A - scans are used for imaging of defects, instead of ultrasonic A-scans.

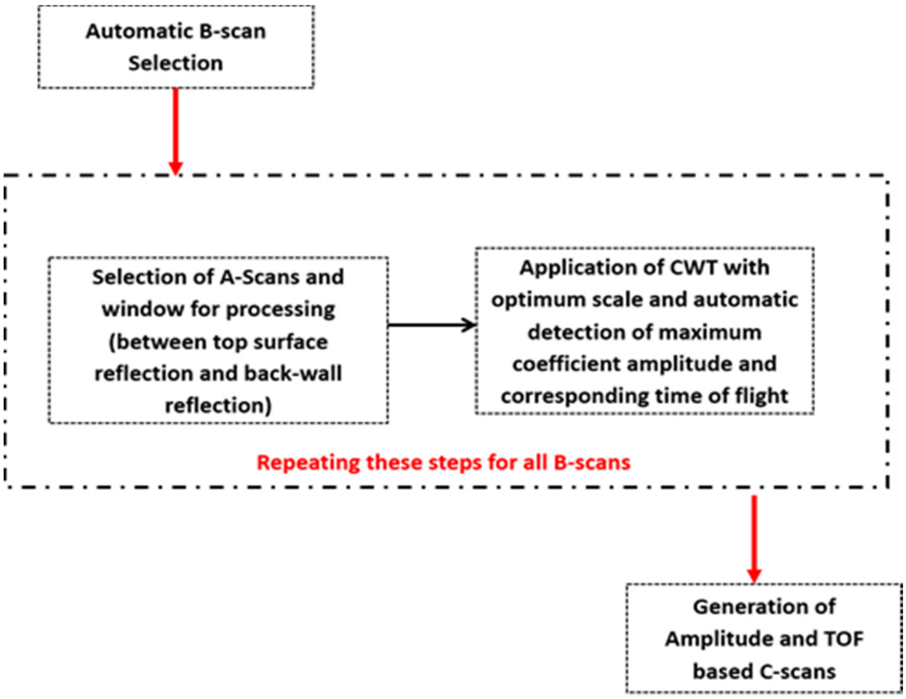

Fig. 3.5. Algorithm used to perform wavelet based C-scan imaging of defects in thick coarse grain austenitic stainless steel specimens.

Appendix 3.1

```
clear all; close all
Z=1:1:60; %total propagation distance of ultrasonic pulse in mm
e=length(Z);
d=zeros(1,e);

S=1.9e-14;      % scattering factor in µs^4/µm^4
GS=200*1.45; % Average grain size
HBW=2.93;     % Half band width of the transducer used in this study
sigma=HBW/2.36;
C=8*S*GS^3*sigma^2;

 for i=1:e
    s=@(f)C*Z(i)*2*1000*f^3 + f-9; % factor of 2 for pulse echo testing;
                                   % factor of 1000 to convert mm into µm

    d(i)=fzero(s,6);
end

plot(Z,d,'r')

PFS=d';  %Peak frequency shift calculated by the model


save ('d_200_Ophir.txt', 'PFS', '-ascii', '-tabs') %saving the data in ASCII format
```

Symbol	Physical meaning	Units
f_0	Incident frequency	MHz
f_c	Peak frequency after shift	MHz
n	Order	Number
D	Depth	mm
σ^2	Variance	MHz
d	Grain size	µm
S	Scattering factor	$\mu s^4/\mu m^4$

Chapter 4. Time-Frequency based Analysis for Understanding Frequency Dependent Attenuation and Quantitative Evaluation of Grain Size

4.1 Introduction

Grain size of a material is an important microstructural feature which influences the mechanical properties such as yield strength, creep and fatigue. Grain size has been widely used for monitoring product quality during manufacturing processes. AISI type 316 austenitic stainless steel is widely used as a structural material in nuclear power plants and petrochemical industries due to its high temperature mechanical properties and good corrosion resistance. Therefore, it is important to nondestructively characterise the microstructure (grain size) of this steel for quality control during fabrication and heat treatment to ensure the desired mechanical properties. This chapter deals with the understanding of the frequency dependent attenuation of ultrasonic waves and quantitative evaluation of grain size in austenitic stainless steel using time-frequency analysis approaches such as short time Fourier transform (STFT) and continuous wavelet transform (CWT).

The usefulness of STFT approach in extending the limit of grain size evaluation by conventional ultrasonic approaches is discussed in detail. A novel methodology developed in this study for selection of optimum window parameter for STFT has also been elucidated. The analysis of ultrasonic signals with STFT has fixed time and frequency resolution, therefore an advanced signal processing technique (i.e., CWT) is also used for the evaluation of grain size in austenitic stainless steel. The details of wavelet based pseudo frequency approach developed for grain size evaluation is discussed in detail. Finally, a comparative analysis is made between STFT and CWT based approaches for quantitative evaluation of grain size. For the first time, time-frequency analysis techniques have been used for microstructural characterization in the present study.

4.2 Experimental

4.2.1 Specimen preparation

The chemical composition of type 316 austenitic stainless steel used in the present study is given in Table 4.1. Specimen blanks of AISI type 316 stainless steel were obtained from bar stock material. These blanks were solution annealed at different temperatures varying from 1373 to 1623 K for different time durations ranging from 15 to 180 minutes followed by water quenching to obtain different grain sizes. Subsequently, all the specimens were given a common treatment at 1323 K for 30 minutes followed by quenching in water, in order to obtain a uniform structure with similar substructural features except the variation in the grain size [91]. Specimens of size 40 mm (L) × 30 mm (W) with 10 mm thickness were prepared from these specimen blanks to examine the effect of grain size on spectral content of the ultrasonic signal. Subsequently, surface grinding of the specimens was carried out to obtain plane parallelism to an accuracy of better than ± 3 μm.

Table 4.1. Chemical composition (wt%) of AISI type 316 austenitic stainless steel

Elements	C	Si	Mn	S	P	Cr	Ni	Mo	Fe
wt%	0.06	0.60	1.80	<0.01	0.034	16.36	12.1	2.2	Balance

4.2.2 Microstructural characterization

Optical metallographic examinations have been performed to examine the microstructure of the heat treated specimens. The specimens were prepared using standard metallographic technique by electrolytic etching with 60% nitric acid in water to reveal the grain boundaries. The linear intercept method as per ASTM standard E112–96 [92], was used to measure the average grain sizes of the specimens. The details of the heat treatments given and the grain sizes obtained are presented in Table 4.2. The typical micrographs of the specimens with different average grain sizes 30, 78 and 210 μm, respectively are shown in Fig. 4.1 (a-c).

Table 4.2. Details of the heat treatments given to AISI type 316 austenitic stainless steel specimens and the corresponding grain sizes obtained by metallographic examinations are presented.

Specimen Ref. No.	Heat Treatment**	Grain Size (μm)*
P0	As Received	30 ± 5
P1	1373K/1h/WQ	78 ± 5
P2	1373K/1.25h/WQ	83 ± 8
P3	1573K/1.5h/WQ	106 ± 10
P4	1623K/0.5h/WQ	121 ± 10
P5	1623K/1h/WQ	138 ± 15
P6	1623K/3h/WQ	210 ± 15

Note: WQ – Water Quench ** Followed by 1323 K/30 min/ WQ
* From optical metallography (ASTM standard E112-96)

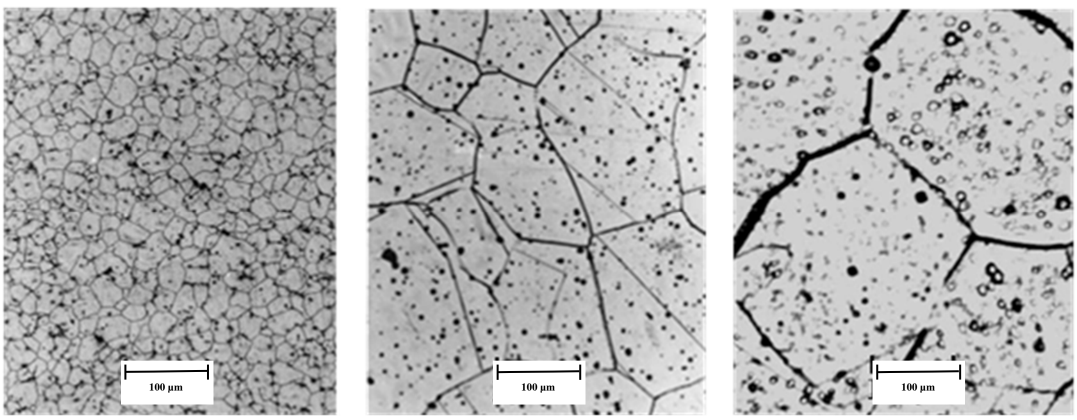

(a) (b) (c)

Fig. 4.1. Photomicrographs of the austenitic stainless steel specimens with different grain sizes (a) 30 μm, (b) 78 μm and (c) 210 μm.

4.3 Results and discussion

4.3.1 Short time Fourier transform

STFT is a widely used time-frequency tool for analysing ultrasonic signals. However, time and frequency resolutions in the STFT processed signal are governed by window length used. The time resolution increases with decrease in window length, but the frequency resolution decreases with decrease in window length and vice versa. The frequency resolution can be increased by zero padding, however, a shorter window length leads to spectral leakage. In view of this, it is essential to devise a suitable procedure for the optimisation of window length to obtain meaningful information with STFT processing. A methodology has been developed in the present study to determine the optimum window length for STFT processing, and this is discussed in detail in section 4.3.1.1.

4.3.1.1 Optimisation of window length for STFT analysis

A novel approach for the optimization of window length has been devised in this study. The proposed approach makes use of a reference signal for this purpose. The A - scan signal (one dimensional) obtained from the water-specimen surface reflection was processed with STFT for different Hamming window lengths to generate spectrograms. The changes in the spectral content and -3 dB bandwidth values of the ultrasonic signal were obtained from spectrograms generated with corresponding window lengths automatically using a software developed in LabVIEW. The details of the LabVIEW program are given in Chapter 3. The maximum amplitude peak location of the time domain signal was used as a reference to obtain peak frequency information by STFT processed signals. The comparison of the STFT and fast Fourier transform (FFT) based results has been used to determine the optimum window length.

In the literature, the optimum window length has been chosen based on theoretical approach, where a prior knowledge of the measurements system characteristics are needed [66]. However, the proposed methodology is based on comparative studies between STFT and FFT based measurements without taking into account the prior information of the measurement system. The comparative approach proposed in this study makes the window optimisation process easy and robust. A typical top surface ultrasonic signal acquired from front surface of a 30 μm grain size specimen using a 25 MHz nominal frequency transducer has been used as a reference signal and this is shown in Fig. 4.2. The signal was time averaged 100 times to avoid random noise. The signal has been chosen with good SNR to avoid any ambiguity due to presence of other frequency components. The amplitude spectrum of the reference ultrasonic signal obtained by FFT is shown in Fig. 4.3.

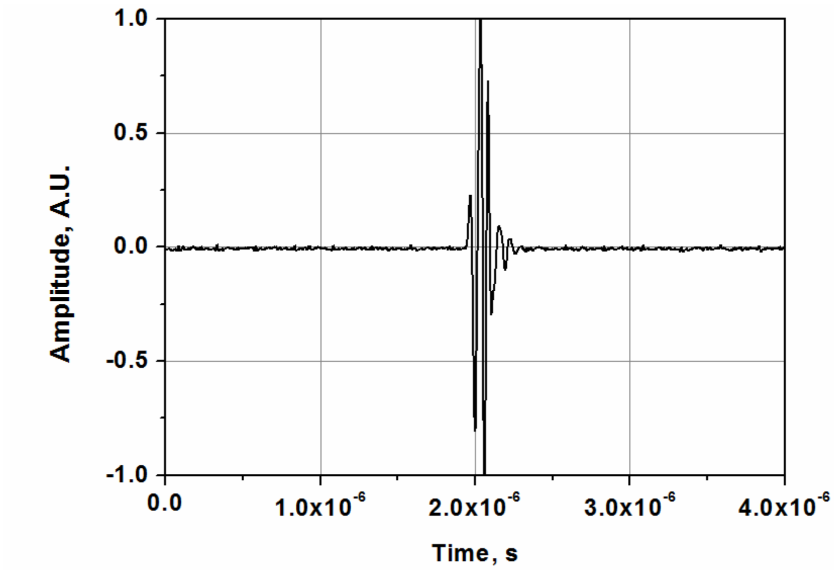

Fig. 4.2. Ultrasonic signal acquired from top surface (water - specimen interface) of 30 μm grain size specimen in immersion mode.

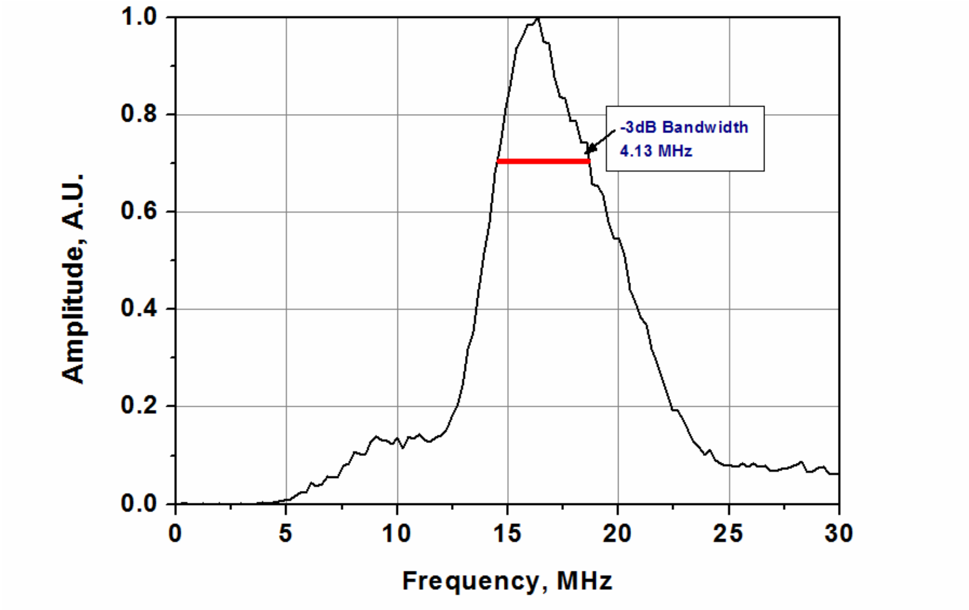

Fig. 4.3. The amplitude spectrum of the reference signal evaluated by FFT (peak frequency ~15.9 MHz and -3 dB bandwidth ~4.13 MHz).

A typical increase in the window length with multiples of 64 data points is used to monitor the change in the spectral distribution of the ultrasonic signal by STFT processing. The typical change in the spectral distribution with window lengths is shown in Fig. 4.4. It can be observed that with increase in the window length, bandwidth of the spectral distribution decreases and peak frequency can be determined with better accuracy.

The variations in the peak frequency and -3 dB bandwidth of the signal with window length are shown in Fig. 4.5. It can be noticed from Fig. 4.5 that, with increase in the window size from 0.2 to 2.5 µs, the peak frequency decreases from 16.8 MHz to 15.8 MHz and the -3 dB bandwidth decreases from 5.8 MHz to 4.2 MHz. For the window lengths of more than 1.024 µs (512 data points), the peak frequencies and the – 3 dB bandwidths obtained from STFT are comparable to those obtained from the FFT of selected echo as shown in Fig. 4.3.

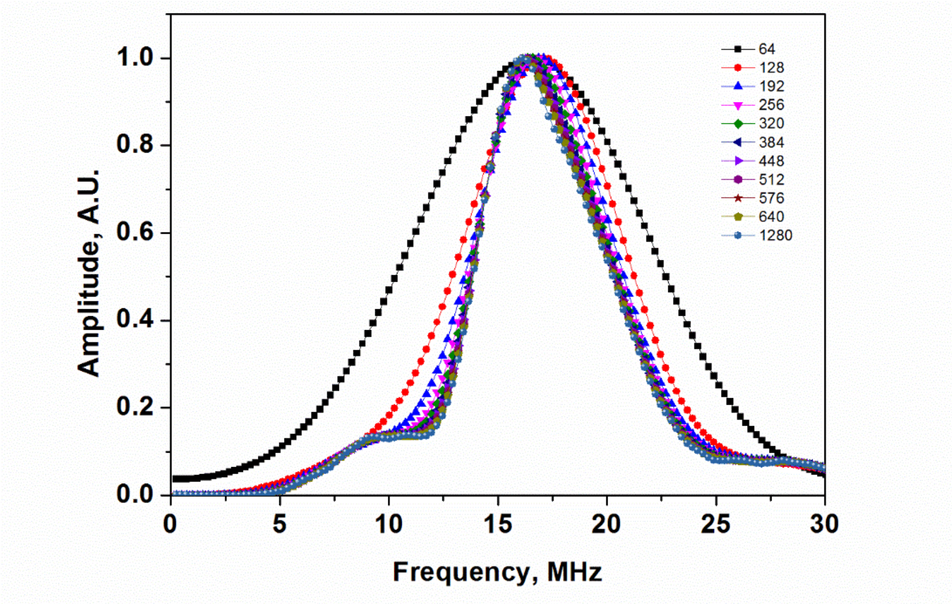

Fig. 4.4. Typical variation in the peak frequency with increase in window length from 64 to 1280 data points (0.12 μs to 2.5 μs) calculated using STFT of the reference signal. The frequency resolution increases with increase in the window length which can be clearly observed by better localisation of peak frequency and decrease in the bandwidth of the processed signal.

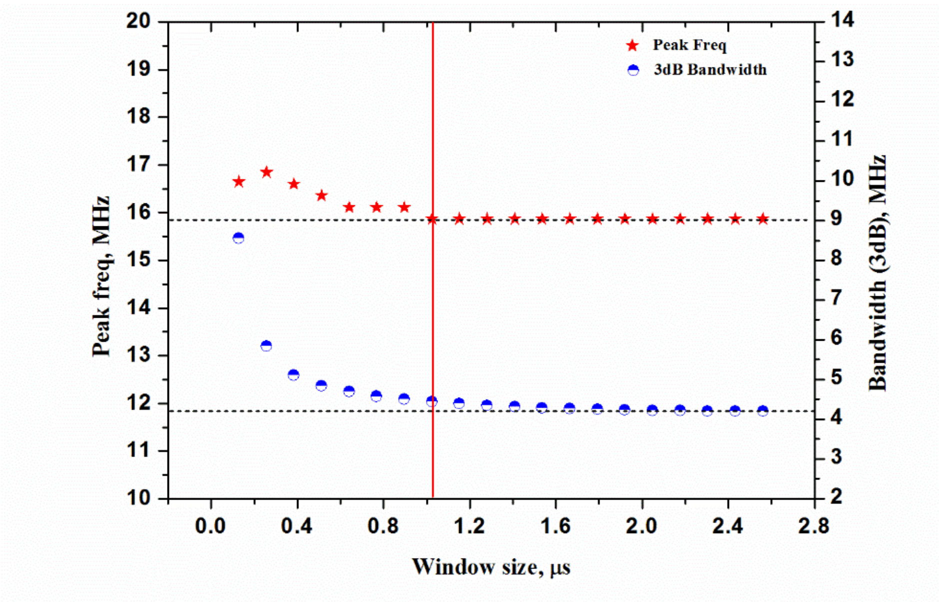

Fig. 4.5. Effect of time window size for generating spectrogram on the measured peak frequency and -3 dB bandwidth. Dotted lines show peak frequency and -3 dB bandwidth obtained by FFT. (The results are shown for the top surface echo of specimen with 30 μm grain size, for which the centre frequency and -3 dB bandwidth were measured to be 15.9 MHz and 4.13 MHz, respectively).

Based on the analyses performed, a window length of 1.024 μs (512 data points) has been selected for STFT analysis of all the ultrasonic signals used in the present study. This optimization makes selection of time window objective, robust and totally automatic. The selection alleviates and reconciles the trade-offs regarding the spectral leakage (because of too small time window), and vague target of interest (because of too large time window) in STFT spectrogram. The A-scan (one dimensional) signals corresponding to different grain size specimens were normalised with respect to the peak amplitude of the first back-wall echo signal and windowed with a continuously moving Hamming window of 1.024 μs (512 data points) length. The maximum and minimum frequencies corresponding to backscatter are calculated by analysing the spectrograms. Average of five readings for the peak frequency is obtained for each specimen. The maximum scatter in the measurement of peak frequency is ± 0.20 MHz for all the specimens at the back-wall echo locations.

4.3.1.2 Frequency dependent attenuation analysis using STFT

Typical RF ultrasonic signal obtained from the specimen with an intermediate grain size (121 μm), and its spectrogram with optimum window size are shown in Fig. 4.6 (a) and (b), respectively. The spectral content at the cursor location in the spectrogram is shown in Fig. 4.6 (c). It can be seen from Fig. 4.6 (a) that the backscatter amplitude during the water path (before the front surface reflection) is negligible. However, as the beam enters into the material, a sudden increase in the backscatter amplitude can be observed clearly after the water-specimen interface echo. By careful observation of the spectrogram, it can be noticed that the peak frequency of the first back-wall echo is ~7 MHz followed by a successive decrease for the multiple back-wall echoes. The typical attenuation pattern of the back-wall echoes can be visualised from the spectrogram. However, the backscatter shows a band of frequencies (14-24 MHz), whose spectral content is less affected with ultrasonic wave propagation. The frequency content of the ultrasonic signal at back wall and backscatter can be simultaneously visualised by spectrogram with time information. This demonstrates the superiority of this time-frequency analysis method for the analysis of non-stationary ultrasonic signals obtained from coarse grained austenitic stainless steel. The frequency information available with spectrogram can be extracted by moving the cursor manually (shown in red colour in Fig. 4.6 (b)) or user defined algorithms for automated measurements. The change in the spectral content of the first three back-wall echoes of the ultrasonic A-scan signal obtained by STFT spectrogram for an intermediate grain size (121 μm) specimen is shown in Fig. 4.7. This figure clearly shows that amplitude of the back - wall echoes decreased and the amplitude spectrum shifted marginally towards lower frequency with increasing propagation distance (second and third back-wall echoes) of ultrasonic wave.

Fig. 4.8 (a) and (b) show a typical RF ultrasonic signal obtained from 210 μm grain size specimen and its STFT spectrogram, respectively. The spectral content at the first back-wall location corresponding to cursor location in spectrogram is shown in Fig. 4.8 (c). It can be clearly noticed from the time domain signal Fig. 4.8 (a) that the back-wall echo signal is completely merged into the backscatter noise and it is difficult to extract meaningful information by the time domain analysis. But careful observation of the spectrogram indicates strong amplitude peak for ~5 MHz frequency at first back wall echo location and a feeble reflection at second back-wall echo location. The backscatter frequency content is similar to that observed in the spectrogram of the ultrasonic signal obtained from 121 μm grain size specimen as shown in Fig. 4.6.

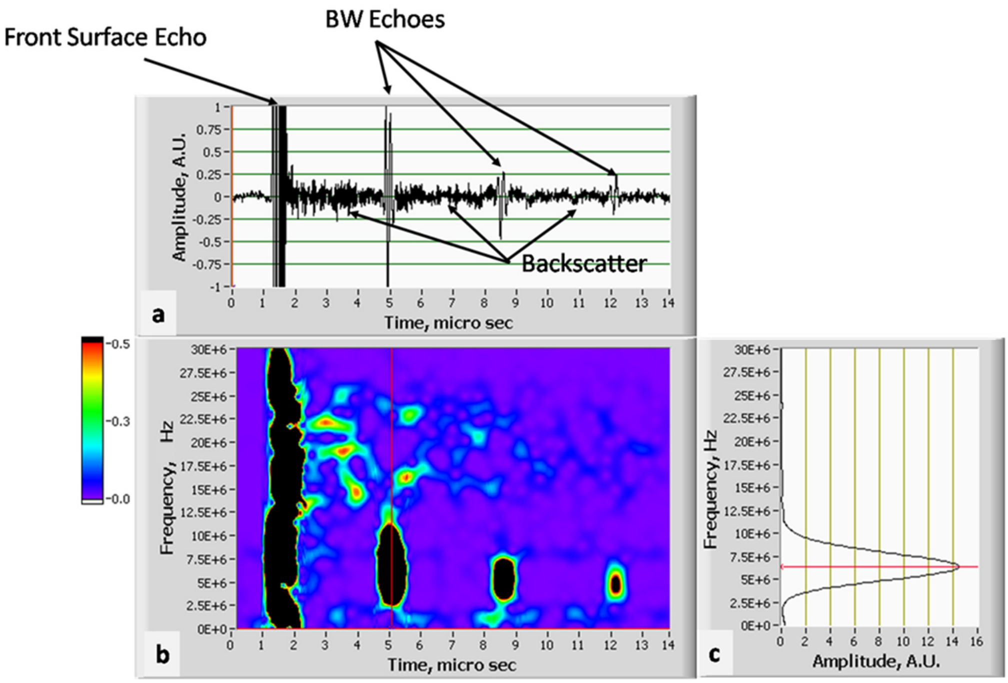

Fig. 4.6. (a) Time domain ultrasonic signal from the specimen of 121 μm grain size (obtained by 25 MHz unfocussed transducer), (b) its spectrogram and (c) frequency content of first back-wall echo peak location by STFT (typical at cursor location, shown in red colour).

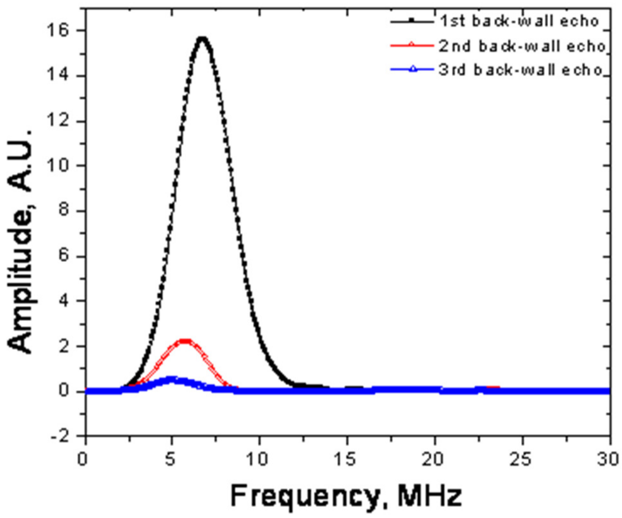

Fig. 4.7. The spectral content of the first three back wall echoes obtained by STFT processing of ultrasonic A-scan signal obtained from 121 μm grain size specimen.

The typical backscatter analysis by the STFT spectrograms for ultrasonic signals obtained from different grain size specimens shows that the frequency content of the backscatter varies in the range of 14-24 MHz for all the specimens. However, the peak frequency of the first back-wall echo is much lower as compared to the peak frequency of the front surface reflection (~16 MHz) and decreases with increasing grain size. With increase in the grain size, the amplitude of the backscatter increases and the amplitude of the back-wall echoes decreases. The observed response is attributed to the enhanced scattering of the ultrasonic beam with increase in grain size.

The effect of grain size on the peak frequencies of the front surface (FS) echo, first three back-wall echoes, spectral content of backscatter for all the grain size specimens (30-210 μm) obtained from the STFT spectrograms is illustrated in Fig. 4.9. As multiple peaks were observed in the spectra of the backscatter, providing a single peak frequency would be misleading, therefore a range of frequencies is shown for the frequency content of the backscatter signal. This range has been qualitatively evaluated from the spectrograms of the ultrasonic signals obtained from each grain size specimen. The details of the peak frequency values obtained by the application of STFT on experimentally obtained A-scan signals are listed in Table 4.3.

.

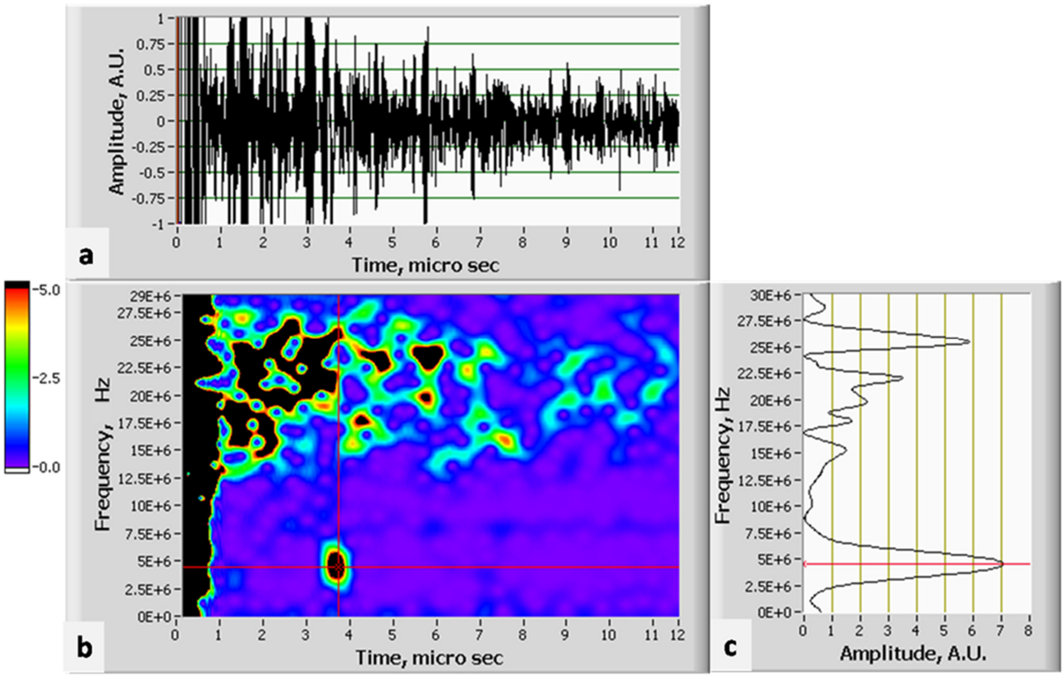

Fig. 4.8. (a) Ultrasonic time domain signal obtained from a 210 µm grain size specimen, (b) its spectrogram and (c) frequency content of first back-wall at cursor location.

Table 4.3. Details of ultrasonic peak frequencies obtained by STFT at the front surface (FS), first back-wall (FBW), second back-wall (SBW) and third back-wall (TBW) echo signals in different grain size specimens.

Specimen Ref. No.	Grain Size (µm)	Peak Frequency, FS (MHz)	Peak Frequency, FBW (MHz)	Peak Frequency, SBW (MHz)	Peak Frequency, TBW (MHz)
P0	30	15.6	15.2	14.8	14.7
P1	78	15.9	8.56	7.88	7.23
P2	83	16.1	8.33	7.61	6.9
P3	106	16.1	7.08	6.23	5.71
P4	121	15.6	6.51	5.45	4.61
P5	138	16.1	6.12	4.93	4.59
P6	210	16.1	4.46	3.63	**

** The third back-wall echo information could not be obtained for 210 µm grain size specimen

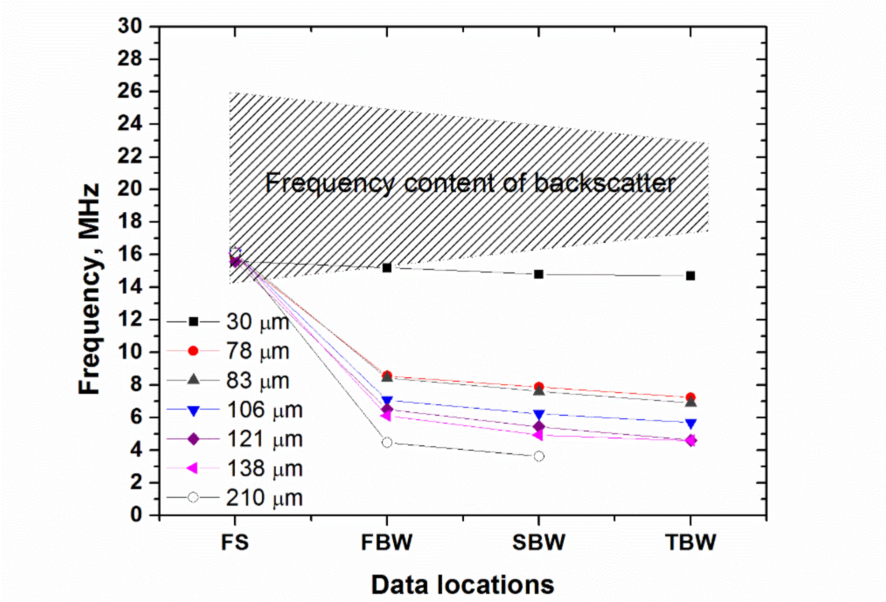

Fig. 4.9. Variation in the peak frequencies of front surface (FS) reflection, first back-wall (FBW), second back-wall (SBW) and third back-wall (TBW) echoes and spectral distribution of the backscatter estimated using STFT for different grain size specimens is illustrated.

It can be seen clearly from Fig. 4.9 that sharp decrease in the frequency content of the incident frequency takes place, when the beam enters into the medium. The frequency content of the subsequent back-wall echoes also decreases rapidly with increasing grain size. However, the maximum backscatter frequency decreases slowly as compared to the frequency of the back-wall echoes. As reported by Nagy et al. [46], the backscatter signal is much less attenuated by scattering than the transmitted coherent wave. This hypothesis was demonstrated by ultrasonic experiments conducted on specially designed specimens. However, the spectral content of the backscatter and back-wall echo can be pictorially visualised by processing a single A-scan signal with STFT.

The scattering in polycrystalline materials is dominated by Rayleigh scattering when the wavelength of the ultrasonic waves (λ) is greater than the grain size (d). In the present study, the ratio of the grain size to the wavelength lies in the range of

0.08 to 0.55 (V = 5750 m/s, λ = 360 μm for 16 MHz centre frequency and *d* in the range of 30 to 210 μm) indicating Rayleigh scattering is predominant.

At the water-steel interface, a high frequency ultrasonic beam (~16 MHz centre frequency) enters into the material. As the scattering is a function of the fourth power of the frequency in the Rayleigh scattering regime ($\alpha_s = S\, d^3.f^4$), the higher frequency components of the signal get preferentially scattered in all directions. The high frequency backscattered energy is received by the transducer and comparatively lower frequency beam continues to propagate deeper into the material and return to the transducer as a low frequency back-wall echo. This explains the higher frequency content of the backscatter and lower frequency content in the back-wall echo. The high frequency scattered energy keeps returning to the transducer due to multiple scattering and reflections of the originally scattered energy from the grains and the specimen boundaries in the direction of the transducer, until they are totally lost in the material due to absorption phenomena. As the absorption phenomena are weak functions of the frequency (as compared to the Rayleigh scattering), the decrease in the frequency content of the backscatter signal is much smaller. This explains the high frequency content (14-24 MHz) of the backscatter even upto the time path of the third back-wall echo. Further, the decay rate of the backscattered signal is observed to be really same for all the specimens having grain size in the range of 30-210 μm. This arises from the fact that the dislocation substructure is expected to be similar [32], due to same final heat treatment given to all the specimens.

The effect of the grain size on the frequency content of the back-wall echoes can also be understood by the spectral analysis of the attenuating ultrasonic wave. It can be assumed that the oscillatory amplitude decays exponentially as the propagation length of the ultrasonic wave increases. If we consider the spectral distribution of the ultrasonic wave, which has an oscillatory pulse of one or two cycles with an exponential decay envelope, the amplitude of the ultrasonic wave g(t) is expressed as [54]

$$g(t) = A\, e^{-\alpha t}\, Sin\,(2\pi f_0 t - \phi) \qquad \phi/f_0 < t < 2 + \phi/f_0 \qquad (4.1)$$

where α is the attenuation coefficient, t is the time, f_0 is the carrier frequency, ϕ is the phase and A is the maximum amplitude of the pulse wave. The spectrum power distribution $|G(f)|^2$ is derived by Fourier transform [54] as

$$|G(f)|^2 \propto \frac{1+\exp(-2\alpha/f_0) - 2\exp(-\alpha/f_0)\cos 2\pi (f - f_0)/f_0}{\alpha^2 + 4\pi^2 (f - f_0)^2} \qquad (4.2)$$

In austenitic stainless steel, more than 95 % of the total attenuation is caused by the scattering [32], therefore α in Eq. 4.2 can be replaced by $\alpha_s = S\, d^3.f^4$. As the grain size increases, α_S increases as a function of its third power (Eq. 4.2). With increase in α_s, the peak frequency of the autopower spectrum shifts to lower values due to the fourth power dependence of α_s on frequency. Because of this, the peak frequency shifts towards lower values with increase in the grain size.

4.3.1.3 Quantitative evaluation of grain size using longitudinal waves

The grain size has been correlated with peak frequency of the autopower spectrum of the first back-wall echo [22]. The peak frequency in this study was linearly correlated with inverse of the square root of grain size. Even though the peak frequency could be correlated with the grain size effectively for smaller grain sizes, unambiguous determination of the peak frequency would not be possible in the specimens with larger grain sizes (>140 μm) due to poor SNR. This can be noticed in Fig. 4.8 (a) that the back-wall echo is completely submerged in the backscatter due to high scattering in the large grain size (210 μm) specimen. The back-wall echo can neither be distinguished in the time domain nor in the frequency spectrum. However, the back-wall echo even with a poor SNR in the time and frequency domains stands out clearly in the spectrogram (Fig. 4.8 (b)). Using spectrogram, it can be clearly understood that the lower frequency peak in the frequency spectrum (Fig. 4.8 (c)) arises from the back-wall echo, while the higher frequency peaks results from backscatter. The simultaneous availability of time and frequency contents of the signal processed by STFT facilitates better localization of back-wall echo position in a noisy signal. This demonstrates the advantage of the joint time-frequency analysis based approach over conventional frequency spectrum based analysis for microstructural characterization.

The peak frequency of the higher order back-wall echoes could also be determined unambiguously using STFT analysis. The inverse square root of the grain size is correlated with the peak frequency of the first, second and third back-wall echoes obtained by STFT and this is shown in Fig. 4.10. The variations in the peak frequency of the first three back-wall echoes exhibited linear relationships with $d^{-1/2}$ as

$$\left.\begin{array}{ll} PF_{FBW} = -2.0 + 2.97\, d^{-1/2} \quad (R = 0.97) & (4.3) \\ PF_{SBW} = -3.45 + 3.15\, d^{-1/2} \quad (R = 0.97) & (4.4) \\ PF_{TBW} = -4.72 + 3.35\, d^{-1/2} \quad (R = 0.96) & (4.5) \end{array}\right\} \text{Valid for real values of peak frequency}$$

where, PF_{FBW}, PF_{SBW}, and PF_{TBW} are the peak frequencies of the first, second and third back-wall echoes, respectively and d is the average grain size measured by metallography technique. The slope of the above correlation increases from the first to the third back-wall echo, this indicates that the sensitivity of the spectral peak frequency based methodology for grain size measurement improves with increasing wave-material interaction distance. The extrapolated fitting curves for the three different back-wall echoes will cut the abscissa at different points. These points correspond to 2700 μm (for FBWE), 850 μm (for SBWE) and 510 μm (TBWE). These indicate the theoretical limit of grain size measurement using the different back-wall echoes (Eq. 4.3 – 4.5) with present experimental set up.

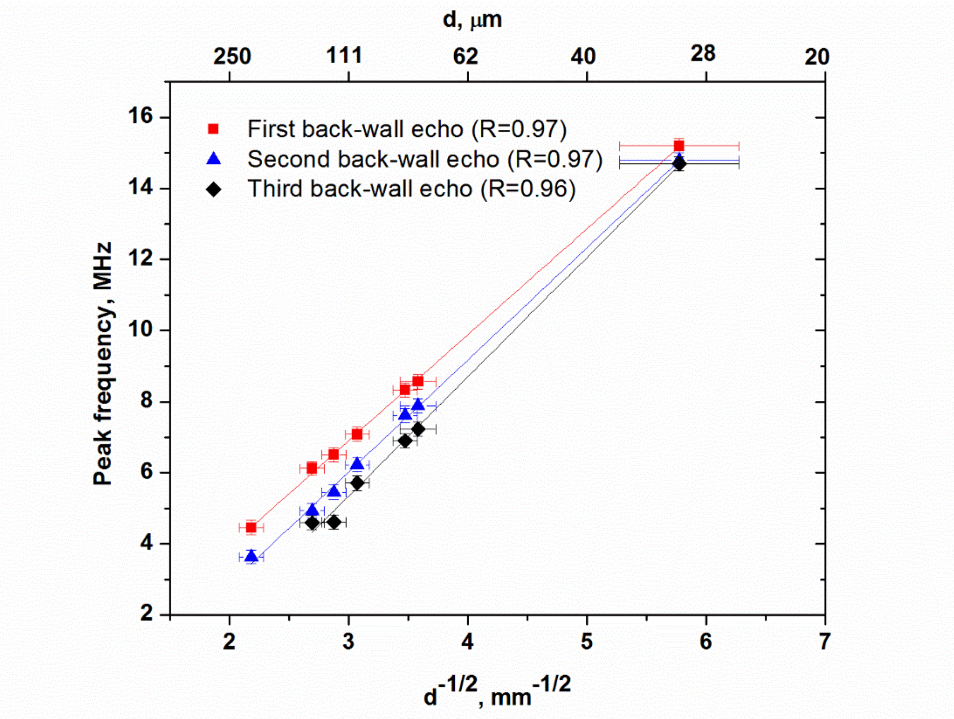

Fig. 4.10. Peak frequencies of first, second and third back-wall echo locations obtained by STFT processing of ultrasonic signals showed a linear correlation with the grain size parameter ($d^{-1/2}$).

Different approaches have been used to correlate ultrasonic scattering with grain sizes. The methods based on ultrasonic scattering showed the increase in the ultrasonic attenuation with increase in the grain size [93]. However, the spectral analysis based methods showed the downward shift in the peak ultrasonic frequency with increase in grain size [47, 54]. The inverse relationship observed by the spectral analysis based approaches is found to be valid in this study also.

4.3.1.4 Quantitative evaluation of grain size using shear waves

In the previous section (4.3.1.3), it has been observed that with the increase in grain size, the higher frequency components of the longitudinal ultrasonic beam gets more scattered as compared to the low frequency components. In this section, the influence of different grain sizes on the spectral content of shear waves is explored. Ultrasonic shear waves are popularly used for inspection of components. Generally, the angle beam inspection is carried out using 45° shear wave. The angle beam shear wave is generated by the principle of refraction and the angle of incidence in material is governed by Snell's law. The shear waves undergo larger attenuation than the longitudinal waves [29]. Hence, the ultrasonic transducer of 10 MHz frequency has been used. The specimens of 10 mm thickness with different grain sizes were used to acquire the ultrasonic signals. The details of heat treatment and grain size in these specimens are given in Table 4.2. To avoid the coupling and pressure variations, immersion measurements were carried out. The transducer was kept at ~19.6° angle with respect to the specimen normal for generating 45° shear waves in the specimen. A typical sketch for data acquisition is shown in Fig 4.11.

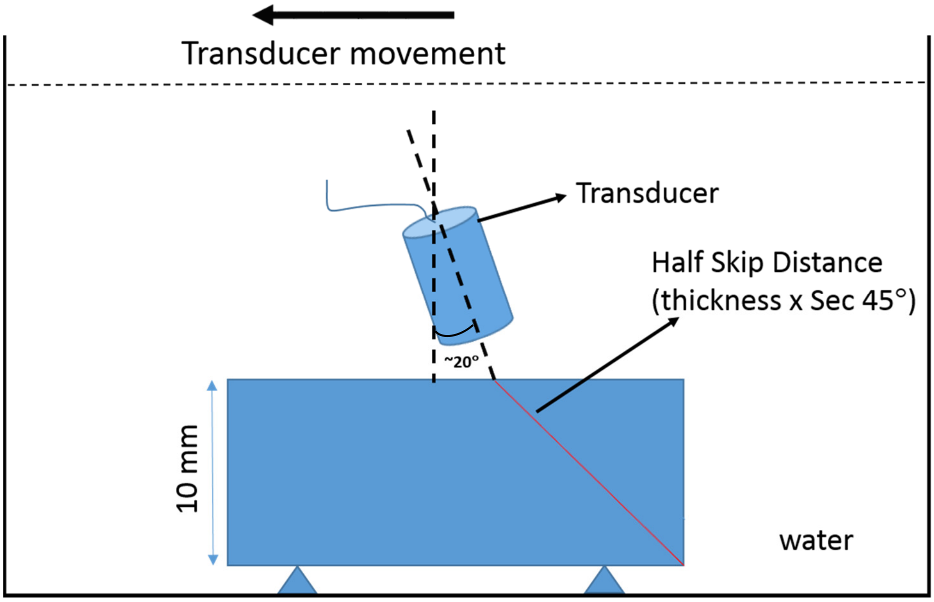

Fig 4.11. Experimental set up used to acquire corner reflection using shear wave

Ultrasonic reflection from the specimen corner acquired at half skip distance (~ 14 mm) was used for analysis. To avoid ambiguity in the corner reflection, ultrasonic B-scans were acquired. A typical B-scan image acquired from 106 µm grain size specimen is shown in Fig. 4.12 (a). It can be observed from the B-scan that with the transducer scanning, shear wave signals at multiple skip distances are also acquired. However, to avoid mode converted echoes corner signal of maximum amplitude at half skip distance is only used for analysis. The ultrasonic radio frequency signal at the maximum amplitude location is used for frequency analysis.

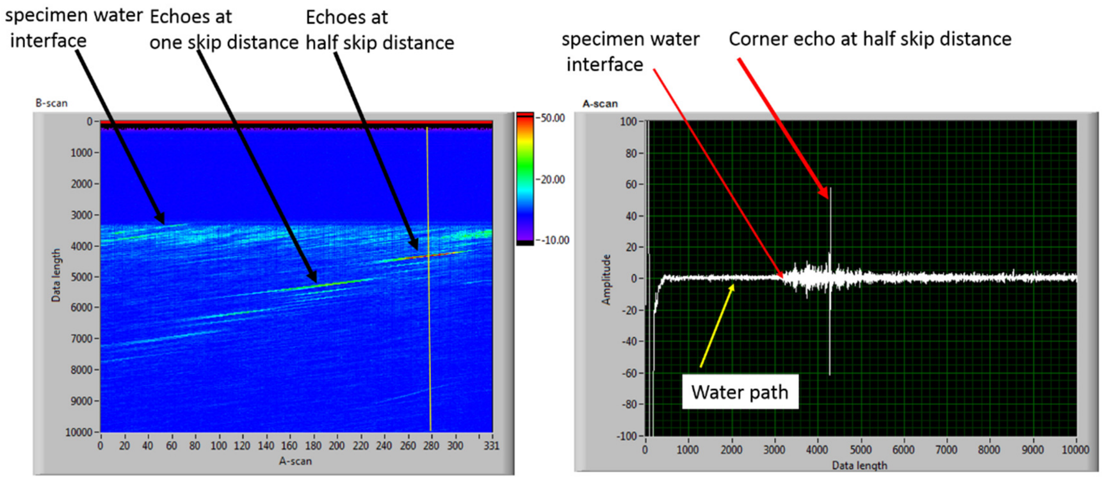

(a) (b)

Fig. 4.12. Typical angle beam B-scan image showing corner reflections at multiple skip distances and (b) radio frequency signal at the half skip corner reflection from a specimen of 106 µm grain size.

The ultrasonic waveform comprising of water steel interface reflection, the back-scattered shear waves and a high amplitude corner reflection from half skip distance can be clearly observed in Fig. 4.12 (b). The frequency analysis of corner reflections from the specimens of different grain sizes was carried out using STFT based methodology discussed in the previous section. The measured peak frequencies in the corner reflection (PF_{CR}), for different grain size specimens showed linear relation with $d^{-1/2}$ (Fig. 4.13), as observed for the longitudinal waves in previous section (4.3.1.3). The variation in the PF_{CR} exhibited linear relationship with $d^{-1/2}$ as

$$PF_{CR} = -4.0 + 2.34\, d^{-1/2} \quad (R = 0.99) \qquad (4.6)$$

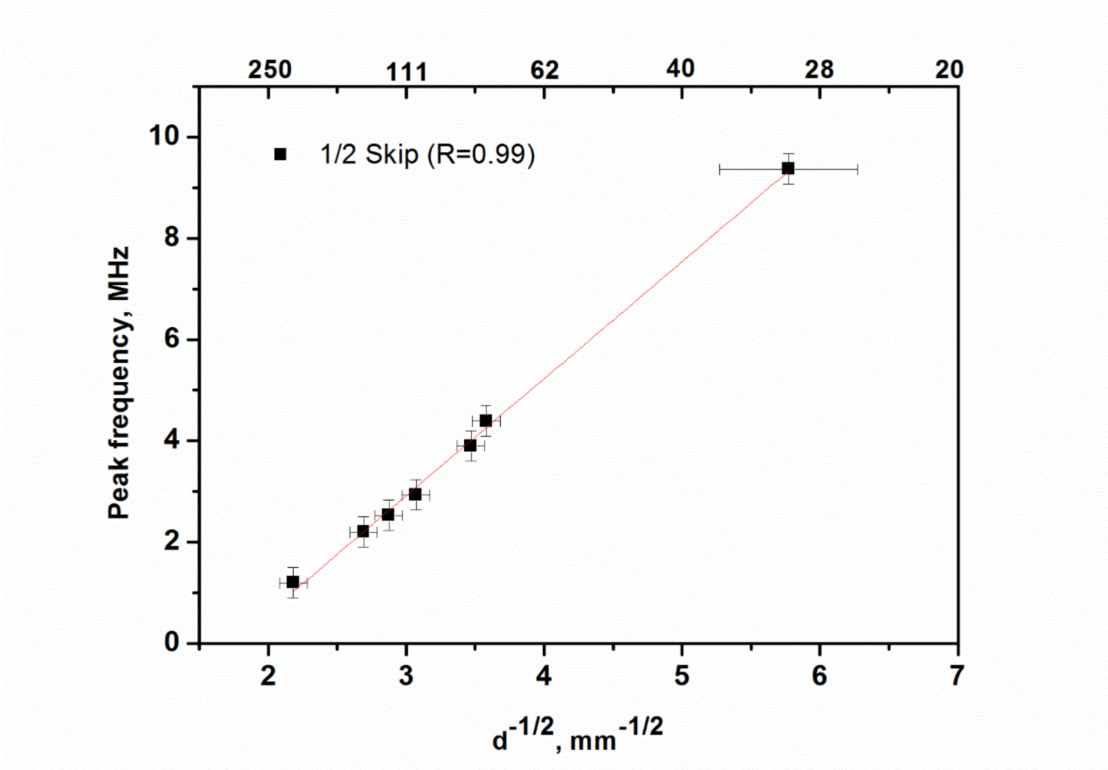

Fig. 4.13. Correlation between peak frequency of shear wave signal from corner reflection and grain size parameter.

The results presented in this section clearly demonstrate that the shear waves also exhibits the phenomenon of downward shift in peak frequency of a specular reflection with increasing frequency dependent attenuation, similar to the longitudinal waves as discussed in the previous section. This clearly demonstrates that, frequency shift based methodology can also be used for analysis of shear wave signals. In the later sections of the thesis, only ultrasonic longitudinal wave signals are analysed. However, the results obtained and discussion will also be valid for shear wave inspection.

4.3.1.5 Conclusions from STFT analysis

- ❖ The short time Fourier transform has been established as a useful tool for microstructural (grain size) characterization applications. This is the first of its kind attempt for the characterization of microstructure using time-frequency approach.

- A novel scheme for optimization of window parameter for STFT is proposed in this study. The optimization of window length based on comparative analysis of STFT and FFT parameters makes this approach robust.
- The spectral content of the ultrasonic signals obtained from coarse grained steels can be analyzed visually in STFT spectrogram, and this has been effectively utilized to analyze the absorption and scattering phenomena simultaneously.
- Using the STFT analysis, it is demonstrated that the limit of grain size characterization using spectral analysis approach can be extended, as this approach could extract reliable frequency information of the ultrasonic back-wall echoes buried in the backscatter.
- The peak frequency values up to three back-wall echoes could be obtained for a range of grain sizes (30-210 µm) using STFT based approach. The variation in the peak frequency of the multiple back-wall echoes exhibited linear relationship with $d^{-1/2}$. The slope of this correlation showed increasing trend from first to third back-wall echoes, which indicated the increased sensitivity of the spectral peak frequency based methodology for grain size measurements. This increased sensitivity has been attributed to extended wave-material interaction.
- The peak frequency obtained from corner echoes of different grain size specimens obtained by using shear waves (45°) also showed linear relationship with $d^{-1/2}$. Hence, the frequency based methodology developed in this study can be successfully used for both longitudinal and shear wave modes.

4.3.2 Continuous wavelet transform

As discussed in the previous section, the STFT based approach has been established as an efficient tool for microstructural characterisation. The optimum window selection procedure has also been standardised. However, the time-frequency resolution achieved by STFT is limited by the window size chosen for the entire analysis. This demands the analysis of the signals with advanced signal processing technique where resolution is not limited by fixed window size. The continuous wavelet transform is an advanced signal processing tool, which has been widely used for processing of ultrasonic signals [7, 72]. The signal can be analysed at different frequencies with variable resolutions. Every spectral component is not resolved equally by CWT as achieved in STFT. The wavelet method is designed to give a combination of good time resolution with poor frequency resolution at high frequencies and good frequency resolution with poor time resolution at low frequencies. The details of the CWT based pseudo frequency approach for evaluation of grain size is discussed in section 4.3.2.1, followed by a comparative examination of the results obtained by STFT and CWT based processing.

4.3.2.1 Optimization of mother wavelet

The choice of wavelet is dependent on the shape of the signal being analyzed. In order to evaluate the capability of different wavelets popularly used for enhancement of SNR for the ultrasonic signals, a comparative study is made. The enhancement of SNR obtained by processing of an ultrasonic signal by popularly used wavelets such as ‘Morlet’, ‘Daubechies’ (db8), ‘Symlet’ (sym5) and ‘Haar’ is compared. The ultrasonic back-wall reflection from a 210 μm grain size specimen has been used for this study. Other than ‘Haar’ all the other wavelets show comparable SNR enhancement as shown in Fig. 4.14. In the literature, 'Morlet' wavelet has shown a Gaussian distribution in the frequency domain [94], and is known to give more accurate results than other wavelets, since the shape of the ultrasonic excitation input is similar to the shape of this wavelet basis function [95]. In view of this, in the present study, 'Morlet' has been used for all the wavelet based processing of signals in the present study.

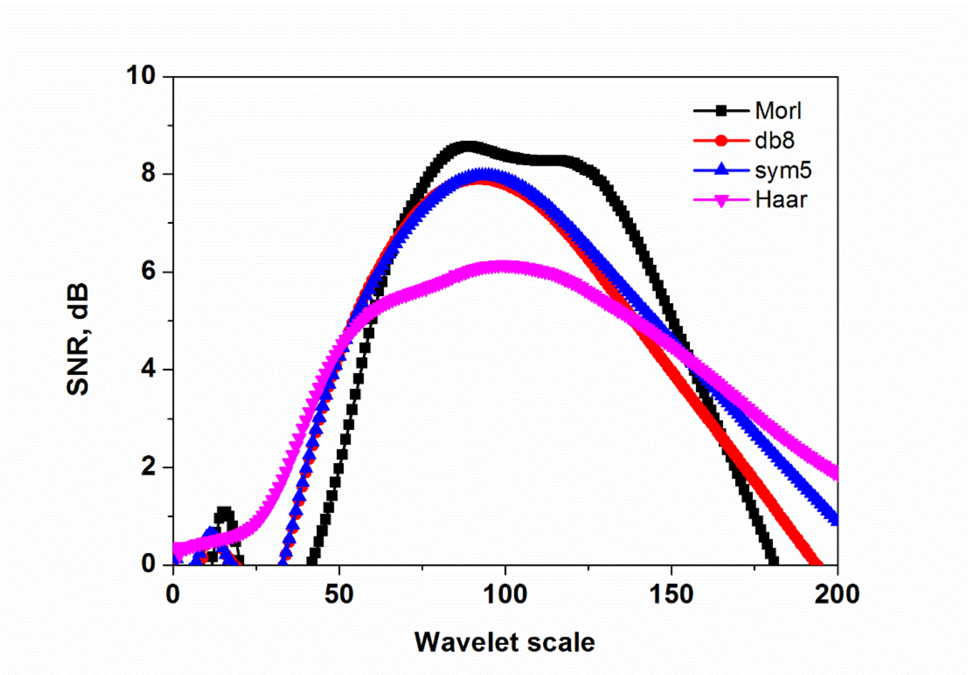

Fig. 4.14. The SNR of ultrasonic signal obtained from 210 µm grain size specimen initially increases with increasing wavelet scales and decreases after reaching maximum. The improvement of SNR was monitored by using different mother wavelets.

4.3.2.2 The Pseudo frequency approach

In order to establish pseudo frequency as an important parameter for grain size characterisation, the correlation between peak frequency and pseudo frequency was established using a top surface ultrasonic reflection obtained from one of the stainless steel specimens used in the study. The system characteristics are also taken care by using the water-specimen surface reflection for standardization. The pseudo wavelet frequencies corresponding to each scale were calculated using a Matlab function 'scal2freq', which utilizes the following expression [96]

$$F_s = F_c/s*dt \tag{4.6}$$

where s is the scale, dt is the sampling period, F_c is the central frequency of the wavelet in Hz, F_s is the pseudo frequency with respect to s (in Hz). The central frequency of the 'Morlet' wavelet used in this study is 0.8125 Hz [96]. Equation 4.6, indicates inverse relationship between pseudo frequency and scale. Since, no precise relationship exists between the scale and the frequency, the term pseudo frequency is used to correlate frequency with the scale. The pseudo frequency may not provide the exact frequency, however it provides a parameter for quantitative characterization.

Ultrasonic signal obtained from the front surface of 138 μm grain size specimen was processed with 'Morlet' wavelet. Typical A-scan signal is shown in Fig. 4.15 (a). The correlation coefficients obtained by wavelet processing has been shown in Fig. 4.15 (b). The variation in the maximum amplitude of wavelet coefficients with scale is calculated and presented in Fig. 4.15 (c). The maximum amplitude of the wavelet coefficients is found to be at scale 21. This indicates that at this scale, the maximum correlation between the ultrasonic signal and the 'Morlet' wavelet is achieved. The amplitude spectra of the coefficients at scale 21 and original ultrasonic signal were compared and the same is shown in Fig. 4.15 (d). The pseudo frequency values for wavelet scales is calculated using Eq. 4.6.

It can be noticed qualitatively from Fig. 4.15 (d) that pseudo frequency behaviour is similar to the actual ultrasonic signal frequency at a particular scale, where the maximum correlation between signal and mother wavelet is noticed.

Specific software is developed in LabVIEW to execute the pseudo frequency approach for various grain size specimens. To make a comparative analysis, the ultrasonic signals used for STFT processing to evaluate grain sizes were also processed by CWT. A typical pseudo frequency plot for ‘Morlet’ wavelet is calculated based on Eq. 4.6 and is shown in Fig. 4.16. The pseudo frequencies are evaluated up to 200 wavelet scales by utilising central frequency of the ‘Morlet’ wavelet $F_s = 0.8125$ Hz [96], and sampling rate of the acquired data 1/dt = 500 MS/s. The correlation between scale and pseudo frequency shown in Fig. 4.16 is used to convert scale to frequency.

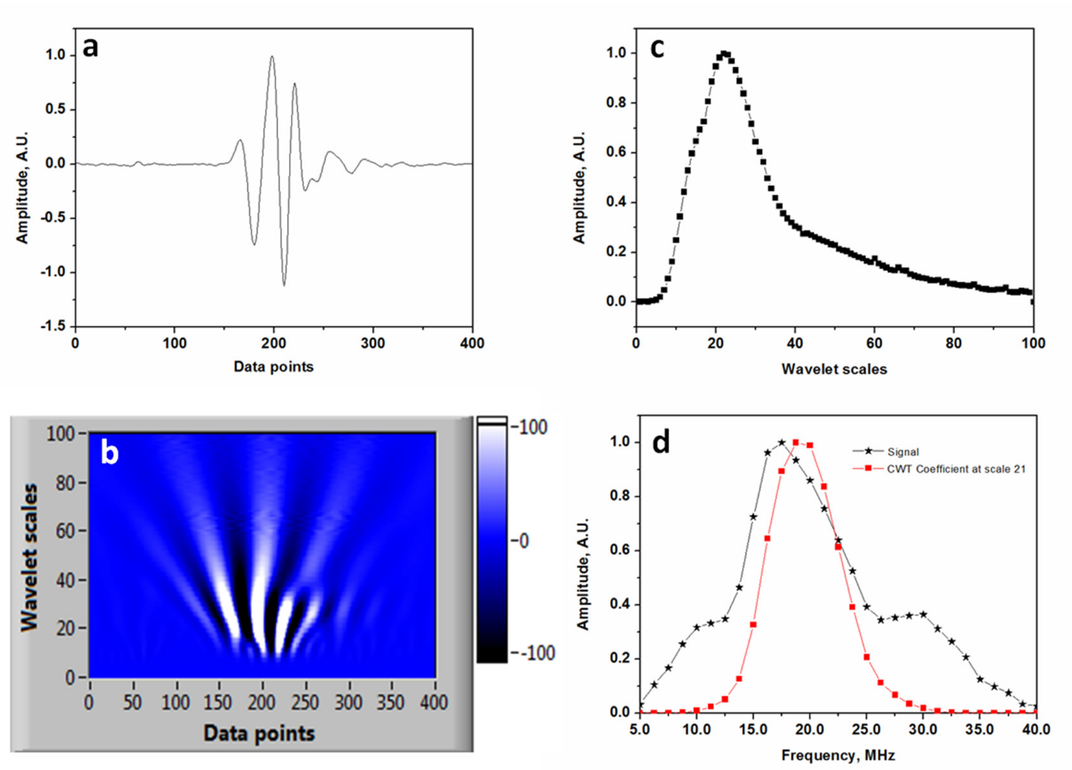

Fig. 4.15. (a) A-scan signal from the top surface of specimen with 138 µm grain size, (b) CWT coefficient plot of the A-scan signal using ‘Morlet’ wavelet, (c) change in the peak amplitude of coefficients with scale and (d) comparison of amplitude spectra of A-scan signal and its wavelet coefficient at scale 21.

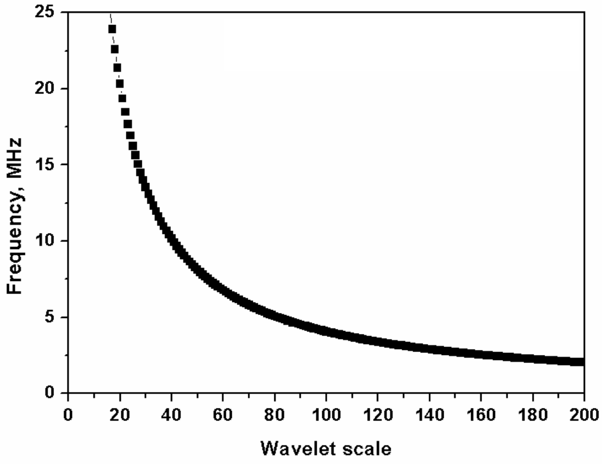

Fig. 4.16. The change in the pseudo frequencies with scales of 'Morlet' wavelet is presented, where the central frequency of 'Morlet' wavelet is 0.8125 Hz [96], and sampling rate of signal is 500 MS/s.

4.3.2.3 Comparison of STFT spectrogram and CWT coefficient plot

Typical A-scan signal obtained from stainless steel specimen of large grain size (210 µm) of 10 mm thickness is shown in Fig. 4.17 (a). The spectrogram and the wavelet coefficients map of the ultrasonic signal using 'Morlet' wavelet are presented in Fig. 4.17 (b) and Fig. 4.17 (c), respectively. Feeble echo amplitude merged in backscatter noise can be observed at first back-wall echo (FBWE) location in Fig. 4.17 (a). The second back-wall echo (SBWE) and third back-wall echo (TBWE) amplitudes are completely submerged in the backscatter. The regions of first three consecutive back-wall echoes (BWEs) are marked with dotted boxes which are identified based on the thickness of the specimen.

The STFT of the signal clearly demonstrates that the frequency content of the backscatter is high (> 12.5 MHz) and the frequency content of first BWE is low (~5 MHz). In the STFT spectrogram, only FBWE could be visualized and no information could be obtained for the SBWE and the TBWE. The wavelet coefficient of the signal shows information up to the TBWE locations as seen in Fig. 4.17 (c).

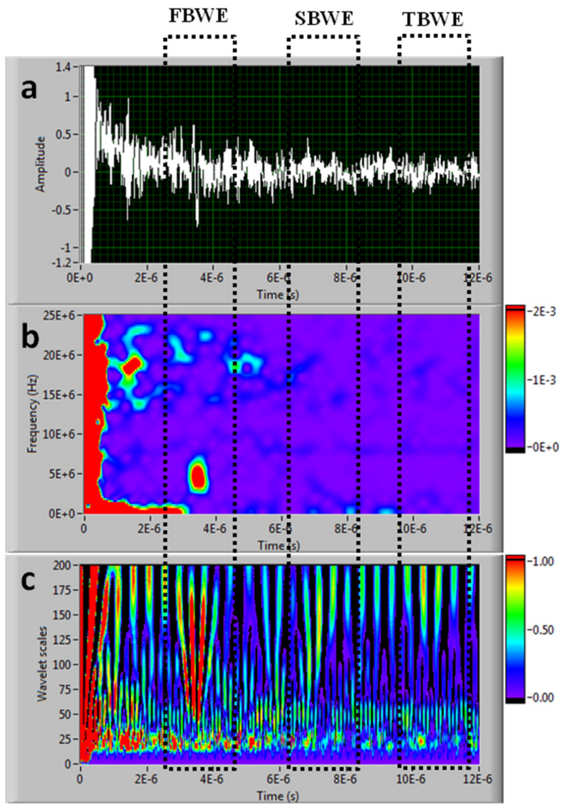

Fig. 4.17. (a) A-scan signal from the 210 μm grain size specimen of 10 mm thickness, (b) STFT spectrogram of the signal and (c) wavelet coefficient plot of the signal. The locations of first three back-wall echoes are highlighted with dotted boxes.

The lower scales corresponding to higher frequency content of the signal and mainly comprises the backscatter. Conversely, the higher scales corresponding to lower frequency content of the signal arises from the back-wall echoes. Further, high scales (> 200), comprises only very low frequency information. This clearly demonstrates that the CWT based analysis is more efficient in processing the noisy signals due to its flexible resolution capabilities compared to STFT.

4.3.2.4 Correlation between SNR and pseudo frequency

The ultrasonic waveforms were normalized with respect to the peak amplitudes of the first back-wall echo signal. The continuous wavelet coefficients were calculated for normalized ultrasonic waveforms obtained for the range of grain sizes (30 - 210 μm). The wavelet coefficients were calculated by continuous wavelet processing using ‘Morlet’ wavelet. The data were processed up to 200 scales and SNR was calculated at each wavelet scale. Specially developed LabVIEW program has been used to obtain the SNR values with each scale up to three back-wall echoes. The back-wall echo regions were considered as the signal and the remaining part of the signal was considered as the noise. Eq. 4.7 is used to calculate the SNR [82] as

$$SNR = 10\ log\left\{\sum_{i=1}^{N_s}(s_i^2/N_s)/\sum_{i=1}^{N_n}(n_i^2/N_n)\right\} \qquad (4.7)$$

where s_i are the amplitudes of points of waveform where back-wall signal is present, n_i are the amplitudes of the points where only noise is present. N_s and N_i correspond to the total number of data points corresponding to signal and noise, respectively.

Typical results obtained for the improvement of SNR of an ultrasonic signal obtained from 210 µm specimen using 25 MHz frequency immersion transducer with wavelet scales are shown in Fig. 4.18. The SNR improves with increasing scale and attains maximum at scales 86, 125 and 143 for FBWE, SBWE and TBWE, respectively followed by a decrease in SNR at higher scales. The scale values for maximum SNR by considering only FBWE and three back-wall echoes together are similar. The higher scales in achieving the best SNR for multiple BWEs is due to decreasing frequency content of the subsequent back-wall echoes. The A-scan signal and wavelet coefficients at scales 25, 50, 86, 125 and 143 are shown in Fig. 4.19. It can be clearly observed that the initial scales 25 and 50 show the high frequency content due to backscatter. At scales 86, 125 and 143, three back-wall echoes provide the best correlation with mother wavelet, and maximum SNR is obtained. At scale 175, only low frequency content is available which does not provide any useful information for the current analysis.

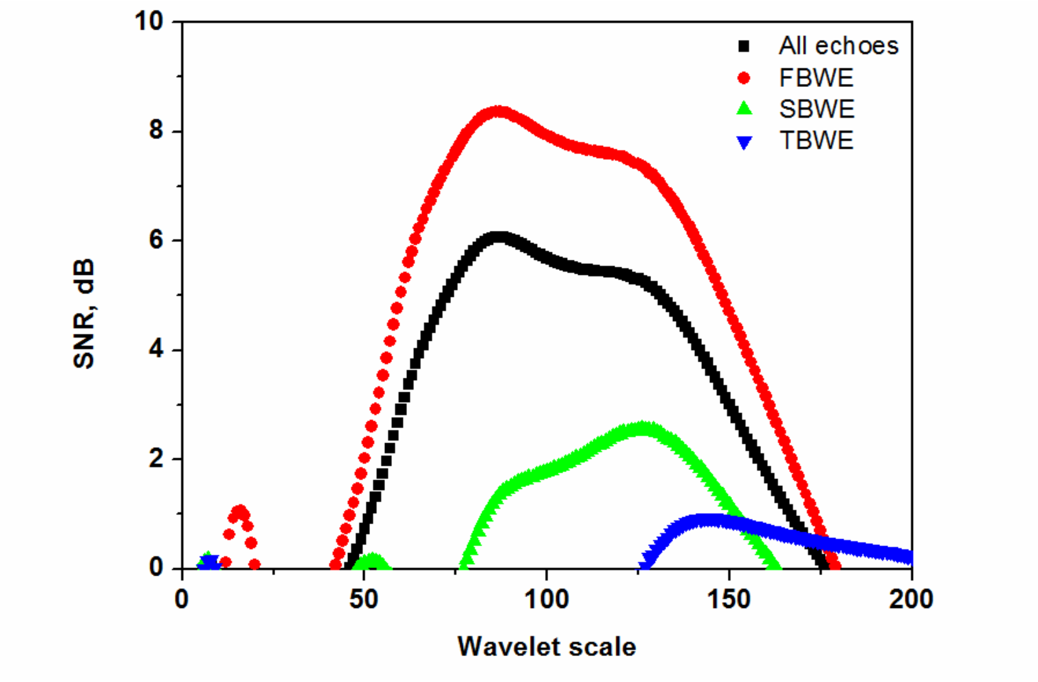

Fig. 4.18. The improvement in SNR with wavelet scales by considering first back-wall echo (FBWE), second back-wall echo (SBWE), third back-wall echo (TBWE) and entire signal for 210 µm grain size specimen. The ultrasonic signal was processed by 'Morlet' wavelet.

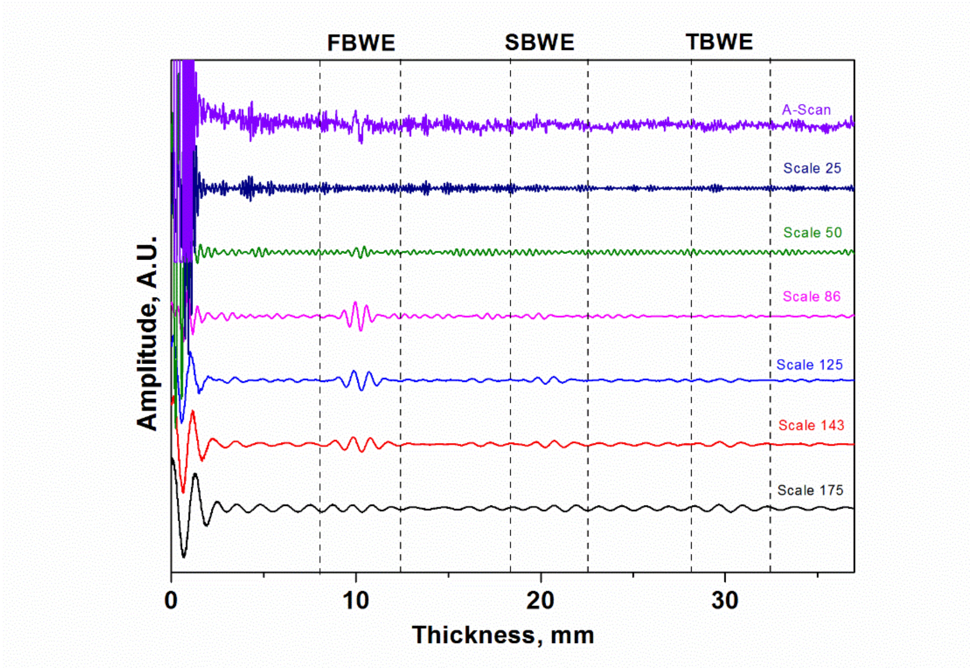

Fig. 4.19. The RF signal obtained from a 210 µm grain size specimen and its wavelet coefficients at different scales (25, 50, 86, 125 and 143 and 175). Scales 86, 125 and 143 correspond to the maximum SNR for the FBWE, SBWE and TBWE respectively.

4.3.2.5 Quantitative grain size evaluation

The ultrasonic signals obtained from different grain size specimens were processed by CWT and improvement of SNR with wavelet scales was monitored. The particular scale for which best SNR is achieved is recorded for all the signals. The pseudo frequencies corresponding to these scales are obtained using the Eq. 4.6. The details of the pseudo frequency values obtained after SNR based CWT processing of ultrasonic signals from different grain size specimens is given in Table 4.4. The flexibility in adopting the CWT has been used to calculate pseudo frequencies up to the TBWE. The calculated pseudo frequencies followed linear correlation with grain size parameter, as shown in Fig. 4.20. The details of the linear correlation obtained are given in Eq. 4.8. The typical variation in the pseudo frequencies obtained by CWT using the three BWEs with grain size is presented in Table 4.4

$$\text{Pseudo } PF_{TBWE} = -3.91+4.02d^{-1/2} \text{ (R=0.99)} \quad \text{(using three BWEs)} \quad (4.8) \left.\vphantom{\begin{matrix}a\\b\\c\\d\end{matrix}}\right\} \begin{matrix}\text{Valid for}\\ \text{real values}\\ \text{of pseudo}\\ \text{frequency}\end{matrix}$$

Table 4.4. Details of pseudo frequencies calculated for the scale values corresponding to optimum SNR by considering three back-wall echoes.

Specimen Ref. No.	Grain Size (µm)*	Pseudo Frequency considering three back-wall echoes (MHz)
P0	30	19.34 ± 1
P1	78	10.69 ± 0.2
P2	83	9.9 ± 0.2
P3	106	8.64 ± 0.1
P4	121	7.38 ± 0.1
P5	138	6.77 ± 0.1
P6	210	4.72 ± 0.1

Note: WQ – Water Quench

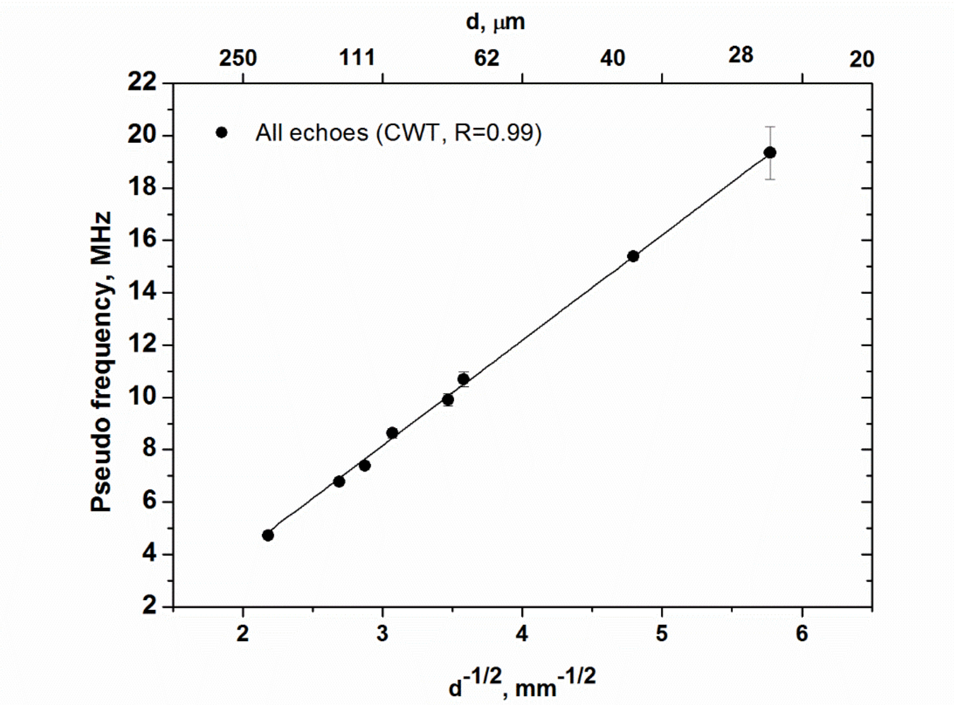

Fig. 4.20. Variations in CWT pseudo frequencies with grain size parameter.

The linear fit of the pseudo frequency and inverse square root of grain size ($d^{-1/2}$) showed very good correlation (R = 0.99). Hence, the CWT based pseudo frequency approach can be used for grain size evaluation of austenitic stainless steel.

4.3.2.6 Comparative analysis between STFT and CWT based approaches

The grain size characterization has been carried out using two time-frequency based approaches STFT and CWT. Fig. 4.21 shows the variation of STFT based peak frequency and CWT based pseudo frequency with grain size parameter. It can be clearly seen from Fig. 4.21 that, both approaches are found to be very useful in analyzing the coarse grained material data for grain size evaluation. The linear fit slope for grain size and pseudo frequency obtained by CWT processing is found to be more compared to linear fit slope between grain size and peak frequencies obtained by STFT processing as shown in Fig. 4.21. Secondly, the linear fit correlation coefficient (R) is found to be 0.96 - 0.97 for STFT based processing and 0.99 for CWT based processing.

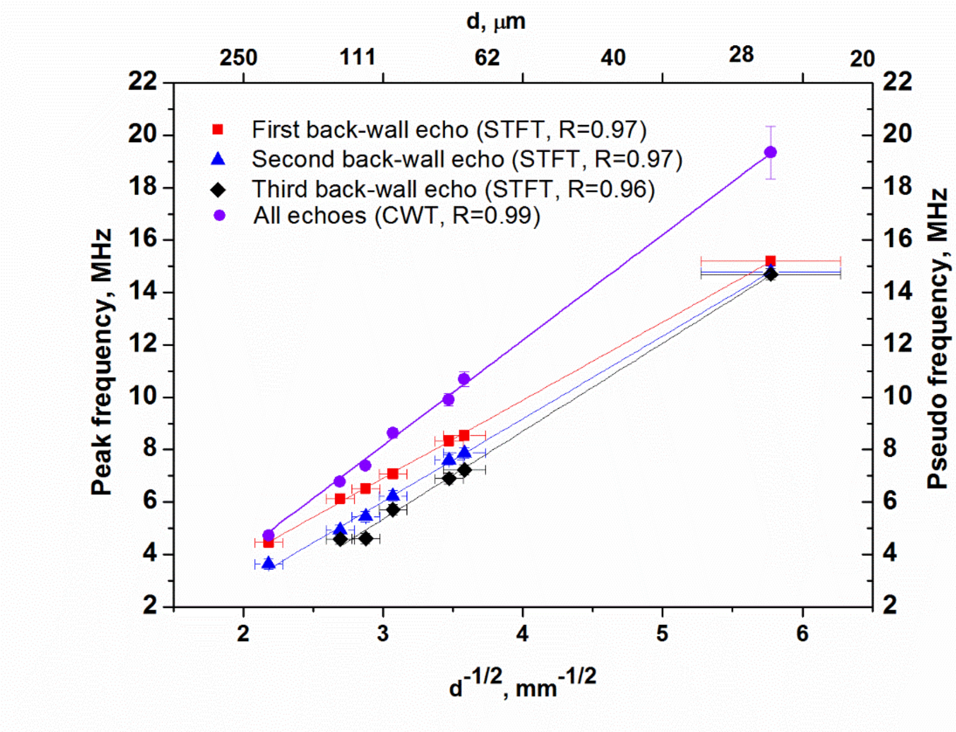

Fig. 4.21. The correlation between STFT peak frequencies and CWT pseudo frequencies with grain size parameter ($d^{-1/2}$).

Which indicates higher sensitivity of continuous wavelet transform based approach with change in grain size changes. This can be attributed to multiresolution capability of CWT analysis with providing high resolution of low frequency components. This is achieved by flexible window size in case of CWT compared to STFT. Further, the correlation of the shape of mother wavelet with signal also played an important role to achieve high sensitivity. The flexibility of application of CWT based approach can also be applied for online grain size characterization. A typical comparison between time-frequency based STFT approach and time-scale based CWT approach for grain size characterization of austenitic stainless steel is summarized in Table 4.5.

Table 4.5. Comparative analysis of STFT and CWT based methods in terms of microstructural characterization of austenitic stainless steels.

Parameters/approaches	STFT	CWT
Window size	Fixed	Flexible
Resolution	Fixed	Flexible
Spectral parameter	Frequency	Scale or Pseudo frequency
Grain size characterization	Yes	Yes, with better sensitivity and understanding

Window size determines the time and frequency resolution, which is fixed in the STFT analysis. However, the analysis by CWT is accompanied with flexible window and the lower frequency components of the signal are better resovled in frequency domain as compared to the high frequency components. Since, in our analysis the low frequency components are buried in high frequency signals, the CWT approach is found to be very useful for the analysis.

4.3.2.7 Conclusions from CWT studies

- The limitation of fixed resolution of STFT has been addressed using flexible CWT analysis for the analysis of ultrasonic signals.
- The SNR based approach for materials characterization using wavelet analysis gives reliable information due to simultaneous analysis of backscatter and back-wall echoes.
- Comparative studies between STFT and CWT showed that the CWT based analysis is more sensitive towards the evaluation of grain size in the range of 30 – 210 µm for type 316 austenitic stainless steel used in this study.

Chapter 5. Continuous Wavelet Transform based C-Scan Imaging of Defects

5.1 Introduction

In the previous chapter 4, details of microstructural characterisation by short time Fourier transform (STFT) and continuous wavelet transform (CWT) have been presented. The application of STFT was very useful in peak frequency estimation at back-wall location from ultrasonic back-wall echo signals sub-merged in backscatter. The time-frequency methodologies adopted for microstructural characterisation in the previous chapter have been extended for defect characterisation and imaging in coarse grain material.

The ultrasonic testing carried out at lower frequency is generally preferred for identification of defects in coarse grained material, as good signal to noise (SNR) ratio can be achieved. However, the ultrasonic inspection performed with lower frequency leads to a poor resolution due to longer wavelength. In most of the practical applications, good near surface resolution is necessary for the detection of finer defects. Therefore, it will be beneficial if the near surface ultrasonic resolution is improved which can be achieved by the use of high frequency ultrasonic waves. Systematic experimental investigations have been carried out using 5 and 10 MHz ultrasonic transducers to understand the influence of ultrasonic frequency on defect detection. The use of high frequency transducer enables higher sensitivity for smaller defects near the surface. The high frequency components of the ultrasonic beam gets scattered with beam travel path which enables comparatively lower frequency inspection at deeper regions.

The STFT based approach has been adopted for the detection of defects located at different depths and obtaining peak frequencies at defect locations. Specially designed coarse grain specimens have been made with side drilled holes (SDH) and flat bottom holes (FBH) at different depths for this purpose. This application of STFT for estimating peak frequencies at defect locations in the presence of backscatter is established. The experimentally observed changes in the spectral content of the propagating ultrasonic waves in scattering media are compared with peak frequency values predicted by existing theoretical model [90]. This model has been suitably modified for our application by incorporating attenuation due to scattering and this has been utilised to predict the shifts in ultrasonic frequency with propagation distance in coarse grain steel.

The peak frequency values at different defect locations showed a systematic variation with depth, which lies in a particular frequency range. This enabled CWT processing of signals at a particular scale for successful imaging of defects. Specific software has been developed for C-scan imaging of defects using conventional and CWT based processing. The results obtained by these processing methods are compared and discussed.

5.2 Experimental

5.2.1 Specimen preparation

Three different specimens of AISI type 316 stainless steel (100 mm diameter and 50 mm thickness) were prepared by suitable heat treatment at different temperatures to obtain different grain sizes. Metallographic examination has been carried out to reveal the grain structure of the specimens. The typical micrographs of these three specimens are shown in Fig. 5.1. The linear intercept method as per ASTM standard E112–96 was used to measure the average grain size [92]. The details of heat treatments given to these specimens and grain sizes obtained are presented in Table 5.1.

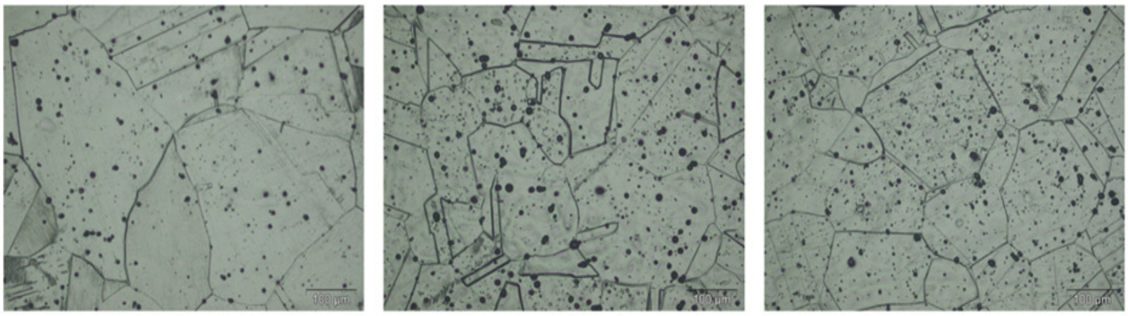

(a) (b) (c)

Fig. 5.1. Photomicrographs obtained by metallography for (a) Specimen 1- 360 µm, (b) Specimen 2- 200 µm and (c) Specimen 3 -200 µm.

Table 5.1. Details of the heat treatments given to AISI Type 316 stainless steel specimens and grain size obtained, these specimens were used to fabricate artificial defects.

Specimen Ref. No.	Heat Treatment	Grain Size (µm)*
Specimen 1	1573/5h/WQ	360 ± 20
Specimen 2	1373K/5h/WQ	200 ± 20
Specimen 3	1373K/5h/WQ	200 ± 20

Note: WQ – Water Quench; * From optical metallography (ASTM standard E112-96)

The two specimens, namely Specimen 1 (360 µm grain size) and Specimen 2 (200 µm grain size) were used to fabricate flat bottom holes (FBH) of different sizes up to different depths. The schematic of the side drilled holes fabricated in these two specimens is given in Fig. 5.2, and the dimensional details of the defects are presented in Table 5.2.

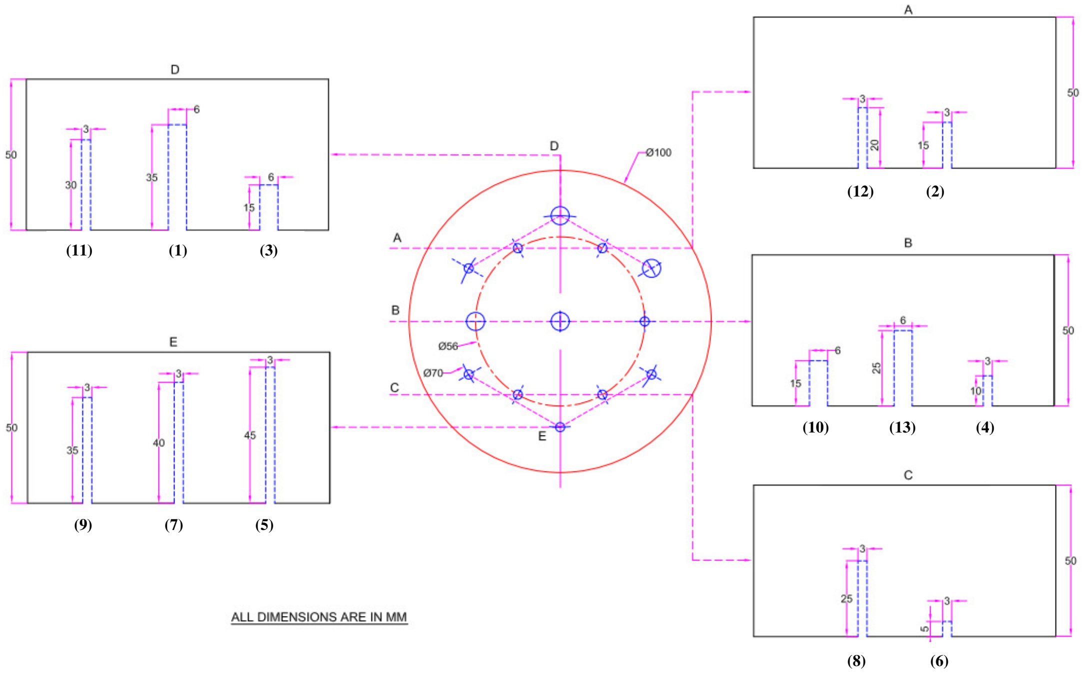

Fig. 5.2. Schematic of Specimen 1 (360 µm grain size) and Specimen 2 (200 µm grain size) used in this study for evaluation of peak frequency shift of ultrasonic waves with propagation distance. The defect identification numbers are also given below the defect dimensions.

Table 5.2. Dimensional details of flat bottom holes (FBH) fabricated in the Specimen 1 (360 µm grain size) and Specimen 2 (200 µm grain size), the FBH were made by electric discharge machining (EDM) process.

Sl. No.	Defect Ref. No.	FBH depth from scanning surface (mm)	FBH Diameter (mm)
1	1	15	6
2	13	25	6
3	3, 10	35	6
4	5	5	3
5	7	10	3
6	9	15	3
7	11	20	3
8	8	25	3
9	12	30	3
10	2	35	3
11	4	40	3
12	6	45	3

Specimen 3 (200 µm grain size) was used to fabricate side drilled holes (SDH) at different depths. The schematic sketch of Specimen 3 is shown in Fig. 5.3. The dimensional details of the SDHs fabricated in Specimen 3 are presented in Table 5.3. Single SDHs were fabricated at different depths to understand the ultrasonic frequency shifts with beam propagation distance. Inclined SDHs in pairs with decreasing distance towards the centre of specimen in the same plane were made to test the resolution capability of CWT. The ultrasonic data were acquired by immersion method in pulse echo mode by 10 MHz unfocussed transducer. The data was sampled at 100 MS/s. The longitudinal ultrasonic velocity is found to be 5740 ± 10 m/s in these specimens. The time of flight of ultrasonic waves is represented by data points with a multiplier factor in C-scan images.

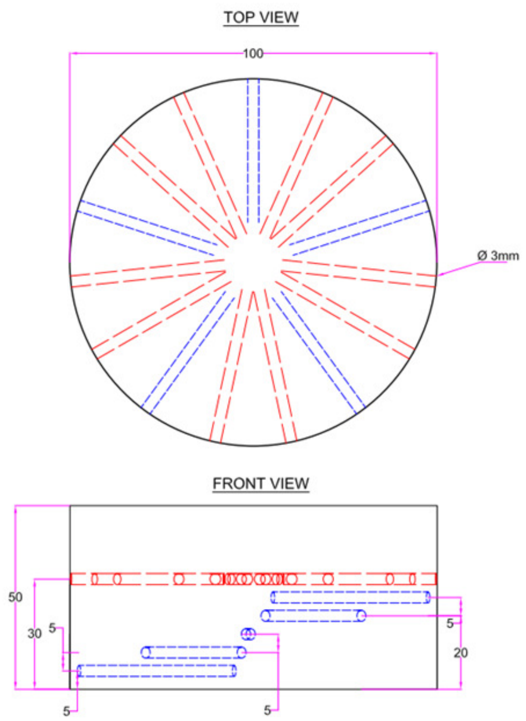

Fig. 5.3. Schematic of Specimen 3 with side drilled holes (SDH) made at different depths (fine dotted lines, blue colour) as well as in same plane (coarse dotted lines, red colour) in inclined manner so the distance between two holes decreases towards centre of the specimen.

Table 5.3. The location of the centre of side drill holes (SDHs) fabricated in Specimen 3 is presented. All the holes were made of 3 mm diameter. Since both the sides are available for scanning, the depth of centre of SDHs from both surfaces are given.

Defect Ref. No.	SDH depth from side1 scanning surface (mm)	SDH depth from side 2 scanning surface (mm)
H1	25	25
H2	30	20
H3	35	15
H4	40	10
H5	45	5
H (6-15)	20	30

5.3 Results and discussion

5.3.1 Conventional C-scan imaging

Ultrasonic signal of top surface reflection from Specimen 2 and its amplitude spectrum obtained by 5 MHz transducer are shown in Fig. 5.4 (a) and (b), respectively. The amplitude spectrum shows that the peak frequency of the transducer is 3.5 MHz. Typical amplitude and time of flight based C-scan images obtained with conventional C-scan imaging method are shown in Fig. 5.5 (a) and (b), respectively. These C-scan images clearly show that four defects in the Specimen 2 (defect ref. nos. 2, 4, 6, 12) could not be imaged with 5 MHz ultrasonic transducer. All these defects are smaller in diameter (3 mm) and located at the depth range of 30-45 mm. However, the defect of larger diameter (6 mm) located at 35 mm depth could be detected and imaged. This clearly suggests that the larger defects can be successfully detected, while smaller defects are missed at similar depths.

5.3.2 Optimisation of ultrasonic frequency

The smaller size defects, which could not be imaged by conventional C-scan processing is attributed to lower reflection amplitudes from defects. The smaller amplitudes from defects leads to poor SNR. This demands the processing of signals to improve SNR for enhanced imaging. However, improving the SNR of signals acquired at lower ultrasonic frequency will still have the inherent limitation of poor resolution due to longer wavelength. Hence, an alternative approach is adopted for utilising high frequency ultrasonic waves for imaging the defects. The ultrasonic signals obtained from defects are merged in backscatter. Hence, the STFT methodology developed for grain size characterisation was used to understand the spectral distribution of defect echoes and the backscatter. This approach is found to be useful in the detection of defects and to evaluate the ultrasonic frequencies at defect locations.

The ultrasonic signal obtained from 3 mm diameter 25 mm deep FBH and its STFT spectrogram are shown in Fig. 5.6 (a) and (b), respectively. The frequency of the defect echo and back-wall echo is about 2 MHz, which clearly indicates a shift in the peak frequency of the incident ultrasonic beam even at 3.5 MHz incident frequency. As the smaller defects situated at deeper depths could not be imaged even at lower frequency, an alternate inspection approach using higher frequency transducer was adopted. Since, the SNR decreases by using the high frequency transducer, the time-frequency approaches are used to detect and image the defects.

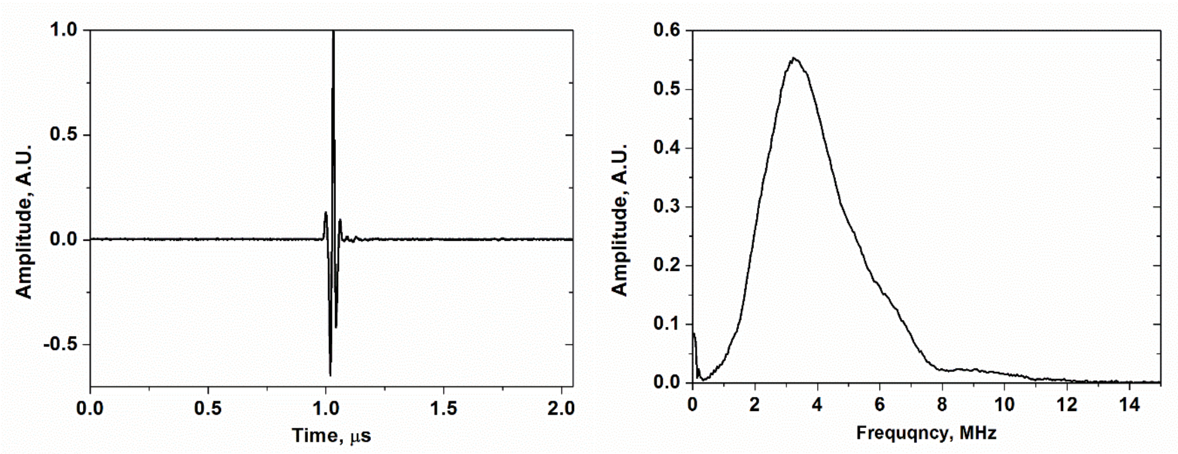

(a) (b)

Fig. 5.4. (a) The ultrasonic signal obtained from water-specimen surface using 5 MHz transducer and (b) its amplitude spectrum.

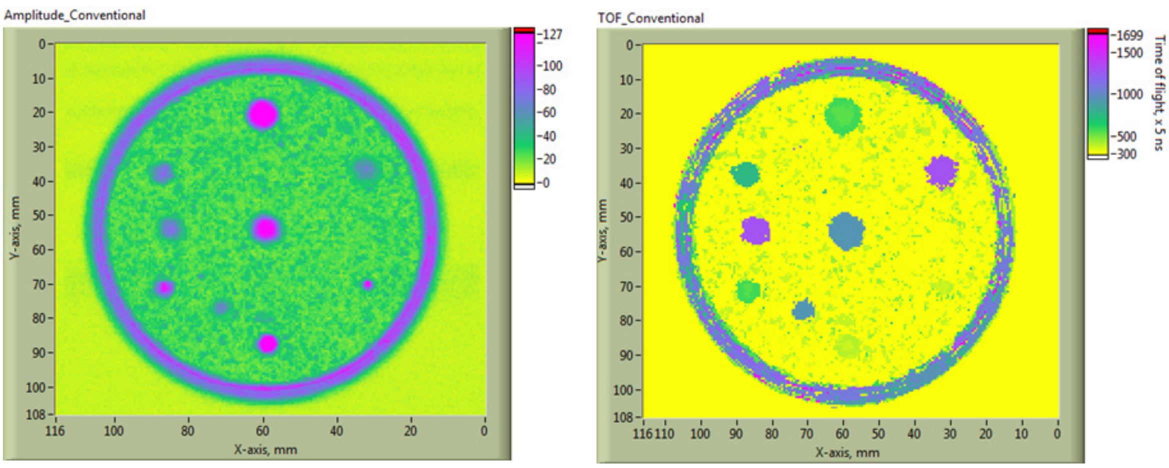

(a) (b)

Fig. 5.5. Ultrasonic C-scans obtained by conventional time domain method for Specimen 2 (a) amplitude based and (b) time of flight (TOF) based, using 5 MHz immersion transducer.

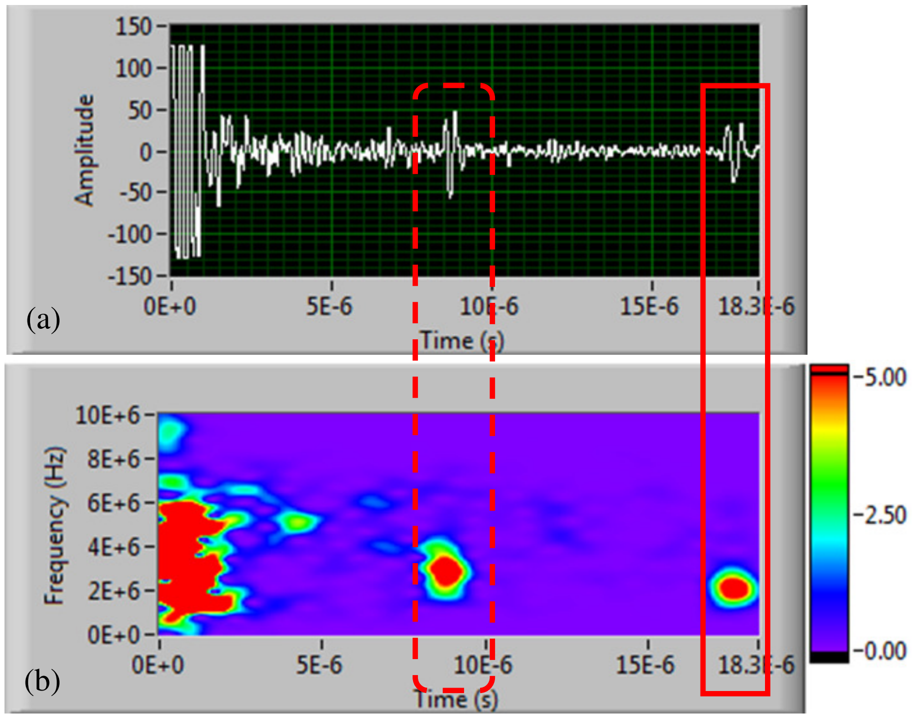

Fig. 5.6. Ultrasonic reflection from a 3 mm dia. FBH at 25 mm depth in Specimen 2 using 5 MHz transducer (shown by dotted rectangle, red colour) and (b) its STFT spectrogram. The back-wall echo is observed at the end of the signal (shown by solid rectangle, red colour).

Increase in the surface roughness, decreases the amplitude of the ultrasonic reflection from the back-surface of the specimens [97]. It has also been observed that with increase in the surface roughness, the shift in the high frequency component is more as compared to the lower frequencies [98]. However, these shifts are negligible compared to the frequency shifts observed in different grain size specimens used in the present study.

5.3.3 Evaluation of frequency shifts using STFT

To develop the approach for high frequency imaging of defects, ultrasonic data was acquired using 10 MHz frequency transducer for all the specimens. Due to the scattering of high frequency components of ultrasonic waves in coarse grained material, the echoes of interest are completely merged in the backscatter and this leads to difficulties in the estimation of spectral information at the region of interest by conventional methods. STFT processing is found to be very useful in estimating ultrasonic peak frequencies at the locations of the artificial reflectors. The optimum window length was chosen based on the selection procedure discussed in Chapter 4. The signals were zero padded to achieve length of 2048 data points. The frequency resolution of 0.1 MHz was achieved during the STFT analysis.

5.3.3.1 Specimen 1 (360 µm grain size)

The ultrasonic A-scan signal from 25 mm deep FBH in Specimen 1 and its STFT spectrogram are shown in Fig. 5.7 (a) and (b), respectively. The frequency information at the defect location obtained from spectrogram is shown Fig. 5.7 (c). The defect location is identified based on the time of flight calculation performed for this defect. It can be clearly observed from the A-scan signal (Fig. 5.7 (a)) that even though the defect indication is completely merged in backscatter, frequency content of the defect signal and backscatter can still be distinguished in the spectrogram. The frequency content at the back-wall echo location can also be identified clearly and is indicated by an arrow in Fig. 5.7 (c). The grain noise is found to be much higher which is attributed to the larger grain size of Specimen 1. The peak frequency from the reflector at 25 mm was found to be ~1 MHz. From this it is clear that the FBH of 6 mm diameter up to 25 mm depth can be easily identified. This demonstrates the usefulness of the STFT approach. However, due to very large grain size, only 6 mm diameter FBH up to 25 mm depth could be detected. Further analysis of this specimen is not carried out in this study.

5.3.3.2 Specimens 2 and 3 (200 µm grain size)

The ultrasonic A-scan signal obtained from 30 mm deep FBH in Specimen 2 and its STFT spectrogram are shown in Fig. 5.8 (a) and (b), respectively. The frequency information at the defect location obtained from spectrogram is shown in Fig. 5.8 (c). Fig. 5.9 (a) and (b) show the ultrasonic A-scan signal obtained from 30 mm deep SDH in Specimen 3 and its STFT spectrogram, respectively. The frequency information at the defect location obtained from spectrogram is shown in Fig. 5.9 (c). The defect and back-wall echo locations were identified based on the time of flight calculations. These locations can also be clearly identified in the spectrograms due to their distinct low frequency content. In the spectrograms, defect locations are marked with dotted circles and back-wall echo locations are marked with solid circles. The spectrogram reveals similar peak frequencies corresponding to 30 mm deep defects in both the specimens. These observations suggest that the frequency shifts are independent of the type of reflector. Since, the grain size in both the specimens is similar, it can be concluded that the shift in the peak frequency is only dependent on the ultrasonic beam travel distance and not on the nature of the reflector. By using STFT approach, the peak frequency corresponding to the defects at defect locations is determined. The peak frequency obtained for different size FBHs at different depths are given in Table 5.4 and the corresponding peak frequency obtained for SDH are presented in Table 5.5.

.

.

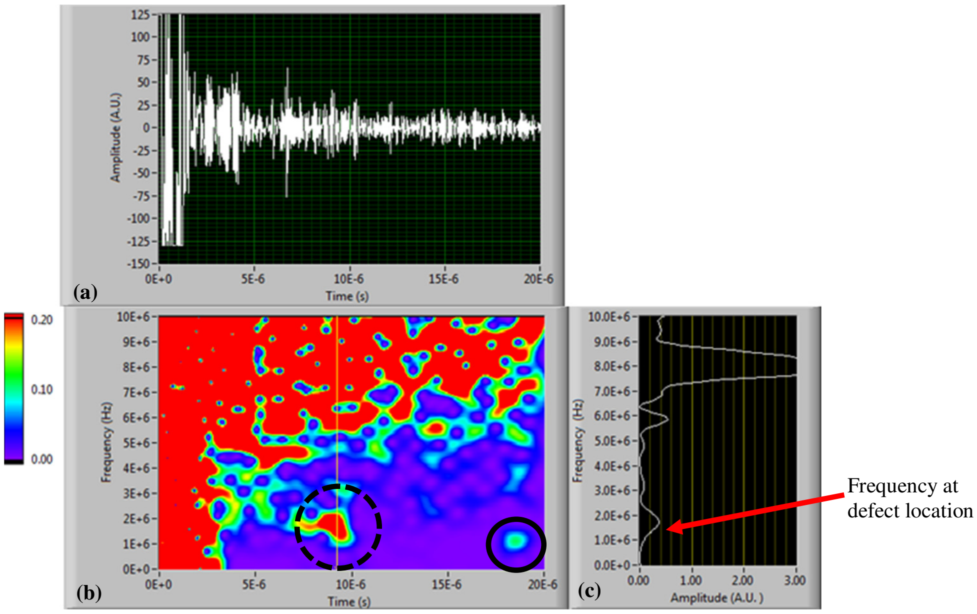

Fig. 5.7. (a) Time domain signal from 6 mm diameter FBH at 25 mm depth in Specimen 1, (b) its spectrogram, where the defect signal location is indicated by dotted circle and back-wall echo location is indicated by solid circle and (c) frequency content at the defect location.

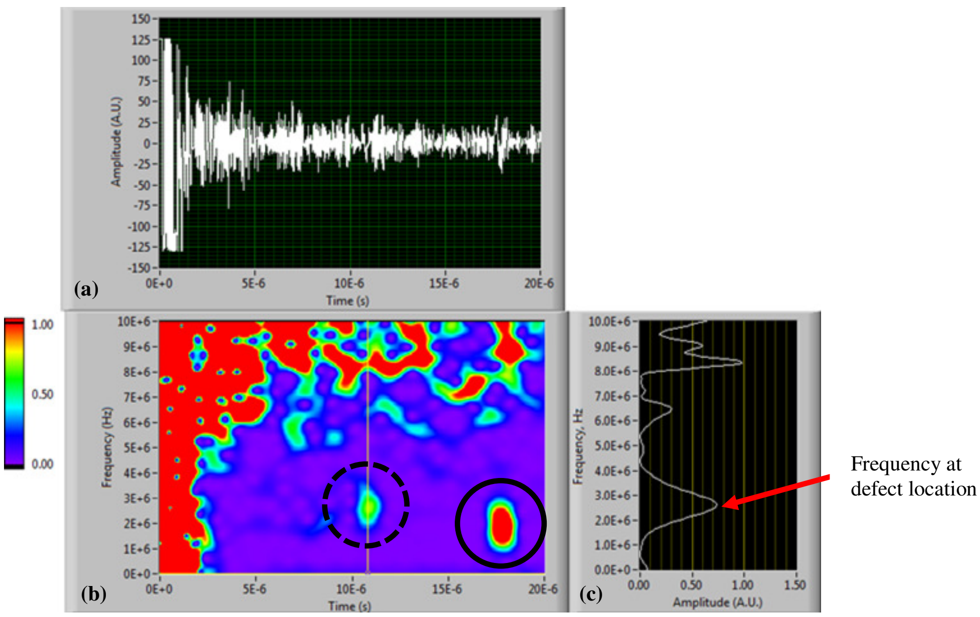

Fig. 5.8. (a) Time domain signal from 3 mm diameter FBH at 30 mm depth in Specimen 2, (b) its spectrogram, where defect signal location is indicated by dotted circle and back-wall echo location is indicated by solid circle and (c) frequency content at the defect location.

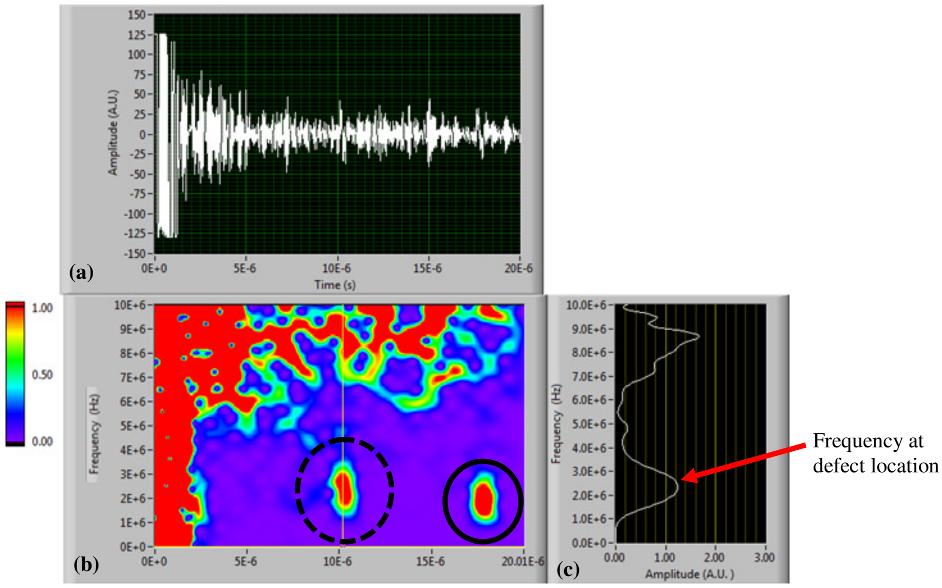

Fig. 5.9. (a) Time domain signal from 3 mm diameter SDH at 30 mm depth in Specimen 3, (b) its spectrogram, where defect signal location is indicated by dotted circle and back-wall echo location is indicated by solid circle and (c) frequency content at the defect location.

Table 5.4. The peak frequency values obtained by STFT for flat bottom holes (FBHs) at different depths in Specimen 2.

Sl. No.	Defect identification number	Defect location from inspection surface (mm)	Defect size (mm)	Peak frequency at defect location (MHz)
1	1	15	6	2.97
2	13	25	6	3.05
3	3, 10	35	6	2.19
4	7	10	3	3.2
5	9	15	3	2.83
6	11	20	3	2.9
7	8	25	3	3.07
8	12	30	3	2.63
9	2	35	3	2.31
10	4	40	3	2.23
11	5	5	3	**
12	6	45	3	**

** frequency information was not estimated to avoid ambiguity of interference from surface echoes

Table 5.5. The peak frequency values obtained by STFT for side drilled holes (SDHs) at different depths in Specimen 3.

Sl. No.	Defect identification number	Defect centre location from inspection surface (mm)	Defect size (mm)	Peak frequency at defect location (MHz)
1	2-1	10	3	2.83
2	3-1	15	3	2.68
3	4-1	20	3	2.51
4	5-1	25	3	2.70
5	2-2	40	3	2.19
6	3-2	35	3	2.17
7	4-2	30	3	2.39
8	5-2	25	3	2.68
9	1-1	5	3	**
10	1-2	45	3	**

** frequency information was not estimated to avoid ambiguity of interference from surface echoes

5.3.4 Model based evaluation of frequency shifts

The mathematical approach adopted by Ophir et al. [90, 99] has been used to develop model based understanding of the shift in the ultrasonic peak frequency. The experimentally observed peak frequency shifts in the two specimens (Specimen 2 and Specimen 3) of 200 μm grain size and 50 mm thickness are compared with the theoretically calculated shifts. The mathematical approach is based on the assumption that a reference ultrasonic pulse propagating through a lossless medium and its Fourier amplitude spectrum has Gaussian envelope [90] as

$$|T(f)| = \frac{1}{\sigma\sqrt{2\pi}} \exp\left[\frac{-(f-f_0)^2}{2\sigma^2}\right] \tag{5.1}$$

where $|T(f)|$ is Fourier amplitude spectrum of the reference pulse in lossless medium, σ^2 is variance of the spectrum and f_0 is peak frequency of the spectrum.

The attenuation of sound intensity in the medium of propagation is a nonlinear function of frequency, and is of the exponential form as

$$|H(f)| = exp[-2\alpha_0 f^n Z] \tag{5.2}$$

where, $|H(f)|$ is frequency dependent attenuation function, n is the exponent of frequency dependence; Z is the total propagation distance and α_0 is an amplitude attenuation coefficient of the medium. In a lossy medium, the received spectrum, $|R(f)|$ is therefore given by

$$|R(f)| = |T(f)|\,|H(f)| = \frac{1}{\sigma\sqrt{2\pi}}\,exp - \left[\frac{(f-f_0)^2}{2\sigma^2} + 2\alpha_0 f^n Z\right] \tag{5.3}$$

where σ is dependent on half power bandwidth (HPBW) of the transducer used and is equal to HPBW divided by a constant factor 2.36. After traversing a path in the medium, the pulse $|R(f)|$ experiences a downshift in its peak frequency. The peak frequency is defined as the frequency at which amplitude spectrum slope is zero. To estimate the frequency downshift, Eq. 5.3 is differentiated with respect to f and is set to zero. For finite frequencies, the resultant equation becomes as

$$2n\alpha_0 Z\sigma^2 f_c^{n-1} + f_c - f_0 = 0 \tag{5.4}$$

The equation describes the location of the downshifted peak frequency f_c as a function of the other parameters present in the Eq. 5.4. The attenuation α_0 can be replaced by the ultrasonic scattering coefficient due to the Rayleigh scattering (α_s) in polycrystalline stainless steel given by

$$\alpha_s = S\ d^3.f^4 \tag{5.5}$$

where S is scattering factor, d is grain size and f is the incident ultrasonic frequency by replacing α_0 by S d^3 and n = 4 in Eq. 5.4, the modified equation can be re-written as

$$8Sd^3Z\sigma^2 f_c^3 + f_c - f_0 = 0 \tag{5.6}$$

The scattering factor for stainless steel was calculated using Eq. 2.6 (Chapter 2), reported by Papadakis [26] for Rayleigh scattering region in cubic materials. To the best of author's knowledge, the value of ultrasonic scattering coefficient in AISI type 316 austenitic stainless steel is not available in literature. The value of scattering factor was calculated by using material and ultrasonic properties which includes, longitudinal ultrasonic velocity V_L = 5750 m/s, shear wave velocity V_S = 3100 m/s, density ρ = 7800 kg/m^3 and elastic constants C_{11} = 200 GPa, C_{12} = 129 GPa, C_{44} = 125 GPa, from literature [100]. The value of scattering factor was calculated as 1.9×10^{-14} μs^4/ μm^4. The diameter of the grains observed in any metallographic section are always less than or equal to the real diameter of the grains in three dimensions. The model based calculations require the mean grain diameter in the three dimensional space. Hence a correction factor is required to be employed. The mean grain diameter was obtained by multiplying the averge grain diameter obtained by a metallographic section with a factor of 1.45 as reported by Papadakis [26].

Equation 5.9 cannot be solved in closed form with the exception of simple cases (where n = 1 or 2). However, for our application (n = 4), closed form solutions are not available. Therefore, the solution was obtained by iterative procedure. The details of the program developed to solve the equation iteratively and to calculate frequency shifts as a function of propagation distance in austenitic stainless steel with grain size of 200 ± 20 μm is given with Appendix 3.1 in Chapter 3.

5.3.5 Comparison of experimental and model based peak frequencies

The experimentally observed peak frequencies in the reflected echoes obtained from artificial defects (FBH and SDH) at different depths are shown in Fig. 5.10. The change in the peak frequency of the top surface echo with varied water path is also shown in Fig. 5.10. Negligible difference in peak ultrasonic frequencies is observed with change in the water path and it lies approximately 9 MHz at all the measured distances (2-50 mm). This clearly indicates that water medium does not alter the spectral content of the propagating ultrasonic waves at the frequency range used in this study. However, it can be clearly observed that the peak frequency shifts towards lower side with the ultrasonic propagation distance in the coarse grain austenitic stainless steel. The depth dependent peak frequency values obtained by theoretical model for stainless steel are in good agreement with the experimental values. Careful observation of Fig. 5.10 indicated that Specimen 2 exhibits slightly higher frequency values for the same propagation distances as compared to Specimen 3. This may arise from the marginal variation in the grain size of the two specimens.

It can be noticed from Fig. 5.10 that the peak frequency values obtained from artificial defects at different depths lie in a small frequency range 1.5-3.5 MHz. This indicates that a wavelet based filtering approach with a single scale corresponding to this frequency bandwidth can be used to improve the SNR and image the defects at different depths.

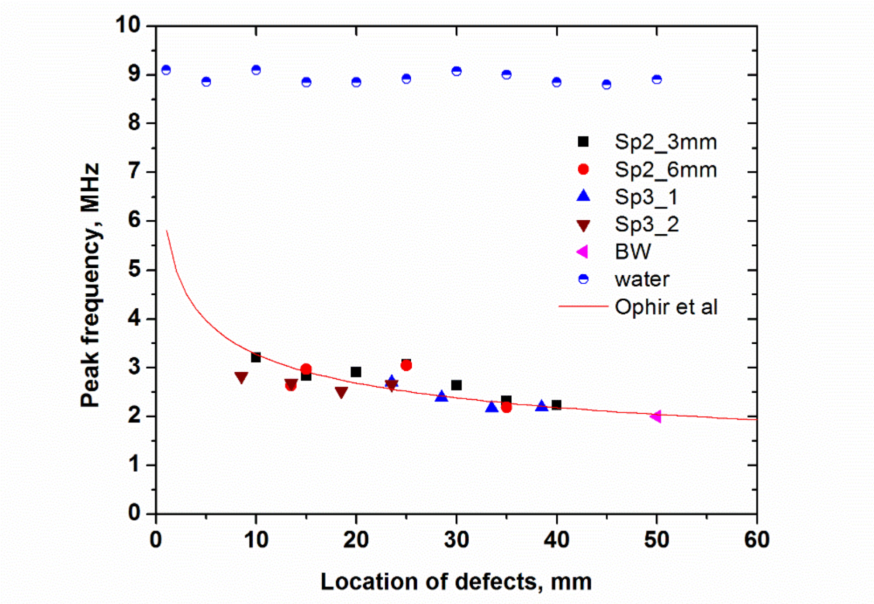

Fig. 5.10. Variation in peak frequency values of ultrasonic waves with propagation distance. The peak frequency values at different depths were evaluated by analysing ultrasonic echoes from artificial defects at different depths using STFT.

5.3.6 Wavelet based C-scan imaging

The CWT has a unique property that it provides very good frequency resolution and poor time resolution for the lower frequency components of the processed signals [68]. Since, the experimental and model results showed the presence of low frequency components at the defect locations, wavelet is an ideal choice for analysis of such signals. The CWT is a simple and powerful time-frequency domain technique, which can enhance SNR based on the selection of scale. Since, the peak frequencies from defect locations lie within small frequency range, one can utilise a single wavelet scale for improvement of SNR and imaging of defects. It is easy to automate the CWT based imaging process by the use of single scale. Further, inherent redundancy of continuous wavelet transform analysis can also be avoided. The application of CWT is also tested for detection of closely spaced defects in Specimen 3. The results presented in this study are based on qualitative analysis of C-scan images generated from Specimen 2 and Specimen 3 by wavelet based approach proposed in this study. It is very important to select proper gating positions to inspect maximum region of a specimen. The improper selection of data may lead to erroneous results. Therefore, ultrasonic data was selected by avoiding high amplitude water - specimen surface reflection. Conventionally, ultrasonic C-scan image is generated by two ways, first by gating the echo at the back-wall location and second between the front surface and the back-wall echo location. When the gating is done only at the back-wall echo location, the specimen with parallel surfaces provides the information about the defects present in the specimen due to shadowing effect, but the defect location can not be obtained. The ultrasonic echo amplitude at back-wall will be reduced depending on the defect size. When the gating is done between the scanning surface and the back-wall, the complete picture of the defects present in the material can be obtained including their position. The C-scan images were generated for both type of gating schemes, as discussed above.

The conventional time domain based C-scan images were generated using peak amplitude and corresponding time of flight in the selected data range for unprocessed signal. The wavelet based C-scan image was generated using peak amplitude of wavelet correlation coefficients at the optimum scale and corresponding time of flight for the selected data. The optimum wavelet scale was chosen based on the experimental and theoretical peak frequency values obtained from different artificial defects at different depths in Specimens 2 and 3, as shown in Fig. 5.10. The 'scal2freq' relation given in Eq. 4.6 was used to find out the optimum scale for 'Morlet' wavelet [96]. The optimisation of mother wavelet and scale-pseudo frequency conversion have been performed as discussed in Chapter 4. The wavelet scale *26* is optimised based on the experimental and theoretical studies carried out to understand frequency shifts in austenitic stainless steel specimens having 200 μm grain size. The optimum wavelet scale *26* has been used to process ultrasonic signals obtained from Specimen 2 and Specimen 3 to generate wavelet based C-scan images.

5.3.6.1 Specimen 2 (Flat bottom holes)

The conventional amplitude and time of flight based C - scan images of Specimen 2 generated by unprocessed signals are shown in Fig. 5.11 (a) and (b), respectively. As expected, no meaningful information can be obtained from these images due to poor signal to noise ratio. Only intermittent weak reflections at a few locations of 6 mm diameter flat bottom holes at 15, 20 and 25 mm depth from the scanning surface were observed in Fig. 5.11.

Fig. 5.12 (a) and (b) show the typical amplitude and time of flight (TOF) based C-scan images of Specimen 2, respectively generated by proposed wavelet based imaging methodology. It can be observed that all the defects present in this Specimen 2 could be imaged including 3 mm FBH located at 45 mm from scanning surface. The defect situated at 45 mm depth from the scanning surface shows a feeble amplitude, which is indicated by an arrow in Fig. 5.12 (b). It can be clearly noticed that wavelet based amplitude image provides better judgement about the size of the reflector compared to wavelet based time of flight image. The comparative analysis of CWT processed C-scan image by 10 MHz frequency (as shown in Fig. 5.12) with conventional C-scan image generated by 5 MHz frequency (as shown in Fig. 5.5), clearly shows that defects missed at lower frequency could also be imaged at higher frequency. This demonstrates the capability of wavelet processing for enhanced defect detection in coarse grained steels. The time of flight based C-scan image has a distinct advantage that it can provide the location of the defect also. For better visualisation of defects in Specimen 2, a 3D contour plot is made for the time of flight information obtained after CWT processing of ultrasonic data. Typical 3D graph is shown in Fig. 5.13, the colour bar represents the depth of the flat bottom holes from the inspection surface. The 3 mm FBH at 45 mm depth is not shown in the figure to visualise other defects with better clarity. The amplitude and TOF based C-scan images of Specimen 2 obtained by conventional time domain method by gating only the back-wall echo region are presented in Fig. 5.14 (a) and (b), respectively. The amplitude and TOF based images appears to be noisy and distinct information of defects could not be obtained by these images. This is attributed to the presence of high amplitude backscatter echoes compared to the defect echoes. To improve the imaging of defects ultrasonic data was processed with CWT, and the same data length utilised for conventional imaging purpose was used for generating wavelet based C-scan images. The amplitude and TOF based C-scan images by wavelet processing at single wavelet scale *26,* are shown in Fig. 5.15 (a) and (b), respectively. The wavelet filtering at optimum scale removes the high frequency noise and provides good sensitivity for detection of defects. Distinct information about the presence of defects was obtained from the C-scan images. The qualitative information about the size of the defects can also be obtained from these images.

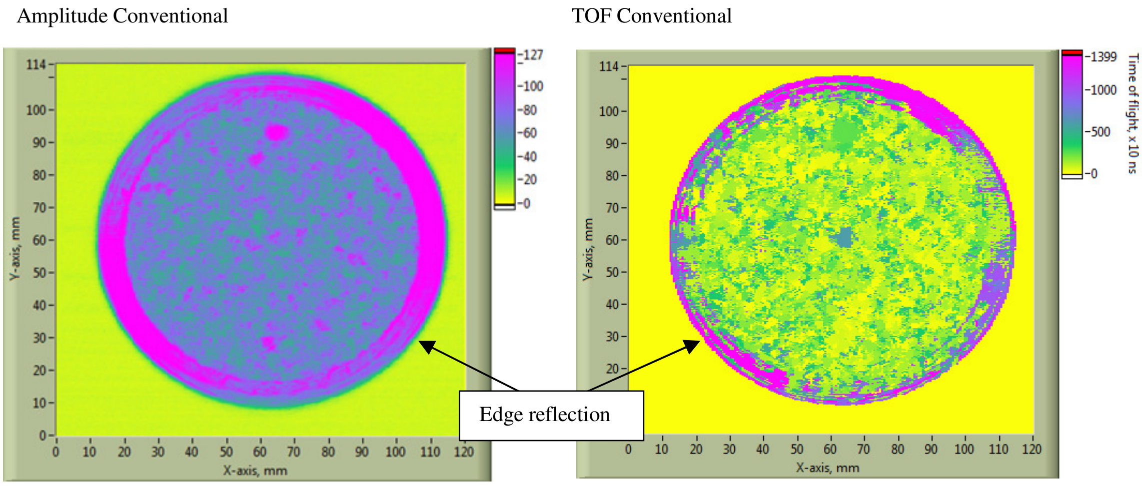

(a) (b)

Fig. 5.11. C-scan images generated by unprocessed data from Specimen 2 (a) amplitude and (b) time of flight based C-scans.

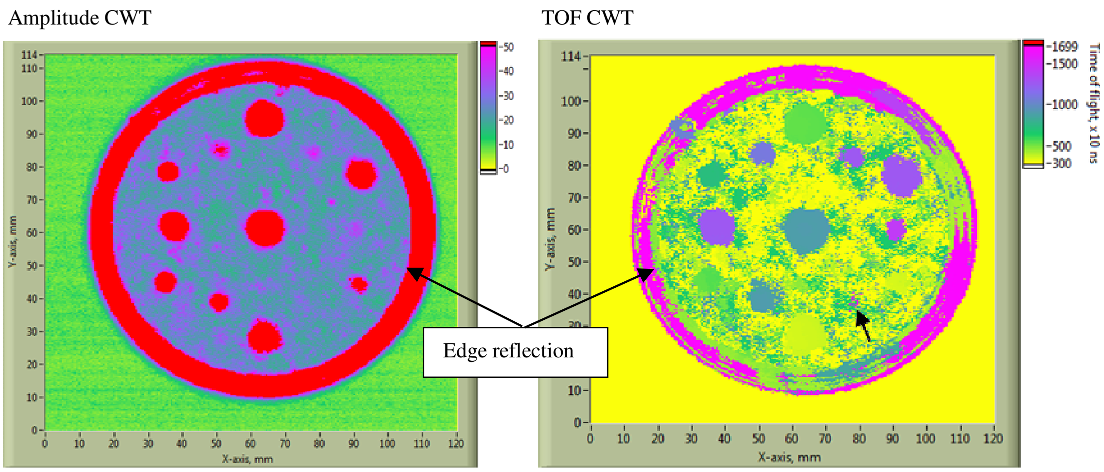

(a) (b)

Fig. 5.12. C-scan images generated by CWT processed data at optimum scale from Specimen 2 (a) amplitude and (b) time of flight based C-scan, arrow indicates deepest defect at 45 mm from scanning surface in the Specimen 2.

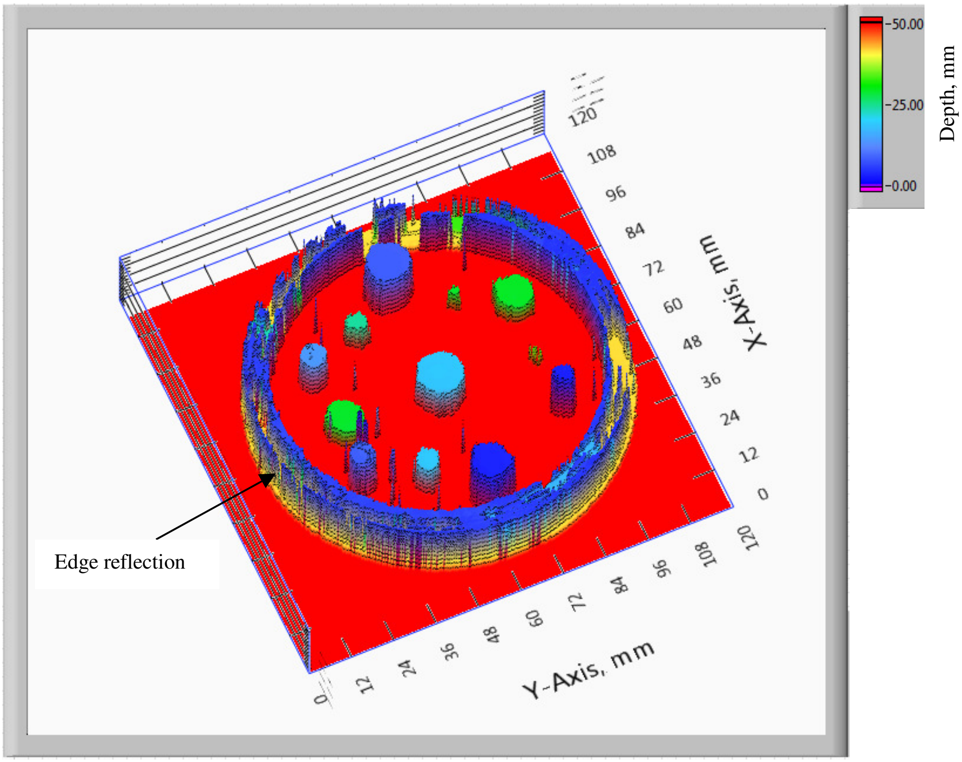

Fig. 5.13. 3D representation of the time of flight data shown in Fig. 5.12 (b), the location of the defects from the top surface in terms of depth is shown in this graph. The reflection from edge of the specimen is indicated by an arrow in the figure.

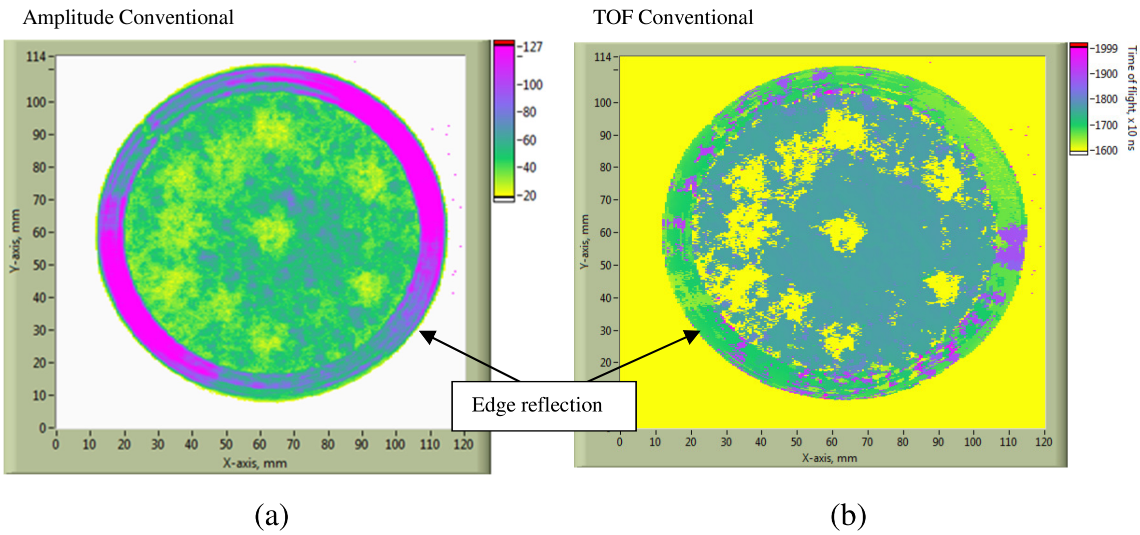

Fig. 5.14. C-scan images generated by unprocessed data from Specimen 2 (a) amplitude and (b) time of flight based C-scans. Only back-wall echo region was used for gating.

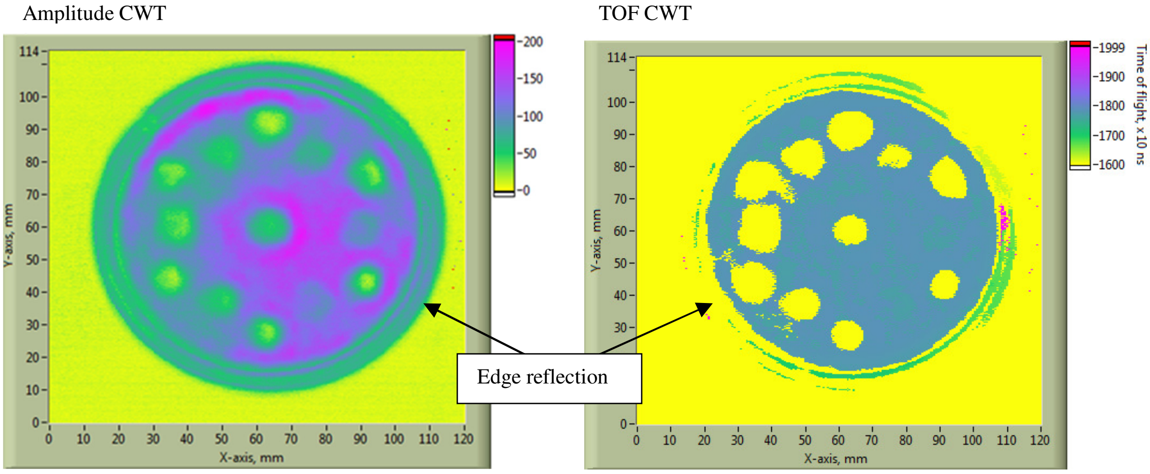

(a) (b)

Fig. 5.15. C-scan images generated by CWT processed data at optimum scale from Specimen 2 (a) amplitude and (b) time of flight based C-scans. Only back-wall echo region was used for gating.

5.3.6.2 Specimen 3 (Side drilled holes)

Various SDHs were made in Specimen 3 in a plane parallel to the specimen surfaces facilitating availability of both sides of the specimen for ultrasonic scanning. When the ultrasonic inspection is carried out from side 1, the centre of the nearest SDHs lies at 20 mm depth, and, the nearest SDHs from side 2 are located at 30 mm depth from the scanning surface. The amplitude and TOF C-scan images of Specimen 3 (side 1) generated by conventional time domain method with the unprocessed data are presented in Fig. 5.16 (a) and (b), respectively. Due to poor signal to noise ratio, no meaningful information could be obtained from these images. However, intermittent reflections can be seen at a few locations of artificial defects.

The typical amplitude and TOF based C-scan images of Specimen 3 obtained from side 1 by CWT processing with optimum scale are presented in Fig. 5.17 (a) and (b), respectively. It can be seen that all the SDHs can be imaged with the optimum scale *26*, which is used during the continuous wavelet transform processing of ultrasonic signals. The TOF based image provided the locations of defect from the scanning surface. The closely spaced ten number of SDHs in the same plane can be imaged and all these defects are shown by same green colour in Fig. 5.17 (b). The other five numbers of SDHs at different depths can also be distinguished according to their locations from scanning surface by different colours are also shown in Fig. 5.17 (b).

The conventional amplitude and TOF based C-scan images of Specimen 3 generated by unprocessed ultrasonic data obtained from scanning performed from side 2 of this specimen are presented in Fig. 5.18 (a) and (b), respectively. The amplitude and TOF based images are noisy and distinct information could not be obtained. However, the intermittent ultrasonic reflections at the locations of the three SDHs made at 5, 10 and 15 mm depth were observed in the conventional C-scan images. These intermittent reflections can be clearly seen from amplitude and TOF based C-scan images shown in Fig. 5.18 (a) and (b), respectively. These intermittent reflections observed in conventional C-scans are attributed to the proximity of the SDHs to the scanning surface. However, no distinct information could be obtained from these images. Fig. 5.19 (a) and (b) show the C-scan images of Specimen 3 obtained from side 2 by CWT processing with the optimum wavelet scale *26*. It can be clearly observed that all the SDHs fabricated in this specimen could be imaged. All the ten SDHs located in the same plane can be clearly distinguished by blue colour in Fig. 5.19 (b). Similarly, the other defects located at different depths were also imaged and can be distinguished by different colours as shown in Fig. 5.19 (b).

For better visualisation of defects in Specimen 3, a 3D contour plot is made from the time of flight information obtained after CWT processing of ultrasonic data. Typical 3D graphs from side 1 and side 2 inspections are presented in Fig. 5.20 and Fig. 5.21, respectively. The depth information of side drilled holes can be obtained from the colour bar given in the figures.

The qualitative analysis of the resolution capability of the CWT for closely spaced defects was performed from the images shown in Fig. 5.17 (a-b) and Fig. 5.19 (a-b). It can be clearly observed that the amplitude based images provide better resolution of the defects compared to the TOF images. When the inspection was carried out from the thicker side of Specimen 3 (side 2), the closely spaced defects can be clearly distinguished up to the centre of the specimen. The wavelet based amplitude images provided better information about the size of the side drilled holes in Specimen 3, compared to the wavelet based time of flight images.

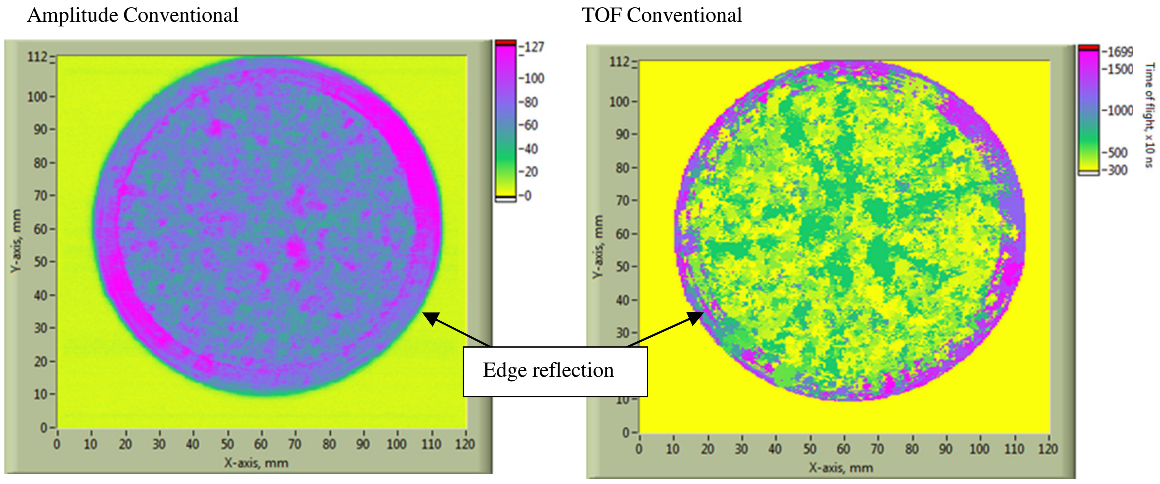

(a) (b)

Fig. 5.16. C-scan images generated by unprocessed data from Specimen 3 (side 1) (a) amplitude and (b) time of flight based C-scans.

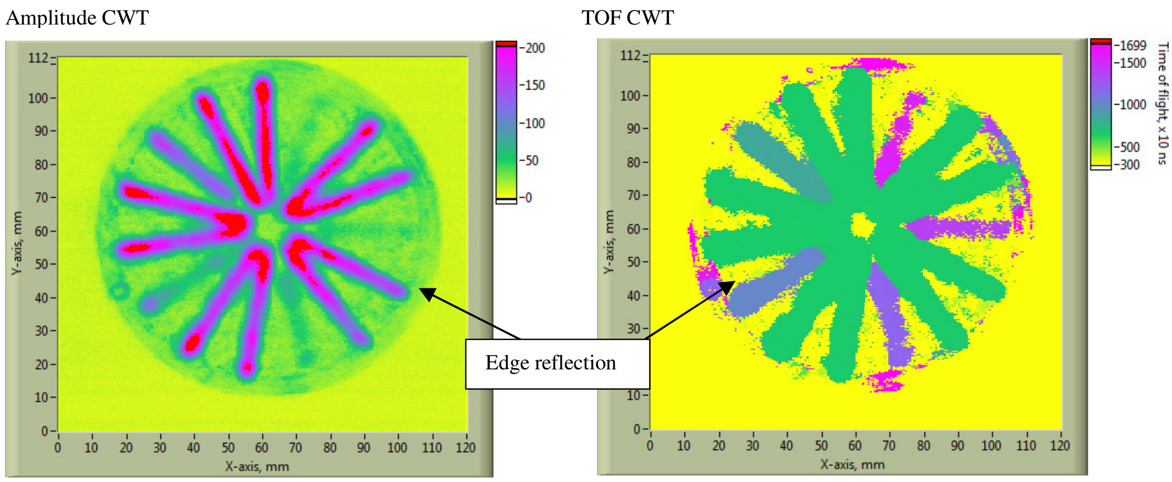

(a) (b)

Fig. 5.17. C-scan images generated by CWT processed data at optimum scale from Specimen 3 (side 1) (a) amplitude and (b) time of flight based C - scans.

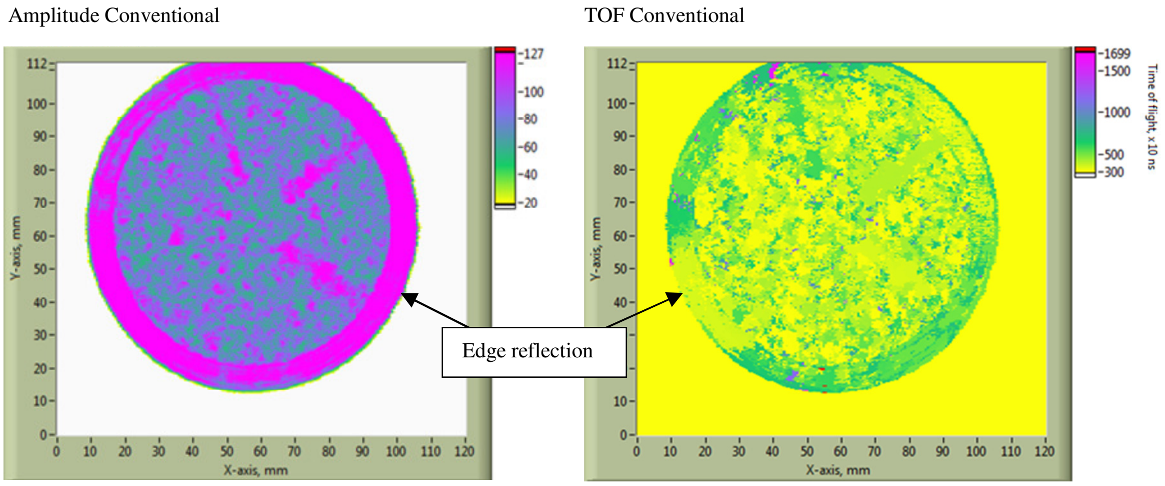

(a) (b)

Fig. 5.18. C-scan images generated by unprocessed data from Specimen 3 (side 2) (a) amplitude and (b) time of flight based C-scans.

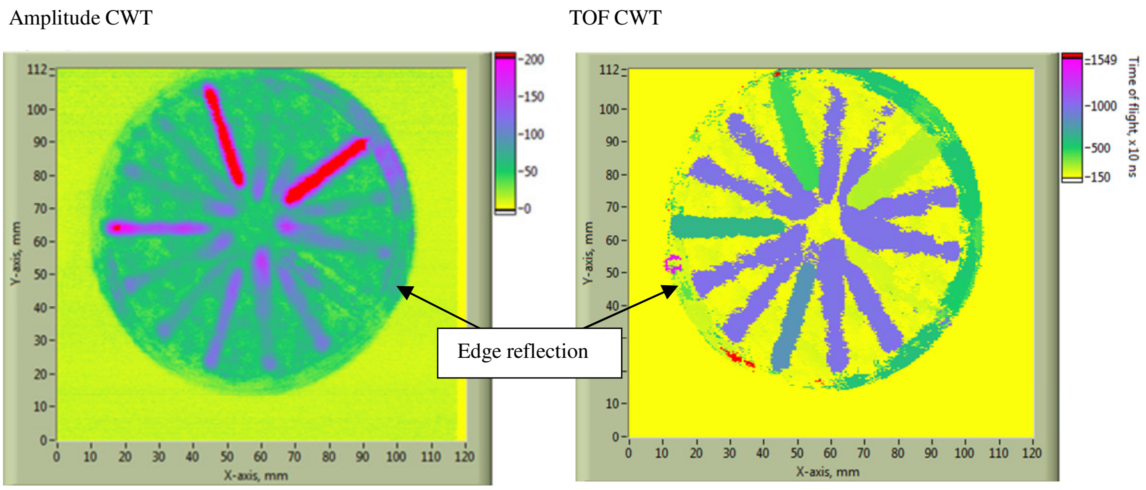

(a) (b)

Fig. 5.19. C-scan images generated by CWT processed data at optimum scale from Specimen 3 (side 2) (a) amplitude and (b) time of flight based C-scans.

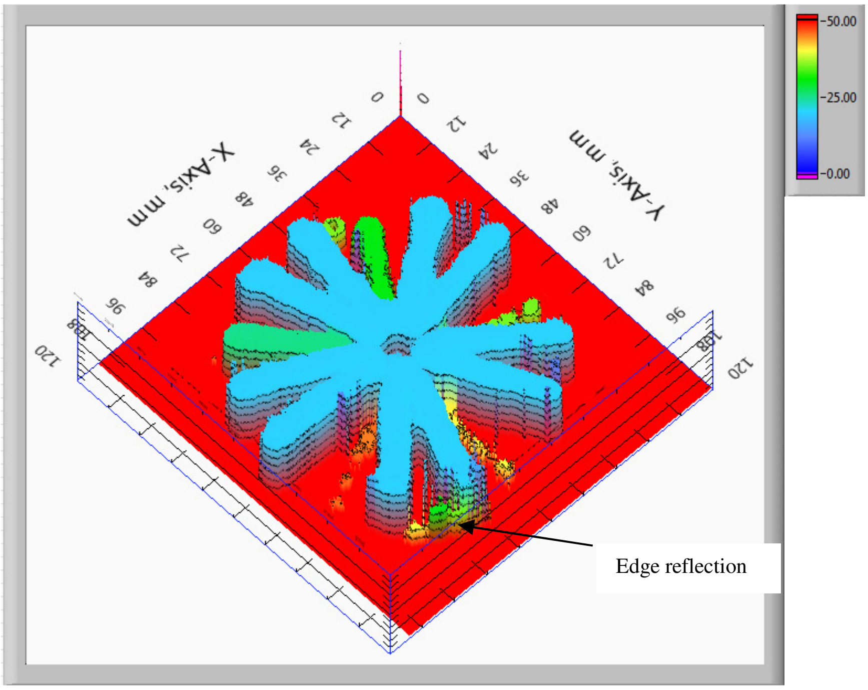

Fig. 5.20. 3D representation of the time of flight data shown in Fig. 5.17 (b), the locations of the side drilled holes from top surface (side 1) of specimen are given in terms of depth.

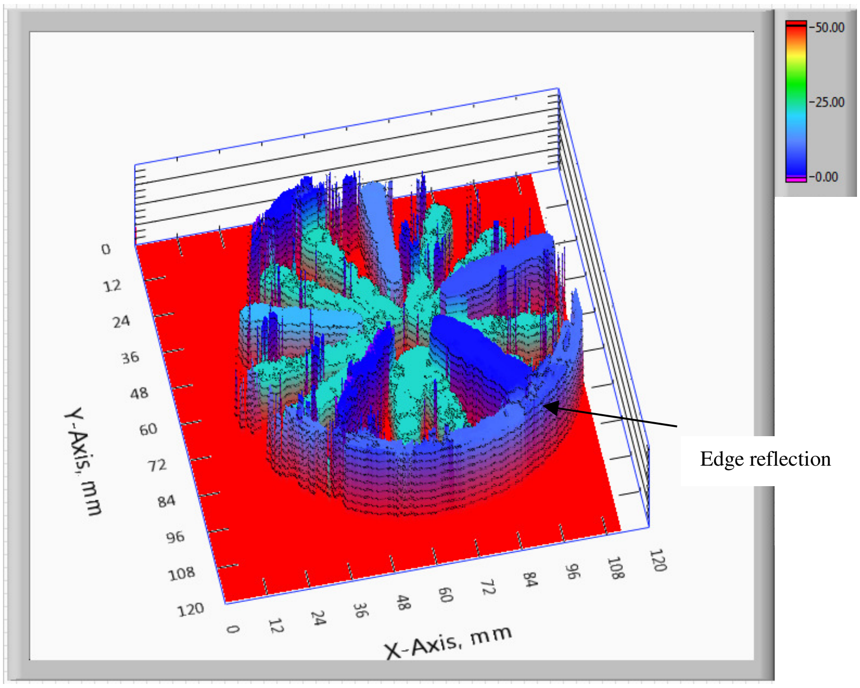

Fig. 5.21. A 3D representation of the time of flight data shown in Fig. 5.19 (b), the location of the side drilled holes from top surface (side 2) of specimen are given in terms of depth.

5.3.6.3 Qualitative evaluation of defect detection sensitivity

Comparative analysis is made for detection of defects using 10 MHz ultrasonic frequency by utilising conventional time domain processing and CWT processing of signals obtained from Specimens 2 and 3. The detection of defects in Specimen 2 by conventional time domain processing of ultrasonic signals using low frequency 5 MHz ultrasonic transducer are also included for comparison. The qualitative analysis of C-scan images obtained by conventional processing clearly indicates that only intermittent weak reflections could be observed at defect locations, and it is difficult to bring out the information about the shape of the reflector. However, the qualitative analysis of wavelet based C-scan images clearly demonstrates that all the defects could be imaged by CWT processing with the optimum scale (scale *26*) and the location of the defects could be obtained by TOF based images. The shape of the reflector can also be clearly traced from the wavelet based C-scan images. This clearly demonstrates the usefulness of the wavelet based imaging compared to conventional method.

The comparison of defect detection capabilities of conventional and wavelet approaches at two different frequencies in Specimen 2 is presented in Table 5.6. The smaller defects (3 mm) at larger depths (30-45 mm) could not be imaged by conventional approach using 5 MHz transducer. At higher ultrasonic frequency of 10 MHz, only intermittent reflections of defects closer to inspection surface or larger in size could be obtained by conventional approach. But by using wavelet approach, all the defects could be imaged even with 10 MHz frequency ultrasonic waves. It can be clearly observed from Table 5.6 and Table 5.7 that the deeper defects missed by conventional approach could be imaged by wavelet approach.

Table 5.6. Qualitative analysis for defect detection capability of conventional and continuous wavelet transform based approaches in Specimen 2.

Sl. No.	Defect Ref. No.	FBH depth from scanning surface, mm	FBH diameter, mm	Detection by Conventional method		Detection by wavelet method
				5 MHz	10 MHz	10 MHz
1	1	15	6	√	√	√
2	13	25	6	√	√	√
3	3, 10	35	6	√	X	√
4	5	5	3	√	√	√
5	7	10	3	√	X	√
6	9	15	3	√	X	√
7	11	20	3	√	X	√
8	8	25	3	√	X	√
9	12	30	3	X	X	√
10	2	35	3	X	X	√
11	4	40	3	X	X	√
12	6	45	3	X	X	√

Table 5.7. Qualitative analysis for defect detection capability of conventional and continuous wavelet transform based approaches in Specimen 3.

SDH depth from scanning surface, mm	SDH diameter, mm	Detection by Conventional method	Detection by wavelet method
		10 MHz	10 MHz
5	3	√	√
10	3	√	√
15	3	√	√
20	3	√	√
25	3	X	√
30	3	X	√
35	3	X	√
40	3	X	√
45	3	X	√

5.4 Conclusions

- ❖ STFT based approach has been established as a reliable method for detection of defects in coarse grain medium.

- ❖ The shift in the peak frequency with ultrasonic propagation distance is investigated by STFT with suitably designed specimens of coarse grain type 316 austenitic stainless steel. The spectral information at the defect locations could be obtained reliably by the proposed STFT approach which could not be achieved by conventional Fourier transform based approach.

- ❖ The experimentally observed shift in the peak frequency is found to be in good agreement with that obtained by an mathematical model based on ultrasonic scattering theory.

- ❖ The peak frequencies obtained from artificial defects located at different depths lies in a frequency band. This enables us to utilise single wavelet scale for imaging all the defects in coarse grain specimens. The developed methodology was also very useful in imaging the closely spaced defects.

- ❖ The STFT and CWT have been established as useful tools for defect detection and imaging with enhanced SNR in coarse grain austenitic stainless steels.

Chapter 6. Ensemble Empirical Mode Decomposition based Adaptive Processing of Ultrasonic Signals

6.1 Introduction

In the previous chapter 5, the ultrasonic imaging of defects in coarse grain austenitic stainless steel specimens using continuous wavelet transform based processing is discussed. However, the wavelet based imaging requires optimisation of different parameters such as mother wavelet and scale. This demands the use of new approaches, which can be used as an adaptive tool for imaging of defects in noisy medium. The Empirical Mode Decomposition (EMD) is a newly developed approach [15], which has been used as an adaptive tool for detection of defects in coarse grain material. A typical comparison of EMD with other time-frequency techniques used in this study such as STFT and CWT is presented in Table 6.1. The EMD approach suffers from mode mixing and in order to overcome this problem, a modified EMD approach known as Ensemble Empirical Mode Decomposition (EEMD) processing of ultrasonic signals is adopted [17]. The comparative analysis between EMD and EEMD processing of ultrasonic signals is made in the present study to understand the influence of these adaptive analysing techniques on the spectral content of the processed signals.

In order to establish a reliable adaptive methodology for defect detection and imaging in coarse grained steels, suitability of the Ensemble Empirical Mode Decomposition (EEMD) processing of ultrasonic signals obtained from coarse grain austenitic stainless steel is explored in this study. The EEMD processing of ultrasonic signals yields different Intrinsic Mode Functions (IMF). The reconstruction of ultrasonic signals can be carried out based on selected IMFs. The studies reported in literature have utilised sum of selected IMFs to reconstruct the ultrasonic signals [16]. However, a novel approach is proposed in this study by applying the signal minimisation algorithm to the selected IMFs obtained by EEMD processed ultrasonic signals. The signal minimisation algorithm has been widely used in split spectrum processing technique [6].

The proposed methodology is applied on ultrasonic signals obtained from various heat treated austenitic stainless steel specimens prepared, with and without defects. Further, a detailed investigation is carried out to reconstruct the ultrasonic signals adaptively with enhanced SNR obtained from a wide range of grain size specimens. The proposed method can be used as an adaptive tool for automatic detection of defects and finding their locations in austenitic stainless steels. The usefulness of proposed methodology is also demonstrated by processing an ultrasonic B-scan acquired from coarse grain specimen with multiple defects.

Table 6.1. Comparison of EEMD with STFT and CWT approaches

Parameters/approaches	STFT	CWT	EMD
Window size	Fixed	Flexible	No window (data driven process)
Resolution	Fixed	Flexible	Adaptive
Spectral parameter	Frequency	Scale or Pseudo frequency	Intrinsic Mode Functions (IMF)

6.2 Experimental

6.2.1 Specimen preparation

Ultrasonic signals from two different types of specimens of AISI type 316 stainless steel have been used in this study. The ultrasonic multiple back-wall echoes obtained from different grain size specimens have been used to study the adaptive nature of the EEMD processing for reconstruction of ultrasonic signals. The details of these specimens are presented in Table 4.2 of Chapter 4. The adaptive nature of EEMD processing with signal minimisation algorithm was then tested for detection of flat bottom holes (FBHs) in Specimen 2. The dimensional details of these FBH are given in Table 5.2 of Chapter 5. The ultrasonic signals have been acquired using ultrasonic immersion transducers of 10 and 25 MHz frequency. The data were recorded with 100 and 500 MS/s sampling rates. Different sampling rates are used to understand the influence of data length on the adaptive nature of EEMD processing.

6.3 Results and discussion

6.3.1 Comparison between EMD and EEMD analysis

A comparative analysis is performed between EMD and EEMD processing of ultrasonic signals to understand the influence of mode mixing. The Matlab routines developed by Flandrin et al. [101] have been used for performing these calculations. In the present study, different amplitudes of noise in the range of 0.1-0.4 times the standard deviation of the signals were utilised for EEMD analysis of ultrasonic signals. The noise amplitude of 0.2 times the standard deviation of signal was found to work well in all the cases investigated in this study.

The noise added in each trial to prevent the mode mixing effect, tends to diminish by $\varepsilon_0/\sqrt{M}$, where ε_0 is the noise amplitude and M is the number of ensembles. Lesser number of ensembles will not be able to prevent mode mixing and larger number of ensembles will increase the computational time. For the signals used in the study the optimum number of ensembles was found to be 100. Further, Hilbert spectra of IMF obtained by EMD and EEMD have been used to evaluate their spectral content. Further, Hilbert spectra of IMF obtained by EMD and EEMD have been used to evaluate their spectral content.

6.3.1.1 Effect of mode mixing

The comparative studies were carried out by processing the ultrasonic signal using EMD and EEMD processing methods to understand the effect of mode mixing. An ultrasonic signal obtained from 10 mm thickness and 78 µm grain size specimen was used for this purpose. The data range is selected including first three back-wall echoes. Fig. 6.1 (a) and (b) show typical IMFs obtained by EMD and EEMD processing of the ultrasonic signal, respectively. Typical Hilbert spectra of IMF-5 obtained by EMD and EEMD processing are shown in Fig. 6.2 (a-b). Hilbert spectrum of IMF-5 obtained by EMD processing shows the significant variations in the spectral content, while, the EEMD processed IMF represents spectral content with minimum variations. The meaningful spectral information obtained by Hilbert spectrum of the IMF is marked by the dashed horizontal lines. In comparison with EEMD, EMD represents nearly two times difference in the spectral content of IMF at the echo locations.

The locations of back-wall echoes, where mode mixing is evident due to EMD processing are circled by solid lines in red colour as shown in Fig. 6.1 (a). The back-wall echoes of the signal, where minimal mode mixing is present due to EEMD processing are circled by dotted lines in black colour as shown in Fig. 6.1 (b). It can be clearly seen that EEMD is able to separate different frequency contents of the signal into different IMFs with minimal mode mixing.

From the above results, it is evident that meaningful reconstruction of ultrasonic signal in coarse grained stainless steel is possible with EEMD processing. In view of this, only EEMD method is used for reconstruction of ultrasonic signals obtained from a range of grain size specimens. The EEMD decomposes the signal adaptively into a finite number of simpler components, thus making a filter bank available for processing the ultrasonic signals for defect signature and noise to be separated [102, 103].

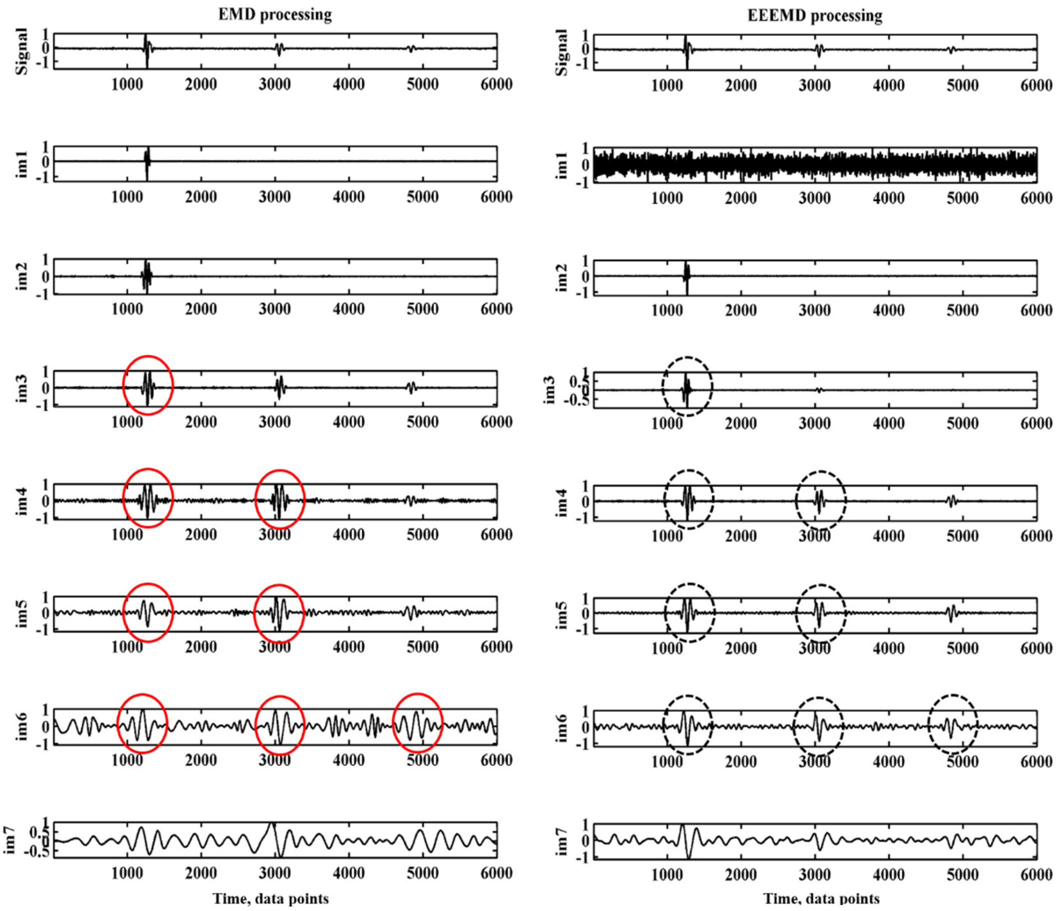

(a) (b)

Fig. 6.1. The comparison of IMFs (im1-im7) obtained by (a) EMD processing, the effect of mode mixing in different IMFs is marked by solid circles and (b) EEMD processing, in comparison to EMD processing the minimal mode mixing is present and marked by dotted circles. The multiple ultrasonic back-wall echoes obtained from 78 µm grain size specimen are selected for the comparison.

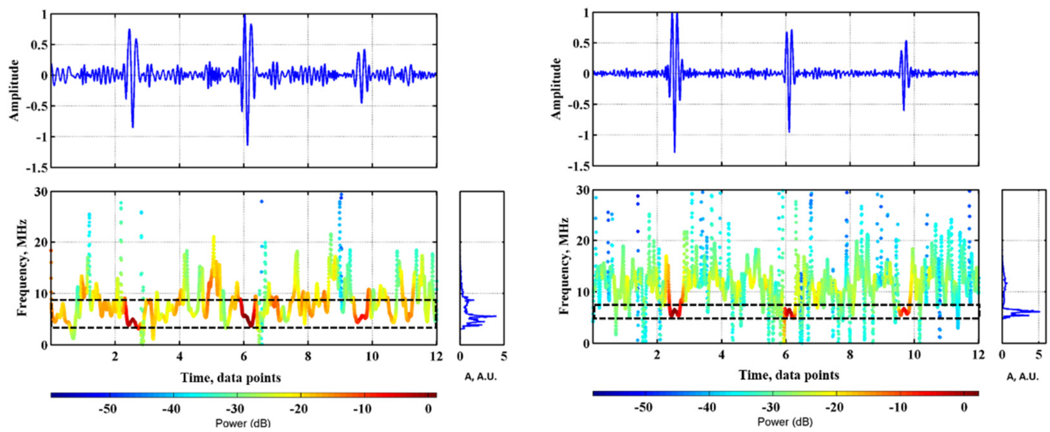

(a) (b)

Fig. 6.2. The Hilbert spectra, for a representative IMF (IMF-5) obtained from (a) EMD and (b) EEMD processing of ultrasonic signals obtained from 78 µm grain size specimen. It can be observed that the mode mixing is significantly reduced by EEMD processing.

6.3.2 Suitability of EEMD processing for signal reconstruction

The suitability of EEMD processing for reconstruction of an ultrasonic signal was evaluated by using an ultrasonic signal with multiple back-wall echoes obtained from 30 µm grain size specimen of 10 mm thickness. The amplitude spectra of different IMFs were obtained after EEMD processing of ultrasonic signal to understand the variation in frequency content of different IMFs.

Fig. 6.3 (a) and (b) show typical ultrasonic signal obtained from 30 µm grain size specimen and its IMFs obtained by EEMD processing with their corresponding amplitude spectra calculated by Fourier transform. The amplitude spectra clearly reveal that the signal comprises of 2-14 MHz frequency. The meaningful signal information is retained even up to the sixth (6^{th}) IMF, where the frequency content of the signal is approximately 1 MHz. The variation in the frequency pattern of different IMFs reveals that with an increasing IMF order the frequency content of the IMF decreases. After the sixth (6^{th}) IMF, very low frequency information is available, which does not provide any meaningful information about the signal. It is difficult to identify the multiple echoes in the seventh (7^{th}) IMF. The frequency content of IMFs follows a systematic pattern, which is achieved adaptively. However, in wavelet processing, the existing filter bank has to be used for processing the signal [7]. In the case of EEMD processing, the useful frequency bandwidth of the ultrasonic signals is determined adaptively, in comparison to the split spectrum processing [6], which demands the separate analysis of ultrasonic signals for the determination of useful bandwidth. Therefore, this method can be very useful for adaptive analysis of ultrasonic signals from coarse grained stainless steels. The useful range of IMFs is evaluated by analysing the ultrasonic signals obtained from a range of grain size specimens, which is discussed in the following section 6.3.3.

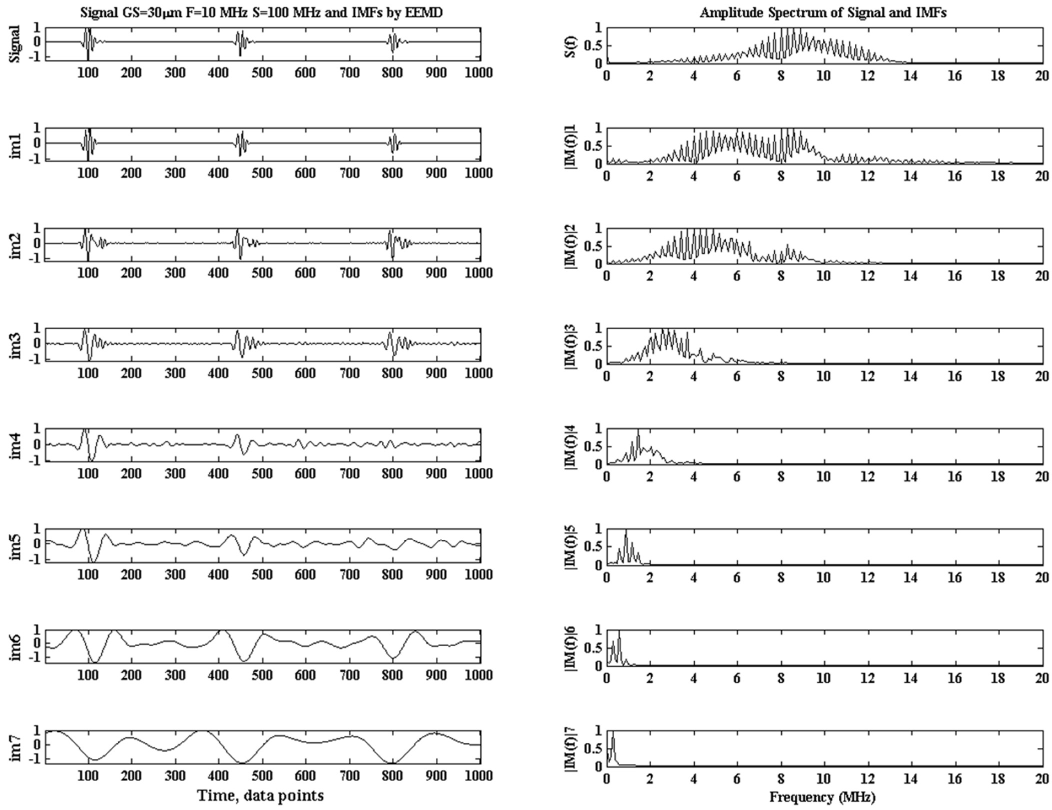

(a) (b)

Fig. 6.3. (a) Typical ultrasonic A-scan signal obtained from 30 µm grain size specimen and its IMFs (im1-im7) obtained by EEMD processing and (b) amplitude spectrum of the signal S(f) and corresponding IMFs (IM(f)-IM(f)7). The ultrasonic signal was acquired with 10 MHz transducer and 100 MS/s sampling rate.

6.3.3 Adaptive reconstruction of signals using EEMD

The adaptive nature of EEMD is tested by processing the ultrasonic signals obtained from a low and a high grain size specimens. These signals were acquired by 10 MHz transducer and sampled at 100 MS/s digitization rate. Fig. 6.4 (a) and (b), show IMFs obtained by EEMD based decomposition from 30 µm and 210 µm grain size specimens of 10 mm thickness, respectively. It can be seen clearly that the meaningful information about the back-wall echoes is available in the IMFs 3-5, irrespective of the large difference in the grain size. Due to adaptive filtering nature of this processing, high frequency grain noise is present in only initial IMFs, and low frequency information is present in the later IMFs. This clearly indicates that the processing of ultrasonic signal based on the selected IMF can provide good signal to noise ratio. This provides an idea to reconstruct the ultrasonic signals obtained from a range grain sizes with enhanced SNR. The observed adaptive nature of this processing can be utilized with selected IMFs to extract the necessary information. In order to analyze the extent of adaptation of EEMD processing for the ultrasonic data used in this study, various ultrasonic signals obtained with different frequencies and sampling rates were analysed. The ultrasonic signals were acquired from a 10 mm thickness specimen with 200 µm grain size, using 10 and 25 MHz transducers with different sampling rates. Fig. 6.5 show the typical IMFs obtained by EEMD processing of ultrasonic signal from (a) 10 MHz probe frequency and 100 MS/s sampling rate, (b) 10 MHz probe frequency and 500 MS/s and (c) 25 MHz probe frequency and 500 MS/s sampling rate. The ultrasonic signals were obtained from a coarse grain specimen in combination of two different ultrasonic frequencies and sampling rates. The two different frequencies were used to generate ultrasonic signals with different spectral content for the same microstructural conditions. The different sampling rates were chosen to vary the data length. It can be clearly noticed from Fig. 6.5 (a) and (c) that the EEMD filters the noise of the signals adaptively and the useful information which is available within a set of IMFs can be obtained. However, the number and level of IMFs are dependent on the probe frequency and the sampling rate chosen for acquiring the ultrasonic signal. The use of higher frequency at higher sampling rate shifts the desired information of the signal to higher IMFs. Therefore in order to make the EEMD based approach completely adaptive, the ultrasonic signals obtained by only one ultrasonic frequency, i.e., 10 MHz and sampling rate of 100 MHz is used to reconstruct the signals.

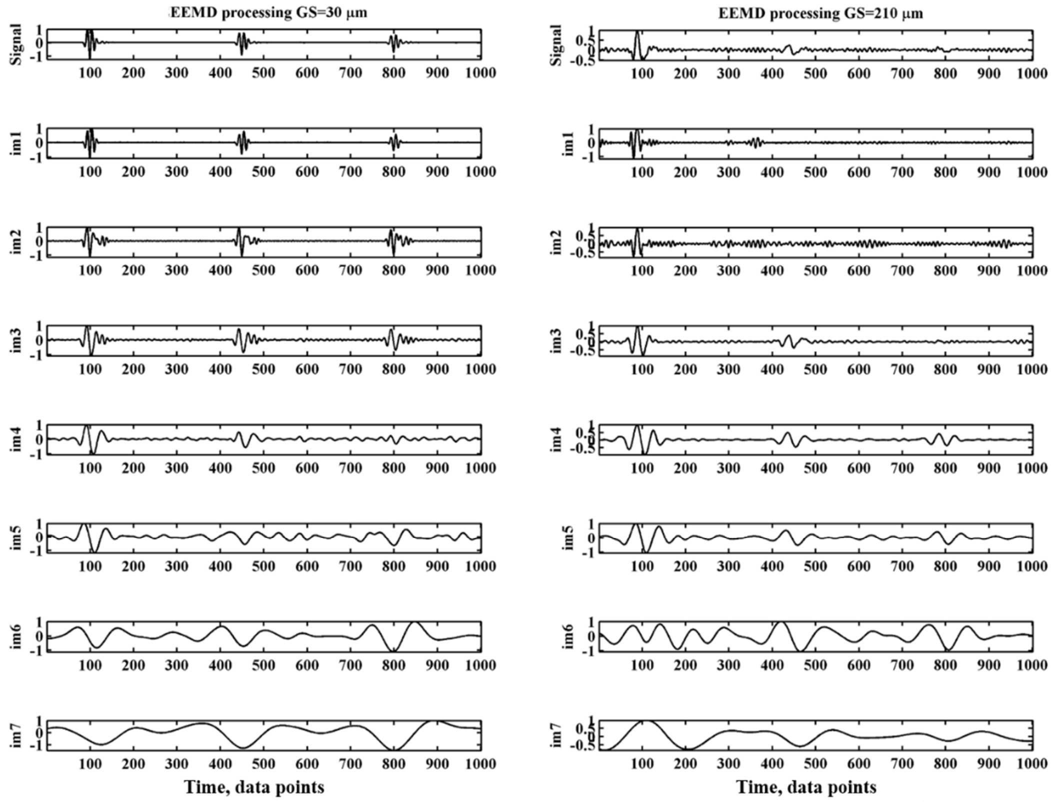

(a) (b)

Fig. 6.4. The IMFs (im1-im7) obtained by EEMD processing of ultrasonic signals obtained from (a) 30 µm and (b) 210 µm grain size specimen. Typical three multiple back-wall echoes are selected for processing. It can be inferred that typical IMFs (3-5) can be used to reconstruct the signal irrespective of the vast difference in the grain size.

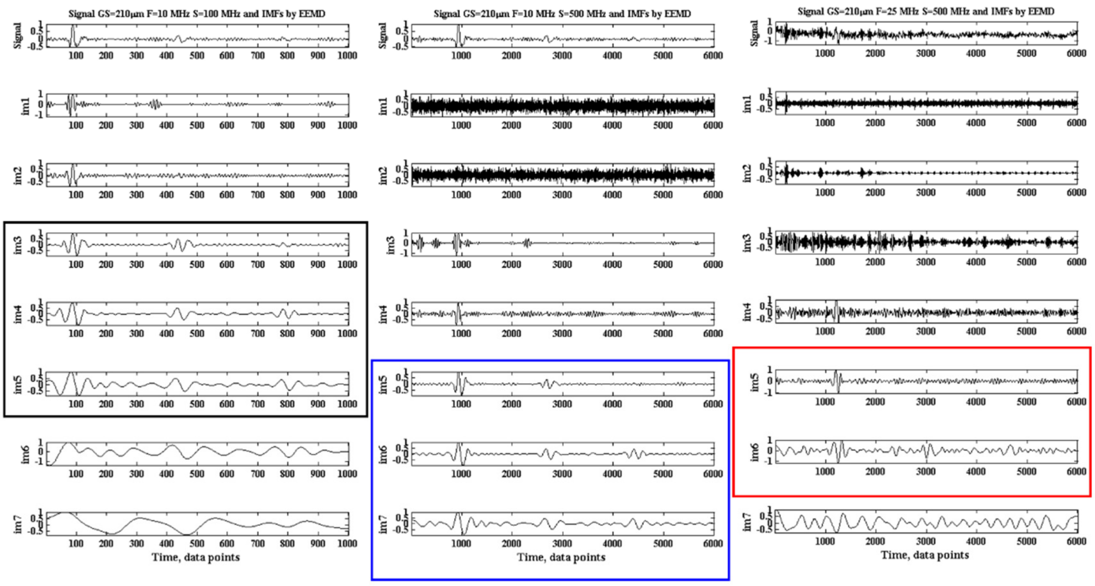

(a) (b) (c)

Fig. 6.5. Comparison of IMFs (im1-im7) obtained by EEMD processing for the ultrasonic signals obtained with (a) 10 MHz probe frequency and 100 MS/s sampling rate, (b) 10 MHz probe frequency and 500 MS/s sampling rate and (c) 25 MHz probe frequency and 500 MS/s sampling rate for 210 µm grain size specimen. The rectangular boxes represent the range of IMFs containing meaningful information of the signal.

The analysis of the signals for a range of grain sizes (30 and 210 µm) as presented in Fig. 6.4 and Fig. 6.5 showed that selected IMFs 3-5 provide the required information about the ultrasonic signal. Fig. 6.6 (a) and (b) show the original ultrasonic signals acquired from 30 and 210 µm grain size specimens, respectively. The signals reconstructed by sum of IMFs (3-5) are shown in Fig. 6.6 (c) and (d), respectively. The signals reconstructed by applications of minimisation algorithm to IMFs (3-5) are shown in Fig. 6.6 (e) and (f), respectively. For the second back-wall echo, ~13 dB higher SNR is observed with minimisation approach as compared to the sum of the selected IMF approach. The improvement in ths SNR is achieved by the adaptive filtering of high frequency components at these IMF levels. The SNR in the signals has been estimated based on the peak amplitude values of the signal (A1) and noise (A2) using the following relation.

$$\text{SNR (dB)} = 20 \log (A1/A2) \tag{6.1}$$

In addition, EEMD processing in conjunction with minimization approach also showed successful reconstruction of ultrasonic signals with enhanced SNR by selecting the IMFs (3-5) only, for the ultrasonic signals obtained from a range of grain size specimens (30-210 µm).

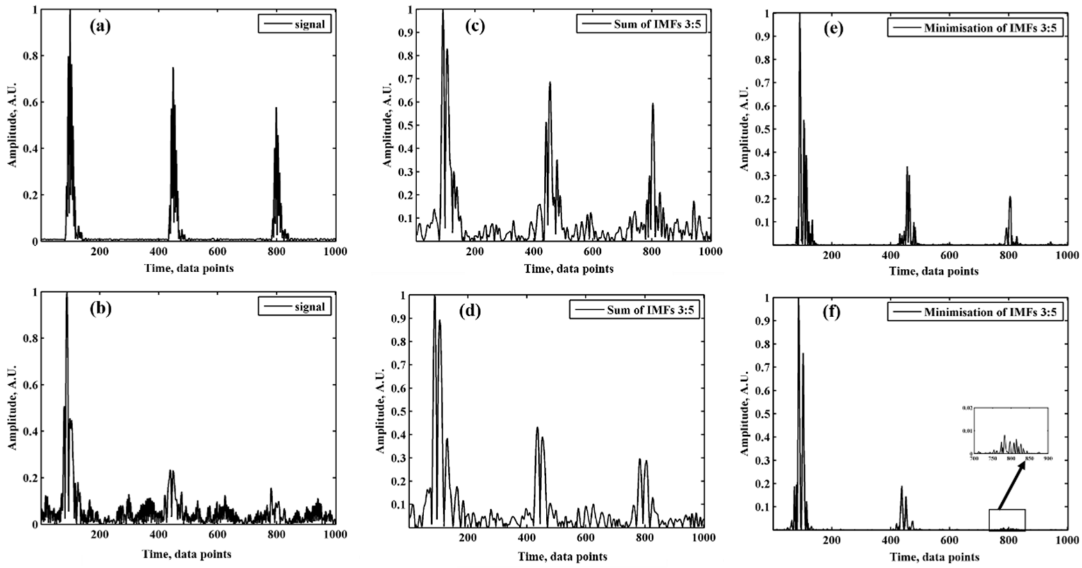

Fig. 6.6. (a-b) shows the ultrasonic signals obtained from 30 and 210 µm grain size specimens, the data range is selected including first three back-wall echoes, (c-d) The reconstruction of the ultrasonic signals by selected IMFs (3-5) obtained by EEMD processing and (e-f) The reconstruction of ultrasonic signals obtained by application of minimisation on selected IMFs (3-5) obtained by EEMD processing. The zoomed part of third back-wall echo is shown in the inset.

6.3.4 EEMD processing for detection of defects

The proposed methodology was extended to validate its usefulness for detection of defects in coarse grained materials. Artificially made FBH at different depths were used for this purpose. Fig. 6.7 (a-c) show the IMFs obtained by EEMD processing of ultrasonic signals recorded from flat bottom holes at (a) 25 mm (b) 30 mm and (c) 35 mm depth, respectively from the scanning surface of Specimen 2. The data range is selected to include the back-wall echo also for the processing. It can be clearly seen that typically IMFs (3-5) can be successively used to reconstruct the signal for different depths of investigation. Fig. 6.8 (a-c) show the actual ultrasonic signals, while Fig. 6.8 (d-f) represent the reconstructed signals with sum of selected IMFs (3 - 5) and Fig. 6.8 (g-i) show the reconstructed signals with application of minimisation on selected IMFs (3-5). It can be clearly seen that application of minimisation enhances the signal to noise ratio of the reconstructed signals. Table 6.2 presents a comparative improvement in the SNR of the signals obtained by the sum and minimisation of selected IMFs. It can be concluded that irrespective of the defect depth i.e., 25 mm - 35 mm, atleast 7 dB additional enhancement in SNR is achieved by IMFs minimisation compared to IMF sum.

The signals analysed with EEMD approach at three different depths (25 – 35 mm) were also analysed by continuous wavelet transform approach. The details of the CWT based approach is discussed in Chapter 5. The SNR in the wavelet processed signals at the optimum scale value was calculated using Eq. 6.1, and found to be 11.8 dB, 7.3 dB and 5.9 dB for the defects located at the depths of 25 mm, 30 mm and 35 mm, respectively. The SNR improvement achieved by CWT approach is found to be less than that obtained by the EEMD approach with minimisation. The superior capability of the proposed method in terms of SNR enhancement and adaptive signal reconstruction, makes it an ideal tool for processing of ultrasonic signals received from coarse grained material.

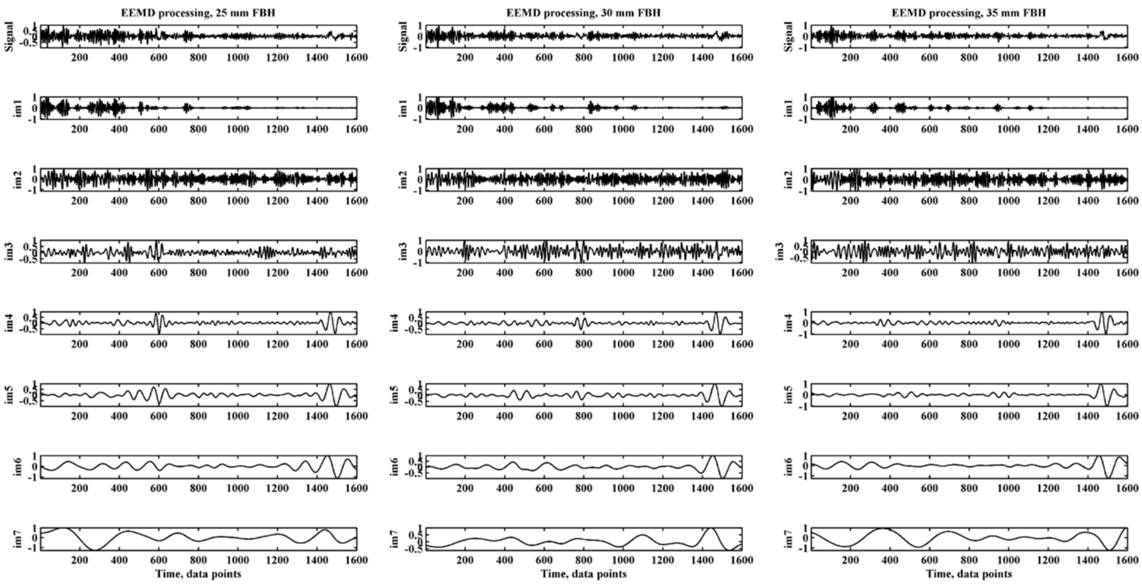

(a) (b) (c)

Fig. 6.7. The IMFs (im1-im7) obtained by EEMD processing of ultrasonic signals obtained from flat bottom holes (FBH) at (a) 25 mm, (b) 30 mm and (c) 35 mm distance from scanning surface in Specimen 2. The data range is selected to include back-wall echo for the processing also.

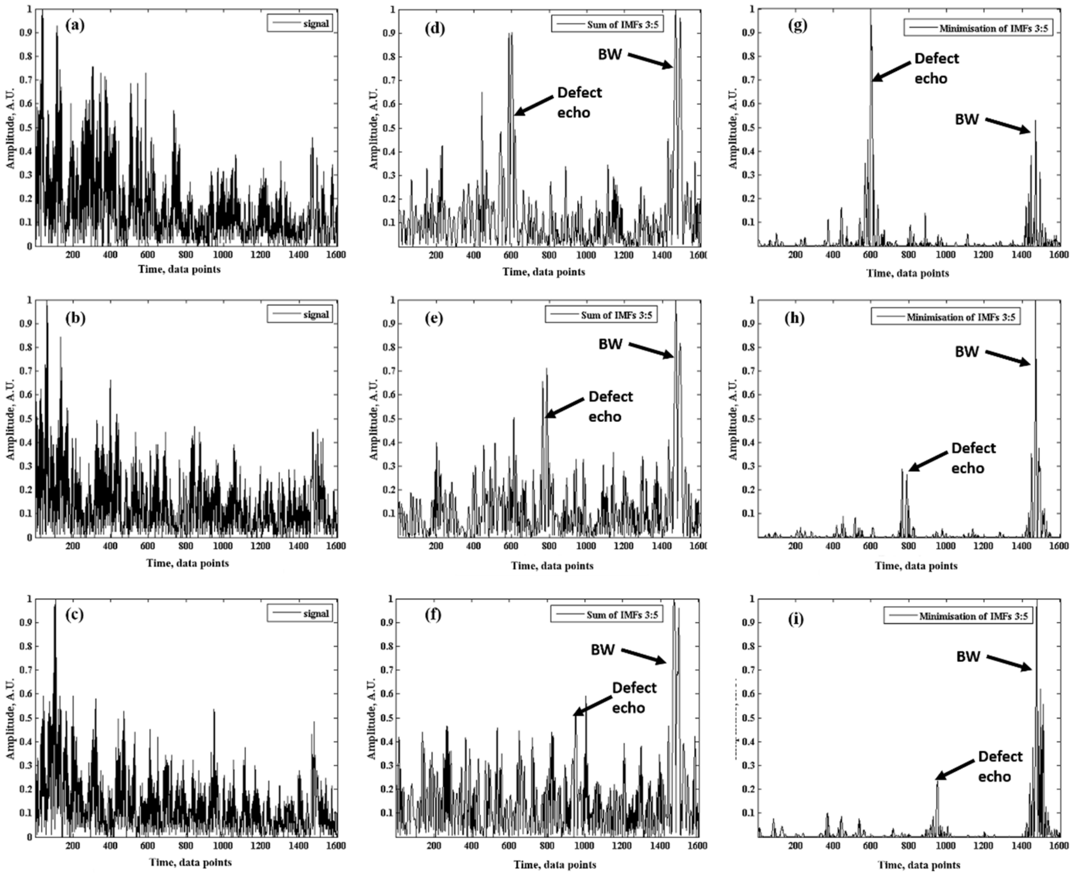

Fig. 6.8. (a-c) shows the ultrasonic signals obtained from flat bottom holes (FBH) at (a) 25 mm (b) 30 mm and (c) 35 mm distance from scanning surface in Specimen 2, (d-f) The reconstruction of the ultrasonic signals by selected IMFs (3-5) sum obtained by EEMD processing and (g-i) The reconstruction of ultrasonic signals obtained by application of minimisation on selected IMFs (3-5) obtained by EEMD processing. The defect and the back-wall echoes are indicated with arrows.

Table 6.2. Signal to noise ratio improvement in ultrasonic signals obtained from artificially made flat bottom holes in 200 µm grain size, 50 mm thickness austenitic stainless steel specimen (Specimen 2).

Depth of FBH from surface (mm)	SNR of raw signal (dB)	SNR of processed signal by Sum (dB) (A)	SNR of processed signal by Minimization (dB) (B)	Extra SNR enhancement due to minimisation (B-A), dB
25	<0	5.6	15.9	10.3
30	<0	3.8	10.8	7.0
35	<0	<0	8.3	8.3

6.4 Adaptive defect detection in a B-scan

The EEMD processing of ultrasonic A-scans in conjunction with minimisation algorithm was found to be useful in detecting the defect signals merged in backscatter with enhanced SNR. The developed methodology was further extended for adaptive defection of defects in an ultrasonic B-scan acquired from Specimen 2. The B-scan is obtained from the specimen containing flat bottom holes at different depths. Fig. 6.9 shows the scan details of the acquired ultrasonic B-scan and the defects covered. The defects located at 15 mm (3 mm diameter), 25 mm (6 mm diameter) and 35 mm (6 mm diameter) from scanning surface are covered in the B-scan, which consists of 180 A-scans. The initial high amplitude water-specimen ultrasonic reflection is not considered for the processing.

The raw B-scan image is shown in Fig. 6.10. The defect locations are marked with dotted circles and numbered as A (15 mm), B (25 mm) and C (35 mm), respectively in the unprocessed B – scan as shown in Fig. 6.10. The range of selected IMFs (3-5) obtained by EEMD processing of individual A-scans were used to reconstruct the signal by the proposed methodology. The comparative analysis of the sum of IMFs and application of minimisation algorithm to IMFs obtained by EEMD is also carried out.

The B-scan image obtained by processing the individual A-scan signals by EEMD and the sum of IMFs (3-5) were used for reconstruction of the signal and is shown in Fig. 6.11. It is clear from the processed image that three FBHs can be identified. However, the presence of significant noise can be seen throughout the image in Fig. 6.11. Fig. 6.12 shows the B-scan image obtained by application of minimisation algorithm to the selected IMFs (3-5) obtained by the EEMD processing.

The image provides very good signal to noise ratio throughout the image and the defects are imaged with enhanced SNR. This clearly demonstrates the usefulness of the proposed EEMD method with signal minimisation for truly adaptive analysis of ultrasonic signals for the detection and imaging of defects in coarse grained austenitic stainless steels.

The application of minimisation algorithm demands the normalization of signals. In case of individual A-scans with defects, the maximum amplitude is obtained corresponding to the defect location. However, in the absence of a defect signal, the normalization will be performed based on the maximum amplitude present in the signal, arising from the noise. An alternative strategy is adopted to remove unwanted high amplitude noise from B-scan by normalizing individual A-scans with the sum of the individual data point amplitudes. This removes the unwanted noise from the processed data. This processing has been applied to both the B-scans obtained after application of the IMFs sum and the minimization methods. The results obtained by this normalization process are shown in Fig. 6.11 and Fig. 6.12.

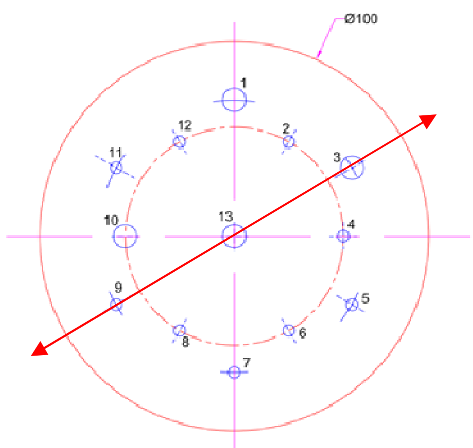

Fig. 6.9. The ultrasonic B-scan was acquired by automatic scanning covering the three flat bottom holes including 9 (3 mm dia., 15mm deep), 13 (6 mm dia., 25 mm deep) and 3 (6 mm dia., 35 mm deep).

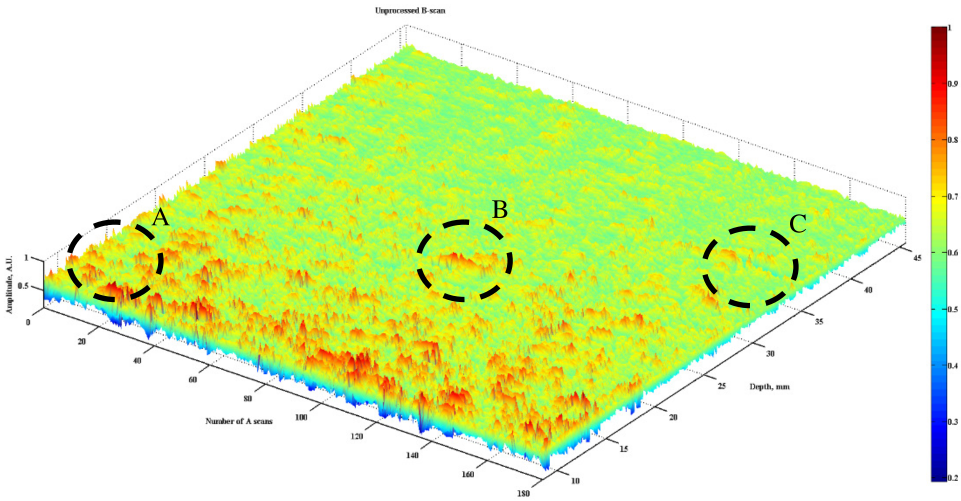

Fig. 6.10. The original B-scan acquired. The ultrasonic frequency used for scanning was 10 MHz and data were acquired at 100 MS/s sampling rate.

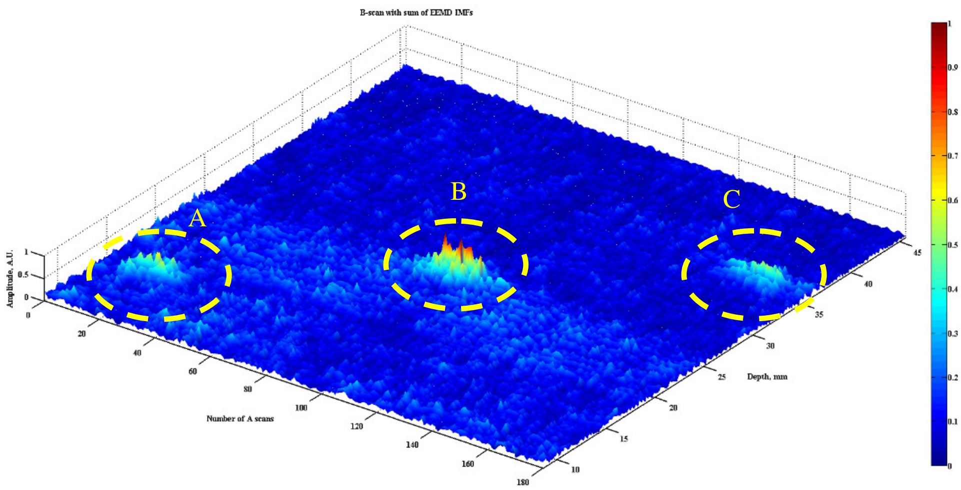

Fig. 6.11. The B-scan reconstructed by sum of IMFs (3-5) obtained by EEMD processing.

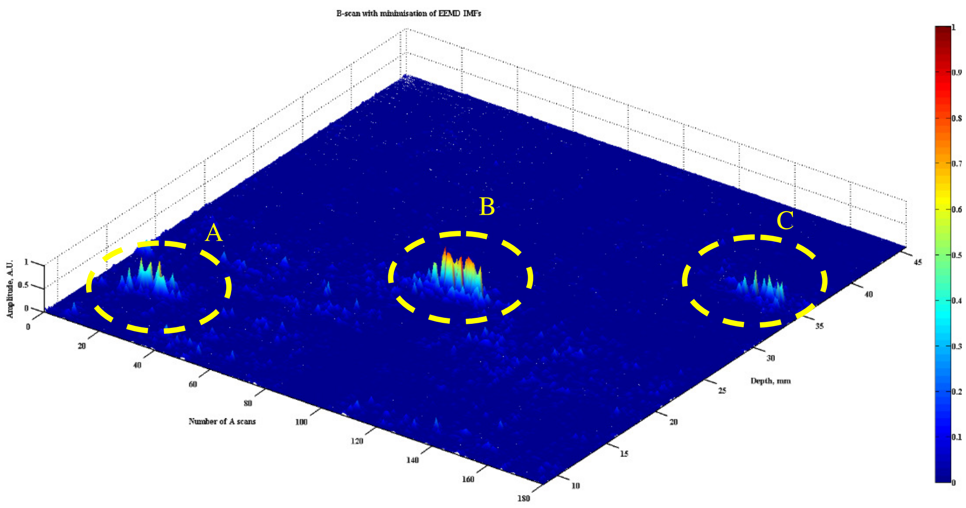

Fig. 6.12. The B-scan reconstructed by applying minimisation algorithm to the IMFs (3-5) obtained by EEMD processing.

6.5 Conclusions

- EEMD has been established as a useful tool for processing of ultrasonic signals obtained from coarse grain austenitic stainless steel, which is able to overcome the mode mixing problem during EMD analysis.

- To the best of the author's knowledge, this is a first of its kind attempt to use combination of EEMD and signal minimisation algorithm for truly adaptive reconstruction of ultrasonic signals with enhanced SNR from a wide range of grain size 30-210 μm.

- The proposed approach showed considerable enhancement of SNR for the ultrasonic signals obtained from artificial defects at different depths. The proposed minimisation method showed at least 7 dB extra enhancement in the SNR as compared to the conventionally used selected IMF sum approach.

Chapter 7. Summary and Future Works

7.1 Summary

In the present study different time-frequency signal processing methods have been adopted to process the ultrasonic signals for the evaluation of grain size, defect detection and imaging. A novel signal processing approach is also proposed for truly adaptive reconstruction of ultrasonic signals with enhanced signal to noise ratio. The ultrasonic signals were acquired from suitably designed coarse grain austenitic stainless steel specimens with higher scattering. This study provides a deeper insight into the use of time-frequency analysis tools for enhanced microstructural and defect characterisation in austenitic stainless steels. The salient results obtained in the thesis are presented below:

- The short time Fourier transform (STFT) has been established as a useful tool for understanding the frequency dependent attenuation and estimation of grain size in austenitic stainless steels. A novel scheme for optimization of window parameter for STFT is also proposed. To the best of the author's knowledge, this is the first of its kind attempt for comprehensive microstructural characterization using time-frequency approach.

- The use of STFT processing demonstrated the possibility of enhanced grain size evaluation compared to conventional spectral analysis based approaches. This is achieved by extraction of reliable frequency information at the back-wall location of the ultrasonic echoes.

- The spectral content of the ultrasonic signals obtained from coarse grained steels can be analyzed pictorially in STFT spectrogram, and this has been effectively utilized for the analysis of the spectral content of back-wall echo and backscatter signals simultaneously.

- The peak frequency values up to three back-wall echoes can be obtained reliably for a range of grain sizes (30-210 μm) using STFT based approach. The variation in the peak frequency of the multiple back-wall echoes exhibited linear relationship with $d^{-1/2}$. The slope of this correlation showed increasing trend from first to third back-wall echoes, which indicated an increased sensitivity of the spectral peak frequency based methodology for grain size measurements. This increased sensitivity can be attributed to extended wave-material interaction.

- The corner echo acquired using 45° shear waves also showed linear relationship with $d^{-1/2}$. Hence, the frequency shift based methodology developed in this study is valid for both longitudinal and shear wave modes.

- The limitation of fixed resolution of STFT has been addressed by using continuous wavelet transform (CWT) for the analysis of ultrasonic signals obtained from coarse grained stainless steel. CWT based pseudo frequency approach has also been successfully used for grain size evaluation.

- The STFT approach established for microstructural characterization was also used for defect characterization. The time-frequency analysis enabled the imaging of defects in higher scattering material at higher ultrasonic frequency, which could not be imaged by conventional low frequency testing. The proposed method enables high frequency based inspection at near surface and comparatively lower frequency based examination for deeper regions.

- The depth dependency of ultrasonic peak frequency shift is investigated by STFT with judiciously designed specimens of coarse grain austenitic stainless steel. The experimentally observed shift in the peak frequency is found to be in good agreement with that obtain by an empirical model based on the ultrasonic scattering theory.

- The imaging scheme based on CWT processing of ultrasonic signals provides a unique opportunity to extract the defect location by time of flight images. The CWT imaging scheme with optimum scale is also found to be very useful in imaging of closely spaced defects.

- Ensemble Empirical Mode Decomposition (EEMD) based processing has been utilized for adaptive processing of ultrasonic signals obtained from coarse grain stainless steels. The EEMD is able to overcome mode mixing problems of Empirical Mode Decomposition (EMD) analysis.

- First of its kind attempt is made to use EEMD processing with signal minimisation algorithm for adaptive reconstruction of ultrasonic signals with improved signal to noise ratio has been made. The proposed method provides significant improvement in the SNR compared to commonly used IMF sum approach.

- The novel combination of EEMD processed IMFs and signal minimisation makes the proposed approach truly adaptive for reconstruction of ultrasonic signals with enhanced SNR in high scattering coarse grain austenitic stainless steels. This enables detection of defects with high sensitivity present at larger depths even in highly scattering materials in comparison to conventional ultrasonic methods.

7.2 Future works

Based on the detailed investigations on the evaluation of grain size and defect detection and imaging in austenitic stainless steel performed in the present study, the important issues need to be addressed in the future work are suggested below:

(1) Time-frequency based approaches have been used in this study to analyse back-wall echo signals obtained from austenitic stainless steel for the evaluation of grain size. Further work should be directed towards the analysis of ultrasonic backscatter signals for grain size evaluation by EMD approach.

(2) The Hall Petch type relationship being observed for longitudinal and shear waves can be further investigated in detail.

(3) The time-frequency based STFT approach is successfully implemented to determine peak frequency in the high scattering medium. It would be of interest, if STFT can be used for phase velocity calculations in austenitic stainless steels with different grain sizes for the examination of the dispersion effect.

(4) EEMD in conjunction with minimisation algorithm has been established as a useful tool for adaptive detection of defects in high scattering austenitic stainless steel. This approach should be examined for adaptive detection of defects in other high scattering materials such as composites and concrete structures.

(5) The usefulness of time-frequency methods for detection and imaging of defects in anisotropic stainless steel weldments need to be explored.

References

[1] J. Krautkramer; H. Krautkramer, Ultrasonic testing of materials, vol. 4th ed., Springer Verlag, 1990.

[2] E P. Papadakis, "Ultrasnoic attenuation casued by scattering in polycrystalline media," in *Physical Acoustics*, vol. IV B, W. P. Mason, Ed., New York, Academic, 1968, pp. 278-304.

[3] S. Qian; D. Chen, Joint time-frequency analysis, methods and applications, Englewood Cliffs, 1996.

[4] R. Polikar, "The story of wavelets, in Physics and Modern Topics in Mechanical and Electrical Engineering, (ed. Mastorakis, N)," World Scientific and Eng. Society Press, pp. 192-197, 1999.

[5] J. Saniie; X M. Jin, "Model-based frequency estimation for ultrasonic NDE application," *IEEE Ultrasonic Symposium,* vol. 2, pp. 1129-1132, 1994.

[6] V L. Newhouse; N M. Bilgutay; J. Saniie; E S. Furguson, "Flaw to grain size enhancement by split spectrum processing," *Ultrasonics,* vol. 20, no. 2, pp. 59-68, March 1982.

[7] A. Abbate; J. Koay, "Signal detection and noise suppression using a wavelet transform signal processor: application to ultrasnoic flaw detection," *IEEE TUFF,* vol. 44, no. 1, pp. 14-26, 1997.

[8] P. Karpur; O J. Canelones, "Split spectrum processing: a new filtering approach for improved signal-to-noise ratio enhancement of ultrasonic signals," *Ultrasonics,* vol. 30 , no. 6, 1992.

[9] R. Philippe; C J. Pritchard, "An overview of split spectrum processing," *NDT.net,* vol. 8, no. 8, August 2003.

[10] Y J. Chen; Y W. Shi; Y P. Lei, "Use of wavelet analysis technique for the enhancement of signal-to-noise ratio in ultrasonic NDE," *Insight,* vol. 38, no. 11, pp. 800-803, November 1996.

[11] E. Pardo; J L. San Emeterio; M A. Rodriguez; A. Ramos, "Noise reduction in ultrasonic NDT using undecimated wavelet transforms," *Ultrasonics,* pp. 1063-1067, 2006.

[12] J. Zhao; P A. Gaydecki; F M. Burdekin, "Investigation of block filtering and deconvolution for the improvement of lateral resolution and flaw sizing

accuracy in ultrasonic testing," *Ultrasonics,* vol. 33, no. 3, pp. 187-194, 1995.

[13] Y-F. Chang; S-C. Chen, "Imaging Hilbert-Transformed Ultrasonic Data,," *Research in Nondestructive Evaluation,* vol. 13, no. 2, pp. 97-103, 2001.

[14] S. Legendre; J. Goyette; D. Massicotte, "Ultrasonic NDE of composite material structures using wavelet coefficients," *NDT&E International,* vol. 34, pp. 31-37, 2001.

[15] N E. Huang; Z. Shen; et al., "The empirical mode decomposition and the Hilbert spectrum for non linear and non stationary time series analysis," *Proceedings of Royal Society London,* vol. 454, no. A, pp. 903-995, 1998.

[16] Q. Li; G. Luo; G. Chen; P. Huang, "Application of empirical mode decomposition for ultrasonic testing of coarse grained materials," *Telkomnika,* vol. 11, no. 9, pp. 5322-5328, September 2013.

[17] Z. Wu.; N E. Huang, "Ensemble empirical mode decomposition: a noise assisted data analysis method," *Adv Adaptive Data Anal,* vol. 1, pp. 1-41, 2008.

[18] T. Wang, M. Zhang, Q. Yu; H. Zhang, "Comparing the applications of EMD and EEMD on time-frequency analysis of seismic signal," *Journal of Applied Geophysics,* vol. 83, pp. 29-34, 2012.

[19] P. Mclntire, Nondestructive Testing Handbook: Ultrasonic Testing, vol. 7, American Society for Testing and Materials (ASTM), 1991, p. 836.

[20] L S. Fu, "Mechanics aspects of NDE by sound and ultrasound," *Applied Mechanics Revivew,* vol. 35, no. 8, pp. 1047-1057, 1982.

[21] Papadakis, E P., "Physical acoustics and microstructure of iron alloys," *International Metallurgical Review,* vol. 29, no. 1, pp. 1-24, 1984.

[22] Anish Kumar, *Correlation of microstructure and mechanical properties with ultrasonic parameters in metallic materials,* IIT Kharagpur: Ph. D. Thesis, 2003.

[23] R L. Roderick; R. Truell, "The measurement of ultrasonic attenuation in solids by the pulse technique and some results in steel," *Journal of Applied Physics,* vol. 23, no. 2, pp. 267-279, 1952.

[24] E P. Papadakis, "Revised grain scattering formulae and table," *Journal of Acosutical Society of America,* vol. 37, no. 4, pp. 703-710, 1965.

[25] E P. Papadakis, "Ultrasonic attenuation and velocity in three transformation products in steel," *Journal of Applied Physics,* vol. 25, no. 5, pp. 1474-1482, 1964.

[26] E P. Papadakis, "Ultrasonic attenuation caused by scattering in polycrystalline metals," *Journal of Acoustical Society of America,* vol. 37, no. 4, pp. 711-717, 1965.

[27] R. Klinman; G. R. Webster; F. J. Marsh; E. T. Stephenson, "Ultrasonic prediction of grain size, strength, and toughness in plain carbon steel," *Materials Evaluation,* vol. 38, no. 10, pp. 26-32, 1980.

[28] W. Gao; C. Glorieux.; S E. Kruger; K V. Rostyne; V. Gusev; W. Lauriks; J. Thoen, "Investigation of the microstructure of cast iron by laser ultrasonic surface wave spectroscopy," *Mater. Sci. and Engg.,* vol. A 313, pp. 170-179, 2001.

[29] A B. Bhatia, "Ultrasonic Absorption," Oxford Univeristy Press, 1967.

[30] D. Eifler; E. Macherauch, "Microstructure and cyclic deformation behaviour of plain carbon and low alloy steels," *International Journal of Fatigure,* vol. 12, pp. 165-174, 1990.

[31] P. Kalyanasundaram; J. Reszat; M. Paul, "Absorption measurements on creep damaged samples using reverberation technique," *Materials Science Forum,* Vols. 210-213, pp. 243-250, 1996.

[32] T. Jayakumar, *Microstructural characterisation in metallic materials using ultrasonic and magnetic methods,* Saarbrucken, Germany: Ph. D. Thesis, 1997.

[33] S. Bolognini; A. Moreau, "Ultrasonic absorption in ultra low carbon steel," *Journal of Applied Physics,* vol. 94, no. 6, pp. 3771-3780, 2003.

[34] H M. Ledbetter, Elastic properites in materials at low temperature, R. P. Clark and A. F. Reed, Eds., Ohio: Americal Society for Metals, Metals Park, 1983, pp. 1-45.

[35] P. Li; S L. Chu; C P. Chou; F C. Chen, "Use of ultrasonic velocity for nondestructive evaluation of ferritic content in duplex Fe-Mn-Al alloy steels," *Scripta Metall. Mater.,* vol. 26, pp. 127-132, 1992.

[36] J C. Shyne; N. Grayeli; G S. Kino, "Acoustic properties as microstucture dependent materials properties," *Proc. Symp. NDE: Microstructural Characterisation and Reliability Properties,* pp. 133-141, 1981.

[37] P. Palanichamy; A. Joseph; T. Jayakumar; Baldev Raj, "Ultrasonic velocity measurements for estiamtion of grain size in austenetic stainless steel," *NDT&E International,* vol. 28, pp. 179-184, 1995.

[38] S. Hirsekorn, "The scattering of ultrasonic waves by polycrystals," *Journal of Acoustic Society of America,* vol. 72, pp. 1021-1031, 1982.

[39] S. Hirsekorn, "The scattering of ultrasoinc waves by polycrystals. II Shear Waves," *Journal of Acoustical Society of America,* vol. 73, pp. 1160-1163, 1983.

[40] P. Palanichamy; A. Joseph; T. Jayakumar;, "Grain size measurements in austenitic stainless steel using ultrasonics," *Insight,* vol. 39, pp. 874-877, 1994.

[41] L. Adler; J. H. Rose; C. Mobley, "Ultrasonic method to determine gas porosity in aluminum alloy castings: Theory and Experiment," *Journal of Applied Physics,* vol. 59, pp. 336-347, 1986.

[42] J E. Gubernatis; E. Domany, "Effects of microstructre on the speed of elastic waves: Formal theory and simple approximations," *Review of Progress in Quantitative Nondestructive Evaluation,* vol. 2A, pp. 833-850, 1983.

[43] D K. Hsu; S M. Nair, "Evaluation of porosity in graphite epoxy composite by frequency dependence of ultrasonic attenuation," *Review of Progress in Quantitative Nondestructive Evaluation,* vol. 6B, pp. 1185-1193, 1987.

[44] A. Hetch; R. Thiel; E. Neuman; E. Mundry, "Nondestructive determinatin of grain size in austenetic sheet ultrasonic backscattering," *Materials Evaluation,* vol. 39, pp. 934-938, 1981.

[45] H. Williams; K. Gobbels, "Ultrasonic attenuation measurement using backscattering technique," in *Review of progress in quantitative nondestructive evaluation*, vol. 8B, 1989, pp. 1747-1753.

[46] Peter B. Nagy; Laszlo Adler, "Scattering induced attenuation of ultrasonic backscattering," *Review of Progress in Quantitative Nondestructive Evaluation,* vol. 7A, pp. 1263-1271, 1988.

[47] Anish Kumar; T. Jayakumar; P. Pananichamy; Baldev Raj, "Influence of grain size on ultrasnoic spectral parameters in AISI type 316 stainless steel," *Scripta Materialia,* vol. 40, pp. 333-340, 1999.

[48] J. Saniie; N M. Bilgutay, "Quantitative grain size evaluation using ultrasonic backscattered echoes," *J. Acoust. Soc. Am.,* vol. 80, no. 6, pp. 1816-1824,

December 1986.

[49] J. Saniie; T. Wang; N M. Bilgutay, "Analysis of Homomorphic processing for ultrasonic grain size characterisation," *IEEE transactions on Ultrasonics, Ferroelectrics, and Frequency control,* vol. 36, no. 3, pp. 365-375, 1989.

[50] D W. Fitting; L. Adler, Ultrasonic spectral analysis for NDE, New York: Plenum Press, 1981.

[51] L L. Morgan, *Crack size evaluation using ultrasonic surface wave spectroscopy,* The City University: P. hD. Thesis, 1975.

[52] A F. Brown, "Materials testing by ultrasonic spectroscopy," *Ultrasonics,* vol. 11, no. 5, pp. 202-210, 1973.

[53] O R. Gericke, "Research Techniques in NDT," in *Ultrasonic spectroscopy*, vol. Vo I, R. S. Sharpe, Ed., London, Academic Press, 1971, pp. 31-61.

[54] K. Honjoh, "Evaluation techniques for austenetic stainless steels through tensile deformation by analysing ultrasonic pulse waves in the frequency domain," *Japan Journal of Applied Physics,* vol. 33, pp. 1554-1560, 1994.

[55] R. Drai; F. Sellidj; M. Khelil; A. Benchaala, "Elaboration of some signal processing algorithms in ultrasonic techniques: application to materials NDT," *Ultrasonics,* vol. 38, pp. 503-507, 2000.

[56] S. Kraus; K. Goebbels, "Improvement of signal-to-noise ratio for the ultrasonic testing of coarse grained materials by signal averaging techniques," in *First Int. Symp. Ultrasonic Materials Characterisation,*, NBS, Gaithersburg, Maryland, (June 7-9, 1978).

[57] J C. Kennedy; W E. Woodmansee, "Signal processing in Non-destructive testing," *J. Testing Eval.,* vol. 3, no. 1, pp. 26-45, 1975.

[58] C. Cudel; M. Grevillot; J J. Meyer; S. Jacquey, "Combining phase and energy detection with mathematical morphology in dual time-frequency representation leads to improved SSP noise robustness," *Ultrasonics,* vol. 39, pp. 291-296, 2001.

[59] S P. Neal; P L. Speckman; M A. Enright, "Flaw signature estimation in ultrasonic non-destructive evaluation using the Wiener filter with limited prior information," vol. 40, no. 4, p. 347, 1993.

[60] X. Li; N M. Bilgutay, "Wiener filter realisation for target detecting using group

delay statistics," *IEEE Trans. SP,* vol. 41, no. 6, p. 2067, 1993.

[61] M A. G. Izquierdo; M G. Hernandz; O. Graullera; L G. Ullate, "Time frequency Wiener filtering for structural noise reduction," *Ultrasonics,* vol. 40, pp. 259-261, 2002.

[62] K D. Donohue, "Maximum likelyhood estimation of A-scan amplitudes for coherent targets in media of unresolvable scatters," *IEEE Trans. UFFC,* vol. 39, no. 2, p. 422, 1992.

[63] Y. Zhu; P. Weight, "Ultrasonic non-destructive evaluation of highly scattering materials using adaptive filtering and detection," *IEEE Trans. UFFC,* vol. 41, no. 1, p. 65, 1994.

[64] Z. Liu; M. Lu; M. Wei, "Structural noise reductoin of ultrasonic signals using artificial neural network adaptive filtering," *Ultrasonics,* vol. 35, pp. 325-328, 1997.

[65] X. Wu; T. Liu , "Spectral decomposition of seismic data with reassigned smoothed pseudo Wigner–Ville distribution," *Journal of Applied Geophysics,* vol. 68, pp. 386-393, 2009.

[66] M A. Malik; J. Saniie, "Gabor transform with optimal time-frequency resolution for ultrasonic application," *IEEE Ultrasonic Symposium Proceedings,* pp. 817-820, 1998.

[67] K P. Soman; K I. Ramachandran; N G. Resmi, Insights into wavelets from theory to practice, New Delhi: PHI , 2010.

[68] R. Polikar, *The wavelet tutorials,* http://users.rowan.edu/~polikar/WAVELETS.

[69] B. G. Ferguson and B. G. Quinn, "Application of the short-time Fourier transform and Wigner-Ville distribution to the acoustic localisation of aircraft," *J. Acoust. Soc. Am.,* vol. 96 , no. 2, pp. 821-827, August 1994.

[70] B. Zhao; O A. Basir; G S Mittal, "Estimation of ultrasound attenuation and dispersion using short time Fourier transform," *Ultrasonics,* vol. 43, pp. 375-381, 2005.

[71] Stephan Mallet, A wavelet tour of signal processing, the sparse way, Academic Press, 2008.

[72] C-H. Chiang; C-C. Cheng; T-C. Liu, "Improving signal processing of the impact-echo method using continuous wavelet transform," in *the Proceedings of 16th World Conference on NDT*, Montreal, Canada, 2004;

http://www.ndt.net/article/wcndt2004/pdf/civil_structures/639_chiang.pdf.

[73] C L. Nogueira, "Wavelet based analysis of ultrasonic longitudinal and transverse pulses in cement based materials," *Cement and Concrete Research,* vol. 41, pp. 1185-1195, 2011.

[74] Shishir Trivedi; Sudhir Misra, "Evaluating changes in fundamental cross - sectional mode of vibrations using a modified time domain for impact echo data," *NDT&E International,* vol. 49, pp. 10-17, 2012.

[75] R. R. Drai, K. Mohamed and A. Benchaala, "Flaw detection in ultrasonics using wavelets transform and split spectrum processing," in *the Proceedings of 15th World Conference on Non-Destructive Testing*, Rome, 2000: http://www.ndt.net/article/wcndt00/papers/idn589/idn589.htm.

[76] E. Oruklu; J. Saniie, "Ultrasonic flaw detection using discrete wavelet transform for NDE applications," *IEEE International Conference on Ultrasonics, Ferroelectrics and Frequency Control Proceedings,* pp. 1054-1057, 2004.

[77] Ki-Bok Kim; David K. Hsu.; Daniel J. Barnard, "Estimation of porosity content of composite materials by applying discrete wavelet transform to ultrasonic backscattered signal," *NDT&E International,* vol. 56, pp. 10-16, 2013.

[78] R. Murthy; N M. Bilgutay; O. Kagan Kaya, "Detection of ultrasonic anomaly signals using wavelet decomposition," *Materials Evaluation,* vol. 55, no. 11, pp. 1274-1279, 1997.

[79] V. Matz; M. Kreidl; R. Smid, "Signal separation in ultrasonic non-destructive testing," *Acta Polytechnica,* vol. 47, no. 6, pp. 3-9, 2007.

[80] G-M. Zhang, C-G. Hou, "Optimal frequency to band ratio of wavelet in ultrasonic non destructive evaluation," *Ultrasonics,* vol. 39, pp. 13-17, 2001.

[81] S-P. Song; P-W. Que , "Wavelet based noise suppression technique and its application to ultrasonic flaw detection," *Ultrasonics,* vol. 44, pp. 188-193, 2006.

[82] J C. Lazaro; J L. San Emerterio; A. Ramos; J L. Fernandez-Marron, "Influence of thresholding in ultrasonic grain noise reduction using wavelets," *Ultrasonics,* vol. 40, pp. 263-267, 2002.

[83] Angam Praveen; K. Vijayarekha; Saju T. Abraham; B. Venkatraman, " Signal quality enhancement using higher order wavelets for ultrasonic TOFD signals from austenitic stainless steel welds," *Ultrasonics,* vol. 53, pp. 1288-1292, 2013.

[84] M S. Mohammed; Kim Ki-Seong, "Shift invariant wavelet packet for signal de-noising in ultrasonic testing," *Insight,* vol. 54, no. 7, pp. 366-370, July 2012.

[85] A. Benammar, R. Drai and A. Guessoum, "Ultrasonic flaw detection using threshold modified S-transform," *Ultrasonics,* vol. 54, pp. 676-683, 2014.

[86] R. Kažys; O. Tumšys; D. Pagodinas, "Ultrasonic detection of defects in strongly attenuating structures using the Hilbert–Huang transform," *NDT & E International,* vol. 41, no. 6, pp. 457-466, September 2008.

[87] Y. Lu; E. Oruklu; J. Saniie, "Application of Hilbert Huang transform for ultrasonic non-destructive evaluation," *IEEE international ultrasonic symposium proceedings,* pp. 1499-1502, 2008.

[88] N. Mariyappa, *Development of SQUID based Magnetocardiography system & Cardiac signal-source analysis using Ensemble Empirical Mode Decomposition,* Mumbai: P. hD. Thesis, HBNI, 2013.

[89] R. Murthy; N M. Bilgutay; X. Li, "Temporal and spatial spectral features of B-scan images," *IEEE Ultrasonic Symposium Proceedings,* pp. 799-802, 1991.

[90] J. Ophir; P. Jaeger, "Spectral shifts of ultrasonic propagation through media with nonlinear dispersive attenuation," *Ultrasonic Imaging,* vol. 4, pp. 282-289, 1982.

[91] S L. Mannan, *Influence of grain size on the flow and fracture in AISI type 316 stainless steel at elevated temperatures,* IISC, Bangalore, India: Ph. D. Thesis, 1981.

[92] "Standard test methods for determining average grain size," ASTM standard E 112-96, 2004.

[93] Klaus Goebbels, Materials Characterisation for Process Control and Product Conformity, CRC Press, Inc., 1994.

[94] P. Goupillan; A. Grossmann; J. morlet, "Cycle-octave and related transform in seismics," *Geoxploration,* vol. 23, pp. 85-102, 1984.

[95] J. Choi; J-W. Hong, "Characterisation of wavelet coefficients for ultrasonic signals," *Journal of Applied Physics,* vol. 107, pp. 114909 (1-6), 2010.

[96] *MATLAB The language of technical computing,* USA: The MathWorks, Inc, 2010.

[97] M. Thavasimuthu; C. Rajagopalan; T. Jayakumar; Baldev Raj, "Effect of front surface roughness on ultrasonic contact testing a few practical observations," *Materials Evaluation,* pp. 1302 - 1309, 1998.

[98] E. Rodriguez; F. Fraudita; Y L. Armorer;, "Effect of surface roughness in ultrasonic testing (Pulse-echo by direct contact) in AISI/SAE 4340 steel samples," *NDT.net,* vol. 8, no. 11, 2003.

[99] J. Ophir, R. E. McWhirt, N. F. Maklad and P. M. Jaeger, "A narrowband pulse-echo technique for In Vivo ultrasonic attenuation estimation," *IEEE transaction on biomedical engineering,* vol. 32 , no. 3, pp. 205-212, March 1985.

[100] K. Benyelloul; H. Aourag, "Elastic constants of austenitic stainless steel: Investigation by the first-principles calculations and the artificial neural network approach," *Computational Materials Science,* vol. 67, pp. 353-358, 2013.

[101] P. Flandrin, *Matlab routines to perform EMD and EEMD,* http://perso.ens-lyon.fr/patrick.flandrin/emd.html.

[102] C-S. Chen; Y. Jeng, "Nonlinear data processing method for the signal enhancement of GPR data," *Journal of Applied Geophysics,* vol. 75, pp. 113-123, 2011.

[103] P. Flandrin; P. Goncalves; G. Rilling, "EMD equivalent filter banks, from interpretations to applications," in *Hilbert Huang Transform*, vol. 5, N. E. Huang and S. S. P. Shen, Eds., Singapore, World Scientific, 2005, pp. 57-74.